Modelling of damage evolution in multiphase engineering materials

Modelowanie rozwoju uszkodzeń w wielofazowych materiałach inżynierskich

Doctoral Thesis

Maciej Ryś

Supervisor:
dr hab. inż. Halina Egner, prof. PK

Institute of Applied Mechanics
Cracow University of Technology
al. Jana Pawła II 37, 31-864 Cracow

Cracow, 2018

Podziękowania

Serdecznie dziękuję dr hab. inż. Halinie Egner za wiele inspiracji oraz motywację do pracy naukowej.

Pragnę podziękować za wsparcie udzielone ze strony Narodowego Centrum Nauki w ramach grantu nr 2015/17/N/ST8/01169.

Wyrażam głęboką wdzięczność mojej Żonie za wsparcie i wyrozumiałość.

Abstract

Austenitic stainless steels are of major engineering importance in many applications due to their excellent mechanical properties, such as high strength, ductility, and corrosion resistance. Such good properties are also maintained at extremely low temperatures and thus austenitic stainless steels are used in many cryogenic applications, for example as cryogenic control/pressure valves or structural materials for elements of the large hadron collider (LHC) operating at 1.9 K, cryogenic transfer lines: tubes, cylinders, thin-walled shells (bellows expansion joints), etc. Under certain conditions and in some thermodynamic states, however, austenitic stainless steels become unstable, and the phase transformation from austenite (γ) to martensite (α') together with the accompanying transformation-induced plasticity (TRIP) effect may occur. In the resulting two-phase microstructure each phase exhibits different thermo-mechanical properties, while the volume fraction of phases in the representative volume of the material evolves. The development of damage, which is responsible for the material degradation, is governed by different mechanisms in each phase: in brittle martensitic inclusions the stress state has a crucial influence on damage, while in soft, ductile austenitic matrix the damage state is mainly determined by plastic flow.

The present dissertation is aimed at developing a complex constitutive and numerical model of a dissipative engineering material, consisting of two phases exhibiting different properties. Damage evolution of different type in each phase is accounted for. The constitutive model is developed within the framework of continuum mechanics and thermodynamics of irreversible processes with internal state variables, on the basis of the local state method. As examples of engineering materials possible to describe using the developed model, austenitic stainless steels of types: 304 and 316L, subjected to mechanical loading are considered.

Streszczenie

Austenityczne stale nierdzewne mają duże znaczenie w wielu zastosowaniach inżynierskich ze względu na dobre właściwości mechaniczne, takie jak wysoka wytrzymałość, ciągliwość i odporność na korozję. Co istotne, stale austenityczne wykazują się tak dobrymi właściwościwościami także w ekstremalnie niskich temperaturach, stąd wykorzystywane są w wielu zastosowaniach kriogenicznych, na przykład jako kriogeniczne zawory sterujące/ciśnieniowe, materiały konstrukcyjne dla elementów dużego zderzacza hadronów pracującego w temperaturze $1,9$K czy w kriogenicznych liniach transferowych: rury, cylindry, cienkościenne powłoki (kompensatory mieszkowe) itp. Jednak w pewnych warunkach termodynamicznych, austenityczne stale nierdzewne wykazują się niestabilnością, która może spowodować przemianę fazową austenitu (γ) w martenzyt (α') wraz z towarzyszącymi jej dodatkowymi odkształceniami plastycznymi. W tak otrzymanej dwufazowej mikrostrukturze, w której udział objętościowy każdej z faz w reprezentatywnej objętości materiału może się zmieniać w czasie (np. podczas plastycznej deformacji), każda faza wykazuje różne właściwości termomechaniczne. Rozwój uszkodzeń, które są odpowiedzialne za degradację materiału, jest wywoływany przez różne mechanizmy w każdej fazie: w kruchej fazie martenzytycznej stan naprężenia ma decydujący wpływ na uszkodzenia, podczas gdy w miękkiej, ciągliwej matrycy austenitycznej rozwój uszkodzeń jest wywoływany głównie przez odkształcenia plastyczne.

Niniejsza rozprawa poświęcona jest opracowaniu ogólnego modelu konstytutywnego i numerycznego dyssypatywnego materiału inżynierskiego, składającego się z dwóch faz wykazujących różne właściwości. Głównym elementem pracy jest uwzględnienie ewolucji uszkodzeń mających różny charakter w każdej z faz. Model konstytutywny opracowany jest w ramach mechaniki kontynualnej i termodynamiki procesów nieodwracalnych z wewnętrznymi zmiennymi stanu, z wykorzystaniem metody stanów lokalnych. Jako przykład materiału inżynierskiego, którego zachowanie może zostać opisane przy użyciu opracowanego modelu, rozważana jest austenityczna stal nierdzewna typu: 304 i 316L, poddana obciążeniu mechanicznemu.

Contents

List of Figures

List of Tables

Chapter 1

Aim and scope of work

Multi-dissipative materials are often characterized by a multiphase microstructure in which each phase exhibits different mechanical properties, and also volume fraction of each phase in the representative volume of the material may be subjected to change. The evolution of damage, which is responsible for material degradation, may be governed by different mechanisms in each phase: in brittle phases brittle damage is observed, on which the stress state has a crucial influence (Murakami, 2012), while in soft, ductile phases the damage state is mainly determined by plastic flow (Lemaitre, 1992; Chaboche, 1999). For this reason each phase has to be considered separately when damage evolution is analysed. On the other hand, phases interact with each other, which is a source of a substantial difficulty in constitutive modelling. All mechanisms have a significant impact on the macroscopic response of a material subjected to mechanical loading. Thus, it is essential to develop advanced constitutive models properly representing the mechanical behavior of multi-dissipative materials.

1.1 Objective and scope of work

The main objective of the present work is the theoretical and numerical research on damage evolution in multi-phase engineering materials. As reference materials metastable austenitic stainless steels (e.g. 304, 316L) have been choosen. Austenitic stainless steels are of major engineering importance in many applications due to their excellent mechanical properties, such as high strength, ductility, and corrosion resistance. Such good properties are preserved practically down to 0K, thus these materials are applied for components of superconducting magnets and cryogenic transfer lines: tubes, cylinders, thin walled shells (like bellows expansion joints), or massive parts like vacuum barriers. Under certain conditions (e.g. during deformation) and in some thermodynamic states, however, in these steels two dissipative phenomena may take place simultaneously in addition to plastic yielding. The first reflects

the metastable nature of the material and consists in a diffusionless transformation (temperature, stress or strain driven) from the primary phase (austenite) to the secondary phase (martensite), together with accompanying transformation-induced plasticity (TRIP) effect. The second phenomenon consists in the evolution of micro damage (microcracks, voids) of a ductile or brittle nature. As the result a two-phase microstructure, in which, each phase exhibits different thermo-mechanical properties, is obtained, and moreover, the volume fraction of phases in the representative volume of the material evolve.
The present Thesis aims at:

1. Development of a constitutive model of the elastic plastic damage two-phase material.
2. Numerical implementation of the proposed model.
3. Identification of the model parameters for 304 and 316L stainless steels.
4. Numerical simulations of chosen structural elements.

The macroscopic constitutive model of a two–phase material will be derived with the use of thermodynamics of irreversible processes framework and local state method. In this approach, the state of a material is entirely determined by certain values of certain independent variables called variables of state. At the macrolevel, the material heterogeneity (on the micro- and mesoscale) is smeared out over the representative volume element (RVE). When Continuum Damage Mechanics (CDM) approach is applied, the true state of the material within the RVE, represented by topology, size, orientation, and number of micro-rearrangements, is mapped to a material point of the so called fictitious continuum. The true distribution of microstructures and correlation between them are measured by the change of the effective constitutive tensors (stiffness or compliance). The microstructural mechanisms are formalized at the continuum level by a suitable set of internal variables of scalar, vectorial, or tensorial nature. Three coupled dissipative phenomena will be taken into account, namely plastic yielding, damage evolution, and martensitic phase transformation. The constitutive model will be derived with the assumption of small strain theory, and rate independent plasticity will be applied, in addition, only isothermal conditions will be considered. Thus rate and temperature independent model of plastic strain induced phase transformation will be employed. The volume fraction of the primary and secondary phases will be described by a scalar variable. It is assumed that the considered two–phase continuum is composed of the austenitic matrix and martensitic platelets, randomly distributed and randomly oriented in the matrix. The martensitic phase is much harder than austenitic one, and thus the austenitic matrix will be treated as an elastic–plastic material which undergoes ductile damage evolution, whereas the martensitic inclusions will show purely brittle response. The damage state in each phase

will be described by second order damage tensor, and a mixture rule will be incorporated to account for the average damage state in the material.

In the Continuum Damage Mechanics, the phenomenon of damage softening is described using the so-called effective state variables of a pseudo-undamaged quasi-continuum. To define these damage effective state variables, various equivalence hypotheses are formulated, for example: the strain equivalence hypothesis, the stress equivalence hypothesis, the strain energy or the complementary energy equivalence hypothesis, or the total energy equivalence hypothesis. The total energy equivalence hypothesis will be used here. Moreover, the aforementioned hypothesis will be extended to other dissipative phenomena like phase transformation as proposed by Egner and Ryś (2017). This formulation enables the definition of internal state variables as well as the effective thermodynamic conjugated forces, which can be indifferently used in stress space and strain space, obtaining symmetric physical properties of a material (symmetric stiffness tensor, compliance tensor, strain hardening modules) even in the case of anisotropy induced by dissipative phenomena, and modelling of coupling between damage variable and other internal state variables in a natural way.

Two dissipative phenomena, ductile damage evolution in the austenitic phase and phase transformation, will be governed by plasticity with a single dissipation potential. In such approach, the ductile damage and the phase transformation progress only when there is plastic flow (strong coupling). Separate damage surface will be incorporated in order to model brittle damage evolution in martensitic phase. Each surface will be subjected to hardening, and kinetic laws will be derived using the generalized normality rule. It will allow to describe the kinetics of dissipative phenomena (plastic flow and brittle damage evolution) independently (weak coupling).

The numerical algorithm will be proposed and implemented via VUMAT subroutine in Abaqus/Explicit FEM program. Parametric studies of the proposed model will be performed to verify the capabilities of the model to reproduce macroscopic response under the applied loading path. The model will be calibrated by means of the experimental data obtained for two typical stainless steels: 304, 316L.
To sum up the work plan covers the following major steps:

1. Development of a constitutive model of the elastic plastic damage multi-phase material
2. Numerical implementation of the developed model
   (a) building a numerical algorithm
   (b) building and testing numerical procedures VUMAT in Abaqus/Explicit
   (c) performing parametric studies to verify the model is capabilities to properly reproduce its macroscopic response under different loading paths

3. Identification of model parameters

4. Numerical simulations of chosen structural elements

1.2 Organization

The present dissertation is structured in the following pattern. Chapter 2 presents state of the art together with literature survey. At the beginning, the plastic strain-induced martensitic phase transformation is discussed. Some basic models are presented briefly. The large portion of the chapter, however, is devoted to the problem of coupling between damage and martensitic transformation in TRIP-assisted steels. As there are hundreds of papers dealing with damage in multiphase steels (including composite materials), the literature survey is restricted only to those which deal with steels in which both damage and martensite are of major importance. The constitutive framework is formulated in Chapter 3. The chaper starts with the definition of a set of internal variables, and, next, in Sections 3.2-3.3 the total energy equivalence hypothesis extended to all the dissipative phenomena regarded is discused in details. Further, in Sections 3.4-3.6 state equations and evolution equations of internal variables are derived with the use of the proposed hypothesis. Numerical implementation of the proposed model is presented in Chapter 4 where two algorithms: for a rate-independent model and a model with the rate-dependent extension but only for regularization purpose, are proposed. To examine the ability of the presented model to properly predict the behavior of brittle and ductile materials, as well as the mixed ductile/brittle material, parametric studies are performed in Chapter 5. Identification of model parameters for 316L and 304 stainless steels and comparison between experimental and numerical resutls in the case of uniaxial tension tests are presented in Chapter 6. As an example, the analysis of an expansion bellows is also shown.

Chapter 2

State of the art and literature survey

2.1 Introduction

Austenitic stainless steels are of major engineering importance in many applications due to their excellent mechanical properties over a wide range of temperatures. These steels combine good mechanical properties with an excellent corrosion resistance, and are therefore commonly used for construction materials in nuclear power plants, especially inside the pressure vessel or in the pipes of primary circuits (Amer et al., 2013). These materials are also among those most widely used for cryogenic temperature applications in various industrial fields, because they exhibit superior material performances at extremaly low temperatures, such as high yield/tensile strength, robust ductility/toughness, and high corrosion resistance/weldability. Therefore, they are employed in a vast range of industrial applications under extreme conditions, for example, as cryogenic control/pressure valves, and they also find use in a liquefied natural gas (LNG) carried cargo containment system. Moreover, the stainless steels of grade 304 and 316 are primary materials used in the reactor components, where they are subjected not only to mechanical loading but also to radiation which has a crucial influence on their behavior (Bailat et al., 2000).

2.2 Plastic strain-induced martensitic phase transformation

Metastable austenitic stainless steels is a class of steel that are susceptible to phase transformation from the austenitic face-centered cubic (FCC) into body-centered cubic (BCC) martensite under applied deformation. Phase transition of austenite into martensite is a non-diffusion process. Sometimes it is referred to as displacive transformation because it involves

moving atoms at very short distances in such a way that relations between neighboring atoms remain unchanged. This evokes a change in the crystallographic structure, but without the diffusion mechanism. This physical phenomenon increases the macroscopic work hardening rate and thus results in a highly nonlinear behavior of material (strong hardening effect due to phase transformation). Moreover, the considered phase transformation is usually accompanied by a significant additional plastic deformation. This mechanical effect was originally considered as TRIP (transformation-induced plasticity). Basically, two mechanisms play a key point for the irreversible deformation of an iron-based alloy during and after martensitic phase transformation: (1) the so called Greenwood and Johnson (1965) mechanism and (2) the Magee mechanism (Magee and Paxton, 1966). The first one explains that the additional plastic deformation is due to the difference of elementary cell volume between the two existing phases, which results in an accommodation process enforcing additional plastic yielding of the surrounding austenite matrix. The latter takes into consideration the fact that martensite platelets are formed with a preferred orientation, and this affects the overall shape of the body; which means that when a small region is transformed, its shape changes.

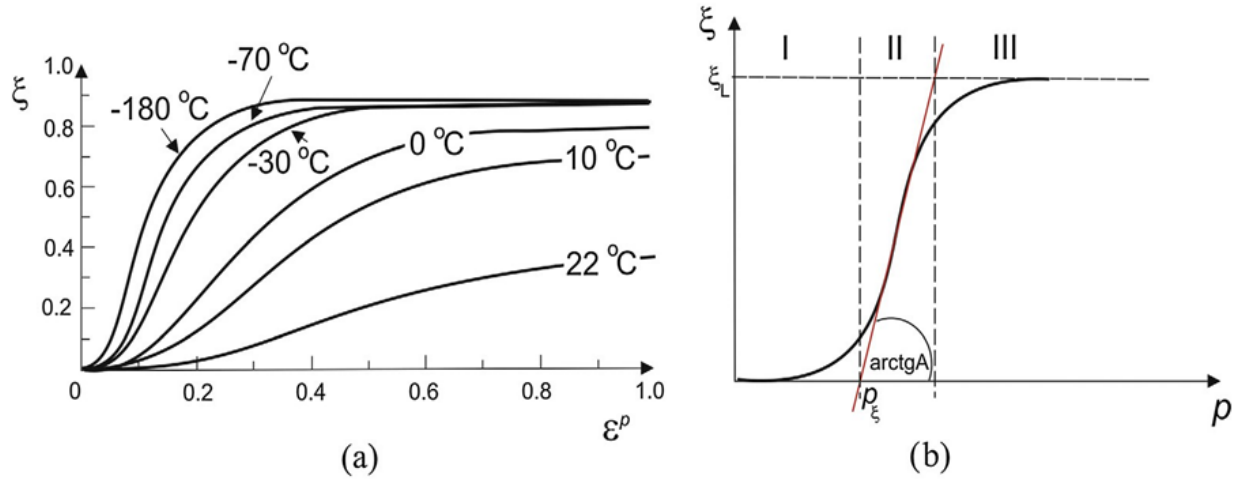

Figure 2.1: (a) Typical experimental curve of volume fraction of martensite versus plastic strain for a stainless steel; (b) linearization of the region II of the martensitic transformation (Egner et al., 2015a).

The experimental curves that describe the kinetics of the phase transformation in the function of plastic deformation are of sigmoidal character (Fig. 2.1). It can be seen that the whole process of austenite transformation into martensite can be divided into three stages (Fig. 2.1b): Stage 1 - initiation of phase transformation in which the rate of transformation is quite small; Stage 2 - rapid increase in the phase transformation kinetics; Stage 3 – the phase transformation slows down and the volume fraction of the secondary phase reaches the

saturation level.

The first physically based description of the kinetics of the plastic strain-induced martensitic transformation was introduced by Olson and Cohen (1975). The authors assumed that the strain-induced nucleation of martensitic embryos appears on the shear band intersections and hence assumed that the increasing number of shear-band intersections depends on the plastic strain, ε^{p}, in the austenite. The following one-dimensional model has been proposed

$$\xi = 1 - \exp\{-\beta[1 - \exp(-\alpha\varepsilon^{\mathrm{p}})]^n\} \tag{2.1}$$

where β is the probability that the intersection will produce an embryo, α represents the rate of shear-band formation, n is a fixed data fit parameter. The sigmoidal curve is applicable over a wide temperature range. In the work of Stringfellow et al. (1992), the authors extended Olson and Cohen model indicating that the volume fraction of the martensite is not only the function of plastic strain but also the local stress state. They included the hardening effect of the martensite platelets and also plastic softening due to martensitic nucleation by introducing an additional strain rate called "nucleation" strain rate decomposed into a deviatoric part and a dilatational part. The deviatoric part is related to the shape change and is assumed to be coaxial with the deviatoric stress, and the dilatational part is related to the volume change. The constitutive model was formulated within the finite strain framework, and the self-consistent method was used to formulate proper equations. The author's proposal, however, is restricted to isothermal conditions, and the strain rate effect was not incorporated in the model. The following formula for the rate of increase in the volume fraction of martensite was proposed

$$\dot{\xi} = (1 - \xi)(A_f\dot{\gamma}_a + B_f\dot{\sigma}_h) \tag{2.2}$$

The factor $(1 - \xi)$ decreases the volume fraction of austenite that can be transformed. The part $A_f\dot{\gamma}_a$ is related to plastic strain induced phase transformation and denotes plastic shear strain in austenite, and A_f is a function of volume fraction of shear bands and the probability that nucleation occurs at a shear-band intersection. The part $B_f\dot{\sigma}_h$ introduces stress dependence in the model, thus σ_h denotes a measure of the triaxiality of the state of stress, and B_f is a certain stress and the driving force for the martensite transformation dependent function. Further extension was made by Tomita and Iwamoto (1995) and Iwamoto et al. (1998) to account for the temperature and strain rate sensitivities of the strain-induced martensitic transformation. Their generalization is based on the observation that the number of intersections of shear bands increases as the strain rate increases. Thus the parameter which appears in function (Eq. 2.2) and which controls the number of shear bands is a function of temperature and power-law function of the plastic strain rate. The authors also observed that the

volume fraction of martensite is much higher for compression than for tension, and thus introduced deformation-mode-dependent transformation kinetics. Moreover, the third invariant of the stress tensor was incorporated in the plastic yield surface to capture a non symmetric response of tension and compression (Tomita and Iwamoto, 2001). They incorporated in the model the decomposition of plastic strain into a classical part and a part related to phase transformation (transformation strain) in a similar way to Stringfellow et al. (1992). Later on, the martensitic transformation concept of Olson and Cohen was adapted to a mesoscopic scale, and crystal plasticity framework was used to build a polycrystalline numerical model (Diani and Parks, 1998). A micromechanical model of martensitic transformation induced plasticity in an austenitic single crystal was proposed by Cherkaoui et al. (1998). The authors derived their model within the framework of thermodynamics of irreversible processes, where Helmholtz free energy was used as a state potential of a two phase material. In the next work (Cherkaoui et al., 2000), based on the micromechanical analysis of the martensitic transformation, the formation of macro domains with moving boundaries together with conditions for the nucleation and growth of martensitic platelets were considered. The proposed models were used in the simulation of texture evolution of an annealed 304 stainless steel (Petit et al., 2007). A thermodynamic transformation criterion for the martensitic transformation within the continuum mechanical framework, and using micromechanical aspects, where the Gibbs potential was used, was proposed by Fischer et al. (1994), Fischer and Reisner (1998), and Reisner et al. (1998). At low temperatures, the second stage of the phase transition (Fig. 2.1b) is becoming more rapid, and thus the phase tranformation can be described by the linear approximation as proposed by Garion and Skoczeń (2002); Garion et al. (2006). Although this model is a significant simplification of Olson and Cohen's proposal, the difference between the two models regarding the stress-strain curve and martensite volume fraction versus accumulated plastic strain is very small (Ryś, 2014). In the work by Han et al. (2004), the authors conducted a series of uniaxial and shear tests at various strain rates. They measured the temperature increase and the martensite content as a function of true strain. A self-consistent model was implemented in an iterative programme based on the radial return method, and a very good agreement was obtained between the experimental results and their numerical simulations. A simple phenomenological stress independent strain–induced martensitic transformation in stainless steel was proposed by Santacreu et al. (2006). The model was further extended to encompass the stress-state-dependency and anisotropy of the martensite evolution by incorporating the Lode angle dependency parameter in the model (Beese and Mohr, 2011, 2012). Most of the abovementioned models are formulated within small strain assumptions, while a multiscale model at fintie strains was proposed by Turteltaub and Suiker (2005); Suiker and Turteltaub (2006). Transformation plasticity in the framework of large

strains was also considered by Hallberg et al. (2007, 2010), where the mechanically induced phase transformation was proposed, and a deep drawing of a cup made of austenitic stainless steel was simulated. A thermodynamically consistent framework of the phase transformation at large deformations was formulated in Mahnken and Schneidt (2010); Mahnken et al. (2012).

Probably, still the most common model incorporating TRIP effect in constitutive modelling used in the industry is that of Leblond et al. (Leblond et al., 1989; Leblond, 1989). This analytical model was obtained from a micromechanical analysis and is based on the assumption that the parent phase has a spherical shape, and TRIP effect occurs by the growth of a spherical product phase core. In the works of Taleb and Sidoroff (2003), and Taleb and Petit (2006) the authors demonstrated that Leblond's model fails to describe certain observed phenomena, especially at the small stress range. The authors also investigated an interaction between TRIP and classical plasticity, as well as a significance of each Greenwood and Johnson, and Magee mechanism during the bainitic and martensitic transformation. A new TRIP model was also proposed with a less rigorous assumption than in Leblond's model. A micromechanical model for the transformation induced plasticity was developed by Diani et al. (1995) using the local tangent approach. Another micromechanically based model was proposed by Fischer and Schlögl (1995), the authors investigated the local stress state in a martensitically transforming micro-region including plastic anisotropy. In the paper of Fischer et al. (1998) the authors proposed a consistent thermodynamic framework to incorporate TRIP in the model, the Gibbs free energy was used as a thermodynamic potential. The authors introduced the transformation condition, and they were able to obtain coupling of the plasticity and the phase transformation in the derived flow rule for the plastic strain rate and the transformation kinetics. The martensitic transformation with TRIP effect in polycrystalline materials subjected to non-proportional loading paths was investigated by Fischer et al. (2000).

2.3 Damage modelling

The damage development occurs in almost all materials. It is related to the appearance and evolution of defects in the material. According to the second principle of thermodynamics, this process leads to an increase in disorder in material structure, e.g. the increase in entropy. Moreover, it is inevitably and irreversibly accompanied by energy dissipation, and its external manifestation is the degradation of mechanical properties (strength and stiffness), thermal properties (coefficient of thermal expansion, conductivity coefficient) and other physical properties. The development of defects leads to micro-cracks, accompanied by further

propagation of macro-cracks, eventually resulting in an oveall destruction of the structural element. The method of describing the development of damage depends on the scale of analysis. We can distinguish an atomic scale (molecular dynamics), a micro-scale (micromechanics), or a macro-scale (continuum mechanics). On the atomic scale, the structure of a material is discontinuous, represented by a lattice or by molecular chains, and the state of defects is determined by a current configuration of atomic bonds, while the breaking of bonds and the formation of new ones represent the evolution of damage. On the micro- or mesoscopic level, the structure of a material is continuous but highly heterogeneous. At this level, the configuration of dislocations is taken into consideration, which motion is often stopped by micro-defects, different types of inclusions, grain boundaries, or the concentration of stress. Damage, in the form of micro-cracks, appears when the local shear stress is beyond the cohesive strength. Inter-granular debonding, as well as decohesion, is also observed on this level. At the micro- and nano- scale, damage is a discrete phenomenon that can be observed at the microstructure level. The evolution of micro-damage can be of brittle or ductile nature. Ductile damage is strongly related to plastic yielding and thus usually occurs within the slip-bands, created in the favorably oriented crystal grains. It is important that ductile damage coupled with plastic flow is dominated by the orientation of the bands, not by the directions of mean stresses. In the case of brittle damage, a crack is initiated without large amount of plastic strain, and the process is strongly dependent on the stress state and, thus, the direction of loading, which results in the anisotropy of the damage evolution. Here, the inter-granular damage mechanism plays a fundamental role. This mechanism is related mainly to the micro-cracks and micro-voids nucleation and evolution at the grain boundaries. At the macrolevel the material heterogeneity, observed on the micro- and mesoscale, is smeared out over the representative volume element (RVE). When continuum damage mechanics approach is applied, the true state of the material within the RVE, represented by the topology, size, orientation, and number of micro-rearrangements, is mapped to a material point of the fictitious continuum. The true distribution of microstructures and the correlation between them are measured by the change of the effective constitutive tensors (stiffness or compliance). The microstructural mechanisms are formalized at the continuum level by a suitable set of internal variables of the scalar, vectorial or tensorial nature. The constitutive tensors for the dissipative material are defined by the use of effect tensors (e.g. damage effect tensor, phase transformation effect tensor, etc.) that map thermodynamic forces from the physical (discontinuous and heterogeneous) to the fictitious (pseudo-continuous and pseudo-homogeneous) configurations. The multiscale approach consists in proposing macroscopic constitutive equations taking into account the local behavior of each subphase in the RVE. A real difficulty is to establish a theoretical formalism linking macroscopic and microscopic scales when one

or several subphases are nonlinear. The limitation of the use of continuum mechanics is that the material is subjected to a critical condition of damage in which the initiation of a macro-crack takes place. In this case, the method of fracture mechanics (FM) is used and a single macroscopic crack is examined by its geometry, size and applied load. Although the process of developing damage is inevitable, there are ways to slow it down. In the case of engineering structures, appropriate tools are used to inhibit the development of defects, such as the use of special FGM materials or an optimal design of structures for lifetime destruction. This, however, requires the development of a complete mathematical description of the dissipative processes taking place in the construction materials. In addition, knowledge of the factors influencing the evolution of damage, including stress state, deformation state, plastic flow, temperature fields, structural changes in crystalline materials or dynamic loads, is also required.

2.4 Damage evolution in TRIP-assisted steels

As was mentioned above, austenitic stainless steels are of major engineering importance in many applications, due to their excellent mechanical properties, such as ductility, high strength or corrosion resistance, over a wide range of temperatures including cryogenic temperatures. As was also mentioned, in these steels two mechanisms are in competition – the damage evolution, which is responsible for the material degradation, and strain induced phase transformation with TRIP effect, which improves some mechanical properties (e.g. strength, ductility) by a composite strengthenig effect (soft matrix is reinforced with a much harder secondary phase), and a dislocation strengthening of the softer matrix as a consequence of the transformation strain accompanying martensitic transformation. The martensitic transformation provides significant modifications of fatigue mechanisms compared with stable alloys, in particular at the mesoscopic scale (e.g. short cracks). Cyclic hardening curves can be characterized by three stages: initial hardening, slight softening and second hardening followed by failure. The second hardening stage is due to the martensitic transformation which starts at some value of the accumulated plastic strain and thus after a critical number of cycles which decreases when the applied plastic strain amplitude increases. Moreover, some experimental studies revealed that the strain induced martensitic transformation has a beneficial effect on the fatigue resistance in low cycle fatigue (LCF). Furthermore, it is often stated that the TRIP effect and the volume expansion related to it result in increasing the average compressive stress, and the damage development may be hindered in the microstructure by delaying the void nucleation. Finally, since the martensitic transformation dissipates energy available for cracking in a stable microstructure, it is understandable that this improves resistance to

damage evolution. However this positive features are strongly dependent on many factors like grain size, carbon content, strain rate or stress triaxiality. On the other hand, there exists some evidence for the presence of micro-damage fields within the martensite sites. Indeed, high carbon content in the primary phase results in a very hard and brittle martensitic product phase, and thus martensitic inclusions may act as potential nucleation sites for crystalline damage, and therefore eventually can have a harmful effect on the integrity of the material. This problem often takes place in the heat affected zone in welds of high-strength, low-alloy steels.

Probably the first attempt in analyzing the correspondence between fracture toughness and martensitic transformation of a high carbon TRIP alloy was thanks to Antolovich and Singh (1971). The experiments were conducted in two temperature regimes: at low temperature regime, where the martensitic transformation occurred, and at high temperature regime, where no phase transformation was observed. The extrapolation techniques were used to compare both results, and it was stated that the martensitic transformation makes positive contribution to the fracture toughness of TRIP alloys because of absorbing energy that could otherwise be available for crack extension. Parks and Stringfellow (1991) implemented their previously derived model (Stringfellow et al., 1992) in ABAQUS and examined tensile necking and crack tip blunting. It was noted that in the absence of transformation the failure due to a process of shear instability occurs faster, and thus the phase transformation at a crack tip results in stabilizing flow and retarding the failure process. This observation was confirmed by fracture toughness experiments performed by Stavehaug (1990). It was observed that the crack propagation in partially transformed materials tends to branch which results in blunting. Finally, it was stated that the observed high toughness of the material is mainly due to the inhibition of shear localization and the deflection of the crack front away from the forward direction. Near crack-tip transformation and localization processes, based on the metallographic study, was further investigated by Olson (1996). A numerical model was provided, and it was noted that the toughening mechanism is related to the stabilization of plastic flow, resulting in the pressure-sensitive strain hardening provided by the strain-induced transformation. The influence of the testing temperature and strain rate on the strain-induced transformation and total elongation in TRIP-aided dual-phase steel was examined by Sugimoto et al. (1992). As suggested by Socrate (1995), on the micromechanical level, in high-strength metastable austenitic steels crack initiation is delayed, since the void nucleation is reduced due to the phase transformation. Moreover, the growing martensitic phase restricts the subsequent void growth. Monotonic and cyclic tests, done on a relatively stable austenitic steel (316LN), were performed by Botshekan et al. (1998) in two temperatures, 300 and 77K. The tensile tests were controlled by the total strain with a constant

strain rate. The tests were interrupted several times to measure the martensite fraction. In low cycle fatigue (LCF) tests various total strain amplitudes were imposed (1%, 1.6%, 2.25%). The experimental tests revealed that higher low-cycle fatigue life was obtained in the tests conducted at 77 K. The authors explained that these results are related to a higher slip homogeneity, which results in a more difficult crack nucleation, and a higher resistance to the early crack growth due to a partial blocking of the short crack paths by martensitic islands. In the work of Stolarz et al. (2001), two specimens made of the high purity metastable austenitic steel (Fe-17Cr-13Ni) with different grain size (D_1=12.5 and D_2=40.5 μm) were subjected to cyclic loading with the same plastic strain amplitude (fatigue test). The authors studied the mechanisms of nucleation and growth of short cracks. It was shown that the phase transformation strongly depends on the grain size, the short crack nucleation is retarded compared with stable microstructures, and the nucleation itself takes place exclusively within martensite islands formed on the surface. The nucleation and propagation mechanism of the short cracks was divided into three stages (cf. Stolarz et al. (2001)):

- The nucleation and propagation of the crack induce plastic zone in the tip of a crack and thus martensitic transformation occur,
- when the transformed zone reaches the grain boundary, crack propagation is temporarily stopped, because the further phase transformation is favoured move along the grain boundary than in the bulk,
- crack propagation is continued in the neighbouring grain without changing direction.

The damage resistance, fracture toughness and austenite to martensite transformation rate in TRIP-assisted steels were investigated in Jacques et al. (2001). Two steels differing in terms of the volume fraction of phases (ferrite, bainite, retained austenite) and by the mechanical stability of retained austenite were examined. A double edge notched plate was tested under tension. The fracture resistance was characterised by means of the J_{R} curves and crack tip opening displacement. It was observed that, at first, in the plastic zone at the crack tip retained austenite is transformed to martensite. On this stage, ferrite-martensite debonding and almost no cracking of martensite grains can be observed. However, further increase in damage sites is predominantly due to the cracking of martensite grains. Moreover, it was observed that after nucleation of a microcrack in the martensitic phase, there is no plastic void growth or microcracking extension, and thus further damage evolution is due to creation of new damage sites. The three-dimensional FE model was based on the finite strain J_2 flow theory with isotropic hardening in ABAQUS. The investigations shown that TRIP effect postpones the plastic localization but, on the other hand, reduces fracture toughness

at crack initiation. Thus, it was stated that the enhancement of resistance to cracking requires limitation of the amount of retained austenite. Finally, the authors concluded that the martensitic transformation is responsible for creation of the damage sites, however it was emphasized that the influence of martensite on the damage evolution depends on the volume fraction of martensite and on mechanical properties of martensite, which are related to carbon content. Indeed, high level of carbon makes martensite very brittle, and thus if martensite is subjected to large tensile stresses, cracking inside the inclusion or along the interface will occur. High-martensite dual-phase steels were investigated by Bag et al. (1999, 2001) by means of studying quasi-static and dynamic fracture toughness and the fatigue-crack growth behavior. It was shown that in the developed steels fracture-toughness increases with increasing the initial volume of martensite in the range of 0.3-0.6 for quasi-static and 0.45-0.6 for dynamic tests. It was also noted that the best range of toughnesses was obtained for specimens with a refined microstructural state. The stability of the retained austenite within the fatigue plastic zone of a low-carbon high strength steel was studied within foil specimens containing fatigue cracks by Huo and Gao (2005). The results have shown that the retained austenite inside the plastic zone at a fatigue crack tip has been transformed into martensite due to plastic deformation. The authors deduced that because of the effect of the energy absorbed and crack closure in the process of the strain-induced martensitic transformation, the propagation rate of the fatigue crack can be reduced. In Chatterjee and Bhadeshia (2006) it was shown that in TRIP steels small hard martensite does not readily crack as the load transfer onto martensite is difficult by straining the microstructure. However, long platelets of martensite transformed from coarse grain austenite lead to early cracking. The influence of the martensitic phase transformation on fracture parameters in the case of deep drawing was examined by Berrahmoune et al. (2006). The martensite content throughout the cup (made of 301LN SS) wall and thickness was determined. It has been found that an increased martensite content has a strong influence on the cracking sensitivity, and it was stated that the increase of the martensite content increases the delayed cracking phenomenon when the drawing ratio exceeds a certain limit. The investigation of the relationship between the microstructure and fracture resistance of TRIP-assisted multiphase steels composed of ferritic matrix with retained austenite, bainite and martensite (as dispersed phases) has been provided by Lacroix et al. (2008, 2006). Three main mechanisms of damage were observed: decohesion between two martensite grains; decohesion between ferrite and martensite grains; cleavage of a martensite grain. It was observed that the crack propagates through martensitic inclusions which are located mainly in ferritic grain, thus the main damage mechanism was decohesion between the martensite and ferrite phase. Moreover, the authors showed that TRIP effect can improve the ductile tearing resistance of thin plates.

In the works of Han et al. (2008, 2009) the mechanical properties of multiphase TRIP-aided steels were examined for various initial volumes of the retained austenite volume fraction as well as its stability condition. The authors stated that the mechanically induced phase transformation of retained austenite has a negative impact on the mechanical properties. Two separate laws for void nucleation and void growth were incorporated, and it was assumed that the void nucleation rate is an increasing function not only of the equivalent plastic strain but also of the volume fraction of martensite. In the works of Uthaisangsuk et al. (2008, 2009, 2011), the influence of a microstructure on damage in TRIP and DP (dual phase) steels have been studied. At the micro scale, two failure modes were found, cleavage (brittle in nature) and dimple (ductile in nature) fracture. It was noticed that the contribution of the fracture mechanism depends on the stress-strain conditions, the internal purity, the volume fraction of retained austenite, and the location of the austenite and martensite islands in the microstructure. It was noted that a fail of a grain of the harder phase within softer matrix results in further ductile damage evolution in the surrounding matrix. However, the main driving mechanism for ductile fracture is void initiation and void growth in the softer matrix. On the one hand, the volume expansion during phase transformation hinders the damage development in the microstructure by delaying the void nucleation but, on the other hand, the volume expansion increases dislocation density which promotes voids nucleation. Moreover, for TRIP steels the presence of martensite in the initial microstructure can lead to an early crack initiation. The increased stress triaxiality accelerates the TRIP effect and crack growth in the microstructure. The strong dependence of the rate of the martensite transformation on the stress triaxiality originates from the volume expansion involved in martensite formation. Ductile damage evolution within soft phase was modelled by the use of continuum mechanics and well known GTN approach (Gurson-Tvergard-Needleman). The void nucleation and the void growth law was incorporated for the ductile damage evolution, and the cohesive model was used to investigate cleavage damage in FE simulations. The phase transformation of retained austenite to martensite was not accounted for. It was also suggested that in composite-like structures damage occurs in surroundings of inclusions due to a high hardness gradient. Therefore, for this reason, the newly formed high strength martensite may act as a source of void nucleation in austenite. The influence of the martensite volume fraction on failure modes in dual phase steels, where the failure was considered in the form of plastic strain localization, was examined by Sun et al. (2009). Lee and coworkers (Lee et al., 2009) proposed a new constitutive model of an austenitic stainless steel. Two types of austenitic steels (304 and 316) were tested under a cryogenic temperature. The phase transformation and evolution of micro-damage were included in the model. The modelling of the plastic behavior was based on the modified visco-plastic damage of Bodner type model. The model

of Tomita and Iwamoto (1995) was used to incorporate phase transformation effects in the constitutive description. The small strain theory was used although the computations were performed up to fracture. The phase transformation occurring in the crack tip region in the austenitic stainless steel 304 was investigated by Hallberg et al. (2012). The authors stated that the martensite which appears in a crack tip region gives rise to fracture toughening of the material. The higher resistance of crack initiation due to the presence of a martensitic phase was also observed. Moreover, it was shown that the formation of martensite at the crack tip may delay or even prevent further crack propagation. This transformation toughening and reduction of crack growth rate has been attributed to crack tip shielding and crack tip blunting, and crack closure due to roughening of the crack surfaces or due to the crack being subjected to compression by the dilatation in the transformed material.

Since the modelling of phase transformation and damage evolution in austenitic stainless steels has been an important element of the research at the Institute of Applied Mechanics (Cracow University of Technology) for many years, it is necessary to present scientific achievements that have been developed. Garion and Skoczeń (2002, 2003) proposed a model of an austenitic stainless steel subjected to loading at cryogenic temperatures where the Mori-Tanaka homogenization scheme was used to include the influence of the martensitic transformation on the hardening process. The authors extended the isotropic ductile damage model of Chaboche-Lemaitre to the case of an orthotropic material by introducing the tensor of texture. The coupling between martensitic transformation and damage evolution, however was not accounted for. In the work of Egner and Skoczeń (2010) the model proposed by Garion and Skoczeń (2003) was reformulated within the framework of thermodynamics of irreversible processes and used to calculate damage evolution in materials characterized by low stacking fault energy (such as copper, stainless steel 316L) in cryogenic conditions. Experimental evidence of the deceleraion of the damage evolution rate due to presence and development of martensite was presented. Mathematical and numerical model with coupling between the martensitic transformation and damage evolution was proposed in Egner and Ryś (2012), and Egner et al. (2015a,b). Moreover, the previous model was extended to account for different types of the damage evolution in both phases, and a mixture rule was postulated in order to obtain the average damage state in the RVE. It was assumed that the brittle damage state in martensite depends directly on the actual stress state. Such approach is quite convenient (e.g. brittle damage may develop independently of plastic flow, and a separate Lagrange multiplier is not required) but leads to inconsistent results of numerical simulations of unloading during cyclic loading. The model was implemented in Abaqus/Vumat via user subroutine to simulate the behaviour of axisymmetric, corrugated thin-walled cryogenic bellows under cyclic loading at cryogenic temperatures in Ryś (2015). The model was also

used in the case of circular bars subjected to torsion in liquid nitrogen and room temperature conditions, 3D FE simulation was compared to the analytical solution of the torsion problem (Ortwein et al., 2016). The ductile damage evolution model used in the abovementioned propositions was based on the Chaboche-Lemaitre model of damage development (extended to acoount for anisotropy), alternative proposition was presented in Ryś (2016), where an isotropic Bonora type model was used. Moreover, the total energy equivalence hypothesis was used to derive particular state equations, and a non-assosiated flow rule was used, which allowed to obtain better correspondence between numerical and experimental results. Finally, in the recent work (Egner and Ryś, 2017), a general theory of the constitutive modelling of multidissipative materials was developed where the total energy hypothesis (originally developed for damage materials) was extended to modelling not only damage but also other dissipative phenomena (e.g. phase transformation). Additionaly to the yield criterion (based on the J_2 theory), analogical damage surface was introduced to model brittle damage evolution. Radiation induced damage in austenitic steels was considered in Ryś and Skoczeń (2017).

It has to be mentioned here that the presented dissertation is based on the previously published works. Especially Chapters 3 and 6 are based on the recent work by Egner and Ryś (2017).

Chapter 3

Constitutive model of a multi-dissipative material

The constitutive model is based on the following assumptions (Egner et al., 2015a; Egner and Ryś, 2017):

1. the partially transformed material is composed of the austenitic matrix and martensitic platelets, randomly distributed and oriented in the matrix,
2. the phase transformation is considered as plastic strain-induced and the austenitic phase is recognized as a rather soft material in comparison to the much harder martensite,
3. the austenitic matrix is subjected to plastic deformation and ductile damage development, whereas the inclusions show purely brittle response,
4. ductile damage in the matrix material and phase transformation are controlled by plasticity (within a single generalized yield function), while brittle damage evolution (in the secondary phase inclusions) is constrained by a separate damage surface,
5. brittle damage yield surface is subjected to isotropic hardening,
6. a rule of mixture is applied to estimate the average level of damage in the RVE,
7. mixed isotropic/kinematic plastic hardening is regarded,
8. strains are small,
9. isothermal conditions are considered,
10. the amount of the secondary phase does not exceed 80-90%.

3.1 Internal variables of state

In the case of the small strain theory, the total strain tensor, $\boldsymbol{\varepsilon}$, can be expressed as a sum of the elastic (reversible) strain, $\boldsymbol{\varepsilon}^{\mathrm{E}}$, and inelastic (irreversible) strain, $\boldsymbol{\varepsilon}^{\mathrm{I}}$: [1]

$$\boldsymbol{\varepsilon} = \boldsymbol{\varepsilon}^{\mathrm{E}} + \boldsymbol{\varepsilon}^{\mathrm{I}} \tag{3.1}$$

In the process of deformation, evolution of material micro-structure may be induced, for example by changes in density and configuration of dislocations, development of microscopic cavities, transition changes from primary to secondary phase, etc. All these rearrangements may contribute to both reversible and irreversible strains (Al-Rub and Voyiadjis, 2003; Egner, 2012), therefore:

$$\boldsymbol{\varepsilon}^{\mathrm{E}} = \boldsymbol{\varepsilon}^{\mathrm{e}} + \sum_{k=1}^{n} \boldsymbol{\varepsilon}^{\mathrm{Ek}}, \quad \boldsymbol{\varepsilon}^{\mathrm{I}} = \sum_{k=1}^{n} \boldsymbol{\varepsilon}^{\mathrm{Ik}}, \quad \boldsymbol{\varepsilon}^{k} = \boldsymbol{\varepsilon}^{\mathrm{Ek}} + \boldsymbol{\varepsilon}^{\mathrm{Ik}}, \quad k = 1, 2, ..., n \tag{3.2}$$

where $\boldsymbol{\varepsilon}^{\mathrm{e}}$ denotes "pure" elastic strain, $\boldsymbol{\varepsilon}^{\mathrm{Ek}}$, $\boldsymbol{\varepsilon}^{\mathrm{Ik}}$ are reversible and irreversible components of the total strain $\boldsymbol{\varepsilon}^{k}$, respectively, induced by k-th dissipative phenomenon. Here, in the particular case of elastic – plastic – damage material with martensitic phase transformation the following decomposition is assumed

$$\boldsymbol{\varepsilon}^{\mathrm{E}} = \boldsymbol{\varepsilon}^{\mathrm{e}} + \boldsymbol{\varepsilon}^{\mathrm{ed}} \tag{3.3}$$

where the total elastic strain, $\boldsymbol{\varepsilon}^{\mathrm{E}}$, is decomposed into the pure elastic strain, $\boldsymbol{\varepsilon}^{\mathrm{e}}$, and the reversible–damage strain, $\boldsymbol{\varepsilon}^{\mathrm{ed}}$. On the other hand, the following three phenomena cause inelastic strain: plastic flow, damage evolution and phase transformation, what results in the following decomposition

$$\boldsymbol{\varepsilon}^{\mathrm{I}} = \boldsymbol{\varepsilon}^{\mathrm{p}} + \boldsymbol{\varepsilon}^{\mathrm{id}} + \boldsymbol{\varepsilon}^{\mathrm{tr}} \tag{3.4}$$

Furthermore, since two types of damage evolution are considered, the irreversible damage strain can be further decomposed into parts related to ductile damage evolution, $\boldsymbol{\varepsilon}^{\mathrm{idd}}$, and brittle damage evolution, $\boldsymbol{\varepsilon}^{\mathrm{ibd}}$

$$\boldsymbol{\varepsilon}^{\mathrm{id}} = \boldsymbol{\varepsilon}^{\mathrm{idd}} + \boldsymbol{\varepsilon}^{\mathrm{ibd}} \tag{3.5}$$

The part of inelastic strain, $\boldsymbol{\varepsilon}^{\mathrm{tr}}$ related to the phase transformation can be decomposed into a deviatoric part, which is related to the shape change due to the TRIP effect, and a volumetric

[1] The standard symbolic notation is employed, where bold-face characters denote second- or fourth-order tensors, a double dot denotes double contraction, e.g. $\mathbf{A} : \mathbf{B} = A_{ijkl}B_{kl}$, and $\otimes$ a tensor product. A superimposed dot denotes the material time derivative (i.e. rate), assumed always to exist.

part (cf. Stringfellow et al. 1992)

$$\boldsymbol{\varepsilon}^{\mathrm{tr}} = \boldsymbol{\varepsilon}^{\mathrm{s}} + \boldsymbol{\varepsilon}^{\mathrm{v}} \tag{3.6}$$

According to the framework of thermodynamics of irreversible processes, the current state of an RVE is entirely determined by known values of a chosen set of internal (hidden) variables whose number and character (scalar or tensorial) depend on a physical mechanism causing the particular microstructural rearrangement and the total strain (or displacement). There are no precise rules of choosing internal variables but, in practice, these variables should be measurable but not controllable (Maugin, 1999). In the case of the proposed model, the following set of independent variables is chosen

$$\{V_\beta\} = \{\boldsymbol{\varepsilon}^{\mathrm{E}}; \boldsymbol{\alpha}^{\mathrm{p}}, r^{\mathrm{p}}; \mathbf{D}^{\mathrm{d}}, \mathbf{D}^{\mathrm{b}}, r^{\mathrm{b}}; \xi\} \tag{3.7}$$

where $\boldsymbol{\varepsilon}^{\mathrm{E}}$ is the elastic strain tensor, r^{p} and $\boldsymbol{\alpha}^{\mathrm{p}}$ are plasticity-related variables corresponding to isotropic (change of size of yield surface) and kinematic (change of location of yield surface) hardening respectively, while ξ is a volume fraction of the martensitic inclusions in the total volume of the RVE. The last symbol in Eq. (3.7), r^{b}, describes the variable related to isotropic hardening of the brittle damage yield surface.

To account for the texture-induced anisotropy of the ductile matrix, and damage-induced anisotropy of the brittle inclusions, the second-rank tensors $\mathbf{D}^{\mathrm{d}}$ and $\mathbf{D}^{\mathrm{b}}$ are, respectively, postulated as the measures of damage, after Egner et al. (2015a). The total material degradation in the RVE is described by the damage tensor $\mathbf{D}$, being a superposition of the ductile part $\mathbf{D}^{\mathrm{d}}$ and the brittle part $\mathbf{D}^{\mathrm{b}}$. The simplest linear rule of mixture is here applied to define the average damage tensor $\mathbf{D}$:

$$D_{ij} = (1-\xi)D_{ij}^{\mathrm{d}} + \xi D_{ij}^{\mathrm{b}} = \left\langle D_{ij} \right\rangle_{\mathrm{RVE}}^{\mathrm{d}} + \left\langle D_{ij} \right\rangle_{\mathrm{RVE}}^{\mathrm{b}} \tag{3.8}$$

It is obvious that a more general formula of the mixture rule can also be used, which is

$$D_{ij} = (1 - m(\xi))\, D_{ij}^{\mathrm{d}} + m(\xi) D_{ij}^{\mathrm{b}} \tag{3.9}$$

where $m(\xi) \in \langle 0, 1\rangle$ is a function satisfying $m(0) = 0$ and $m(1) = 1$.

3.2 The generalized total energy equivalence hypothesis

Continuum mechanics approach used in the present analysis provides the constitutive and evolution equations in the framework of thermodynamics of irreversible processes. The material heterogeneity (on the micro- and meso-scale) is smeared out over the representative volume element (RVE) of the piece-wise discontinuous and heterogeneous material. In continuum damage mechanics the phenomenon of damage softening is described by the use of the so-called effective state variables of a pseudo-undamaged quasi-continuum. To define these damage-effective state variables, various equivalence hypotheses are formulated, for example: (a) strain equivalence hypothesis (Lemaitre, 1971; Lemaitre and Chaboche, 1978), (b) stress equivalence hypothesis (Simo and Ju, 1987), (c) strain energy or complementary energy equivalence hypotheses (Cordebois and Sidoroff, 1982a,b), or finally, (d) total energy equivalence hypothesis (Chow and Lu, 1992; Saanouni et al., 1994). According to these hypotheses, the effective state variables are defined in such a way that respectively strains, stresses, strain energy or complementary strain energy, or the total energy for both real (damaged) and fictitious (pseudo-undamaged) materials are the same.

In the following section, a constitutive description of an austenitic stainless steel is derived based on the total energy equivalence hypothesis but extended to all the dissipative phenomena regarded. The theoretical background of the consistent application of this hypothesis on the macro-scale to phenomena other than damage was presented in the paper by Egner and Ryś (2017).

The formulation based on the total energy equivalence hypothesis satisfies a number of compromises (Saanouni, 2012). In particular, the groups of effective state variables can be equivalently used either in the strain or stress space. The transition from one space to the other can be performed by the application of the Legendre-Fenchel transformation. In the presence of anisotropic and dissipative behaviour, the total energy equivalence leads to symmetric physical properties (elastic modulus, strain hardening modules, etc) for a damaged and phase transformed material. Moreover, it allows to achieve naturally a strong coupling between damage, phase transformation, and all other variables, without neglecting any interaction between various phenomena taking place in the material.

The development of plasticity, damage and phase transformation affects the global mechanical properties of steel, either causing softening (damage) or hardening (plasticity, phase transformation, cf. Egner and Skoczeń (2010); Egner et al. (2015a)). This means that material behavior (both elastic and inelastic) is influenced by the microstructural mechanisms. To account for the influence of the dissipative phenomena on the overall mechanical proper-

ties, the so-called effective state variables can be used in the state and dissipation potentials instead of the classical state variables. These effective state variables are here defined on the basis of the total energy equivalence generalized to all dissipative phenomena (cf. Saanouni et al. (1994); Egner and Ryś (2017)):

> *"At any time* (t)*, to an RVE in its real (deformed, damaged, phase transformed) configuration, described by a set of state variables, we associate an unchanged (undamaged, untransformed) equivalent fictive configuration the state of which is described by the effective state variables – in such a manner that the total internal energy defined over the two (real and fictive) configurations is the same".*

Such formulation involves two main configurations (see Fig. 3.1): a real, discontinuous and

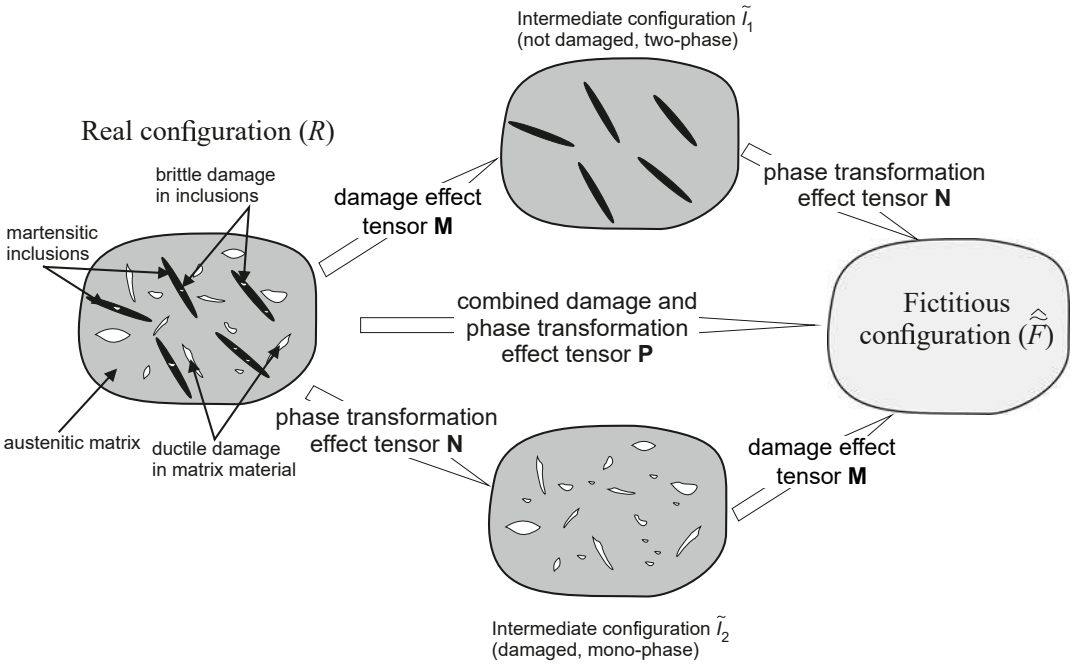

Figure 3.1: Illustration of the generalized total energy equivalence hypothesis.

heterogeneous configuration (R) of a material subjected to three dissipative phenomena: plastic slips, damage and phase transformation, and a fictitious, quasi-continuous and quasi-homogeneous configuration $(\hat{\tilde{F}}) \equiv (\tilde{\hat{F}})$. Mapping from configuration (R) to $(\hat{\tilde{F}}) \equiv (\tilde{\hat{F}})$ may be equivalently performed with the use of two intermediate configurations: $(\tilde{I}_1)$, which is idealized undamaged but phase transformed, and $(\hat{I}_2)$, which is a damaged but idealized untransformed configuration. Each intermediate configuration is characterized by proper effective variables, defined on the basis of the total energy equivalence applied to the real configuration (R) and the intermediate configuration considered. Mapping from the real configuration (R) to fictitious configuration $(\hat{\tilde{F}}) \equiv (\tilde{\hat{F}})$ may therefore be indifferently realized in

two ways: $(R) \rightarrow (\tilde{I}_1) \rightarrow (\hat{\tilde{F}})$ or $(R) \rightarrow (\hat{I}_2) \rightarrow (\hat{\tilde{F}})$, as a combination of two qualitatively different transformations: one of them transforms a highly discontinuous (damaged) configuration to a perfectly continuous (undamaged) one, while the second transforms a highly heterogeneous (multi-phase) configuration to a perfectly homogeneous (mono-phase) configuration.

Using such a unified approach to damage and phase transformation requires two transformation tensors: the classical damage effect tensor (M_{ijkl}), which maps the state variables from the damaged to pseudo-undamaged configuration ($(R) \rightarrow (\tilde{I}_1)$ or $(\hat{I}_2) \rightarrow (\hat{\tilde{F}})$), and a new phase transformation effect tensor (N_{ijkl}). The new tensor maps the state variables from the transformed to pseudo-untransformed configuration ($(\tilde{I}_1) \rightarrow (\hat{\tilde{F}})$ or $(R) \rightarrow (\hat{I}_2)$).

In such approach, all dissipative phenomena are consistently described by the use of the same thermodynamic framework. The representative volume element of a real, discontinuous (due to cavities and microcracks) and heterogeneous (due to phases) material is mapped into a point of a fictitious homogeneous continuum in which all micro-rearrangements are smeared out without resolving the details of the contributing components. The effective state variables

Table 3.1: Pairs of variables related to different configurations defined in the model.

phenomenon	Real configuration (R)	Intermediate configuration $(\tilde{I}_1)$	Intermediate configuration $(\hat{I}_2)$	Pseudo-undamaged and untransformed configuration $(\hat{\tilde{F}}) \equiv (\hat{\tilde{F}})$
plastic flow plastic hardening (kinematic and isotropic)	$(\boldsymbol{\varepsilon}^{\mathrm{E}}, \boldsymbol{\sigma})$ $(\boldsymbol{\alpha}^{\mathrm{p}}, \mathbf{X}^{\mathrm{p}})$ $(r^{\mathrm{p}}, R^{\mathrm{p}})$	$(\tilde{\boldsymbol{\varepsilon}}^{\mathrm{E}}, \tilde{\boldsymbol{\sigma}})$ $(\tilde{\boldsymbol{\alpha}}^{\mathrm{p}}, \tilde{\mathbf{X}}^{\mathrm{p}})$ $(\tilde{r}^{\mathrm{p}}, \tilde{R}^{\mathrm{p}})$	$(\hat{\boldsymbol{\varepsilon}}^{\mathrm{E}}, \hat{\boldsymbol{\sigma}})$ $(\hat{\boldsymbol{\alpha}}^{\mathrm{p}}, \hat{\mathbf{X}}^{\mathrm{p}})$ $(\hat{r}^{\mathrm{p}}, \hat{R}^{\mathrm{p}})$	$(\hat{\tilde{\boldsymbol{\varepsilon}}}^{\mathrm{E}}, \hat{\tilde{\boldsymbol{\sigma}}})$ $(\hat{\tilde{\boldsymbol{\alpha}}}^{\mathrm{p}}, \hat{\tilde{\mathbf{X}}}^{\mathrm{p}})$ $(\hat{\tilde{r}}^{\mathrm{p}}, \hat{\tilde{R}}^{\mathrm{p}})$
phase transformation	(ξ, Y^{CH})	(ξ, Y^{CH})	$(\xi = 0, Y^{\mathrm{CH}} = 0)$	$(\xi = 0, Y^{\mathrm{CH}} = 0)$
ductile damage	$(\mathbf{D}^{\mathrm{d}}, \mathbf{Y}^{\mathrm{d}})$	$(\mathbf{D}^{\mathrm{d}} = \mathbf{0}, \mathbf{Y}^{\mathrm{d}} = \mathbf{0})$	$(\mathbf{D}^{\mathrm{d}}, \mathbf{Y}^{\mathrm{d}})$	$(\mathbf{D}^{\mathrm{d}} = \mathbf{0}, \mathbf{Y}^{\mathrm{d}} = \mathbf{0})$
brittle damage	$(\mathbf{D}^{\mathrm{b}}, \mathbf{Y}^{\mathrm{b}})$ $(r^{\mathrm{b}}, R^{\mathrm{b}})$	$(\mathbf{D}^{\mathrm{b}} = \mathbf{0}, \mathbf{Y}^{\mathrm{b}} = \mathbf{0})$ $(\tilde{r}^{\mathrm{b}}, \tilde{R}^{\mathrm{b}})$	$(\mathbf{D}^{\mathrm{b}} = \mathbf{0}, \mathbf{Y}^{\mathrm{b}} = \mathbf{0})$ $(\hat{r}^{\mathrm{b}}, \hat{R}^{\mathrm{b}})$	$(\mathbf{D}^{\mathrm{b}} = \mathbf{0}, \mathbf{Y}^{\mathrm{b}} = \mathbf{0})$ $(\hat{\tilde{r}}^{\mathrm{b}}, \hat{\tilde{R}}^{\mathrm{b}})$
Total internal energy (isothermal)	U^{t}	$\tilde{U}^{\mathrm{t}}$	$\hat{U}^{\mathrm{t}}$	$\hat{\tilde{U}}^{\mathrm{t}} \equiv \hat{\tilde{U}}^{\mathrm{t}}$

are related to different configurations considered in the model (see Fig. 3.1, Tab. 3.1), and

defined on the basis of the total energy equivalence between subsequent configurations:

$$\begin{aligned} &U^{\mathrm{t}}(\boldsymbol{\varepsilon}^{\mathrm{E}}, \boldsymbol{\alpha}^{\mathrm{p}}, r^{\mathrm{p}}; \xi; \mathbf{D}^{\mathrm{d}}; \mathbf{D}^{\mathrm{b}}, r^{\mathrm{b}}) = \tilde{U}^{\mathrm{t}}(\tilde{\boldsymbol{\varepsilon}}^{\mathrm{E}}, \tilde{\boldsymbol{\alpha}}^{\mathrm{p}}, \tilde{r}^{\mathrm{p}}; \xi; \tilde{r}^{\mathrm{b}}) = \\ &= \hat{U}^{\mathrm{t}}(\hat{\boldsymbol{\varepsilon}}^{\mathrm{E}}, \hat{\boldsymbol{\alpha}}^{\mathrm{p}}, \hat{r}^{\mathrm{p}}; \mathbf{D}^{\mathrm{d}}; \mathbf{D}^{\mathrm{b}}, \hat{r}^{\mathrm{b}}) = \hat{\tilde{U}}^{\mathrm{t}}(\hat{\tilde{\boldsymbol{\varepsilon}}}^{\mathrm{E}}, \hat{\tilde{\boldsymbol{\alpha}}}^{\mathrm{p}}, \hat{\tilde{r}}^{\mathrm{p}}; \hat{\tilde{r}}^{\mathrm{b}}) \end{aligned} \tag{3.10}$$

It is assumed here that the total energy, U^{t}, can be additively decomposed into a sum of elastic energy, U^{e}, kinematic hardening energy, U^{kin}, and isotropic hardening energy, U^{iso}. Thus, the introduced hypothesis can be further formulated in a stronger form, namely all the total energy components are equivalent in each configuration.

$$U^{\mathrm{e}} = \frac{1}{2}\sigma_{ij}\varepsilon^{\mathrm{E}}_{ij} = \frac{1}{2}\tilde{\sigma}_{ij}\tilde{\varepsilon}^{\mathrm{E}}_{ij} = \frac{1}{2}\hat{\sigma}_{ij}\hat{\varepsilon}^{\mathrm{E}}_{ij} = \frac{1}{2}\hat{\tilde{\sigma}}_{ij}\hat{\tilde{\varepsilon}}^{\mathrm{E}}_{ij} \tag{3.11}$$

$$U^{\mathrm{kin}} = \frac{1}{2}X^{\mathrm{p}}_{ij}\alpha^{\mathrm{p}}_{ij} = \frac{1}{2}\tilde{X}^{\mathrm{p}}_{ij}\tilde{\alpha}^{\mathrm{p}}_{ij} = \frac{1}{2}\hat{X}^{\mathrm{p}}_{ij}\hat{\alpha}^{\mathrm{p}}_{ij} = \frac{1}{2}\hat{\tilde{X}}^{\mathrm{p}}_{ij}\hat{\tilde{\alpha}}^{\mathrm{p}}_{ij} \tag{3.12}$$

$$U^{\mathrm{iso}} = \frac{1}{2}R^{\mathrm{p}}r^{\mathrm{p}} + \frac{1}{2}R^{\mathrm{b}}r^{\mathrm{b}} = \frac{1}{2}\tilde{R}^{\mathrm{p}}\tilde{r}^{\mathrm{p}} + \frac{1}{2}\tilde{R}^{\mathrm{b}}\tilde{r}^{\mathrm{b}} = \frac{1}{2}\hat{R}^{\mathrm{p}}\hat{r}^{\mathrm{p}} + \frac{1}{2}\hat{R}^{\mathrm{b}}\hat{r}^{\mathrm{b}} = \frac{1}{2}\hat{\tilde{R}}^{\mathrm{p}}\hat{\tilde{r}}^{\mathrm{p}} + \frac{1}{2}\hat{\tilde{R}}^{\mathrm{b}}\hat{\tilde{r}}^{\mathrm{b}} \tag{3.13}$$

Note that the fictive undamaged and untransformed configuration $(\hat{\tilde{F}}) \equiv (\tilde{\hat{F}})$ is qualitatively different from the virgin material configuration, because the complete description of the current state of the fictive material $(\hat{\tilde{F}}) \equiv (\tilde{\hat{F}})$ requires not only the use of observable variables but also hardening variable pairs $(\hat{\tilde{\boldsymbol{\alpha}}}^{\mathrm{p}}, \hat{\tilde{\mathbf{X}}}^{\mathrm{p}})$, $(\hat{\tilde{r}}^{\mathrm{p}}, \hat{\tilde{R}}^{\mathrm{p}})$, $(\hat{\tilde{r}}^{\mathrm{b}}, \hat{\tilde{R}}^{\mathrm{b}})$, while for the virgin material all internal variables are zero. In other words, in configuration $(\hat{\tilde{F}}) \equiv (\tilde{\hat{F}})$ the information about the current state of "hardening" related to all dissipative phenomena has to be recorded.

3.3 Damage and phase transformation effect operators

A general solution that satisfies equation (3.11) may take the following form:

$$\tilde{\sigma}_{ij} = [M_{ijkl}(\mathbf{D})]^{-1}\sigma_{kl}, \qquad \tilde{\varepsilon}^{\mathrm{E}}_{ij} = [M_{ijkl}(\mathbf{D})]^{T}\varepsilon^{\mathrm{E}}_{kl} \tag{3.14}$$

$$\hat{\sigma}_{ij} = [N_{ijkl}(\xi)]^{-1}\sigma_{kl}, \quad \hat{\varepsilon}^{\mathrm{E}}_{ij} = [N_{ijkl}(\xi)]^{T}\varepsilon^{\mathrm{E}}_{kl} \tag{3.15}$$

$$\hat{\tilde{\sigma}}_{ij} = [P_{ijkl}(\mathbf{D}, \xi)]^{-1}\sigma_{kl}, \quad \hat{\tilde{\varepsilon}}^{\mathrm{E}}_{ij} = [P_{ijkl}(\mathbf{D}, \xi)]^{T}\varepsilon^{\mathrm{E}}_{kl} \tag{3.16}$$

Each of the operators introduced above ($\mathbf{M}$, $\mathbf{N}$, $\mathbf{P}$) should meet appropriate restrictions which result from the basics of linear algebra and physics of a phenomenon under consideration. Namely, the damage effect operator $\mathbf{M}(\mathbf{D})$ should:

- be a positive definite, symmetric, and decreasing function of damage tensors,

- be reduced to the fourth-rank unit tensor in the absence of damage,
- tend toward the fourth-order zero tensor at total fracture of the RVE when the average damage tensor approaches the unit tensor.

The phase transformation effect operator $\mathbf{N}(\xi)$ should:

- be a positive definite, symmetric and monotonic function of phase transformation variable,
- be reduced to the fourth-rank unit tensor in the absence of phase transformation,
- transform the properties of the matrix material into the properties of the secondary phase material when the phase transformation variable reaches unity.

The combined effect operator $\mathbf{P}(\mathbf{D}, \xi)$ should:

- be a positive definite, symmetric but not necessarily monotonic function of damage and phase transformation variables,
- be reduced to the fourth-rank damage effect operator in the absence of phase transformation, and to the fourth-rank phase transformation effect operator in the absence of damage: $\mathbf{P}(\mathbf{D}, 0) = \mathbf{M}(\mathbf{D})$, $\mathbf{P}(\mathbf{0}, \xi) = \mathbf{N}(\xi)$.

To derive the solution that satisfies Eqs (3.12) and (3.13), the following additional assumptions are applied:

a) a given dissipative phenomenon does not affect itself,

b) it is assumed (for simplicity) that phase transformation affects only plastic hardening variables and not damage variables (which remain unchanged),

c) the relations between inelastic tensorial variables (related to kinematic hardening) in subsequent configurations involve fourth-order inelastic operators $\mathbf{M}^{\text{in}}$, $\mathbf{N}^{\text{in}}$, $\mathbf{P}^{\text{in}}$ which exhibit the same features as "elastic" operators $\mathbf{M}$, $\mathbf{N}$, $\mathbf{P}$ (see above),

d) since current state of phase transformation is described with the use of scalar variable ξ, the phase transformation effect tensor (affecting plastic kinematic hardening variables) is here a unimodular fourth-rank tensor:

$$\mathbf{N}^{\text{in}} = h^{\text{kin}}(\xi)\mathbf{I} \tag{3.17}$$

As a result, operator $\mathbf{P}^{\text{in}}$, related to a combination of mappings $(R) \rightarrow (\tilde{I}_1) \rightarrow (\hat{\tilde{F}})$ or $(R) \rightarrow (\hat{I}_2) \rightarrow (\tilde{\hat{F}})$ takes the following form:

$$\mathbf{P}^{\text{in}}(\mathbf{D}, \xi) = h^{\text{kin}}(\xi)\mathbf{M} \tag{3.18}$$

e) damage affects plastic kinematic hardening variables in the same way as elastic strains $\mathbf{M}^{\text{in}} = \mathbf{M}$,

f) the relations between inelastic scalar variables (related to isotropic hardening) are described by the use of scalar functions $g(\mathbf{D})$, $h^{\text{iso}}(\xi)$ and $p(\mathbf{D}, \xi) = g(\mathbf{D})\, h^{\text{iso}}(\xi)$.

According to the above assumptions we obtain:

$$\tilde{X}^{\text{p}}_{ij} = [M_{ijpq}(\mathbf{D})]^{-1} X^{\text{p}}_{pq}, \qquad \tilde{\alpha}^{\text{p}}_{ij} = [M_{ijpq}(\mathbf{D})]^{T} \alpha^{\text{p}}_{pq} \tag{3.19}$$

$$\hat{X}^{\text{p}}_{ij} = \frac{1}{h^{\text{kin}}(\xi)} X^{\text{p}}_{ij}, \qquad \hat{\alpha}^{\text{p}}_{ij} = h^{\text{kin}}(\xi)\, \alpha^{\text{p}}_{ij} \tag{3.20}$$

$$\hat{\tilde{X}}^{\text{p}}_{ij} = \frac{1}{h^{\text{kin}}} (M_{ijkl})^{-1} X^{\text{p}}_{kl}, \qquad \hat{\tilde{\alpha}}^{\text{p}}_{ij} = h^{\text{kin}} (M_{ijkl})^{T} \alpha^{\text{p}}_{kl} \tag{3.21}$$

Accordingly, for the isotropic hardening variables it is:

$$\tilde{R}^{\text{p}} = \frac{R^{\text{p}}}{g(\mathbf{D})}, \quad \tilde{r}^{\text{p}} = g(\mathbf{D}) r^{\text{p}}, \quad \tilde{R}^{\text{b}} = R^{\text{b}}, \quad \tilde{r}^{\text{b}} = r^{\text{b}} \tag{3.22}$$

$$\hat{R}^{\text{p}} = \frac{R^{\text{p}}}{h^{\text{iso}}(\xi)}, \quad \hat{r}^{\text{p}} = h^{\text{iso}}(\xi) r^{\text{p}}, \quad \hat{R}^{\text{b}} = R^{\text{b}}, \quad \hat{r}^{\text{b}} = r^{\text{b}} \tag{3.23}$$

$$\hat{\tilde{R}}^{\text{p}} = \frac{R^{\text{p}}}{g(\mathbf{D}) h^{\text{iso}}(\xi)}, \quad \hat{\tilde{r}}^{\text{p}} = g(\mathbf{D}) h^{\text{iso}}(\xi) r^{\text{p}}, \quad \hat{\tilde{R}}^{\text{b}} = R^{\text{b}}, \quad \hat{\tilde{r}}^{\text{b}} = r^{\text{b}} \tag{3.24}$$

In the present considerations, it is adopted that scalar damage effect function $g(\mathbf{D})$ and hardening functions $h^{\text{kin}}(\xi)$, $h^{\text{iso}}(\xi)$ take the forms (Saanouni et al., 1994; Egner and Ryś, 2017):

$$g(\mathbf{D}) = 1 - \sqrt{D_{ij} D_{ij}} = 1 - D_{eq}, \quad h^{\text{kin}}(\xi) = 1 + h_X \xi, \quad h^{\text{iso}}(\xi) = 1 + h_R \xi \tag{3.25}$$

where h_X, h_R are material parameters.
It should be noted here that the introduced above phase transformation effect scalar functions $h^{\text{kin}}(\xi)$ and $h^{\text{iso}}(\xi)$ are purely phenomenological, however a similar linear function $h^{\text{kin}}(\xi)$ in a kinematic hardening description was proposed by Sitko and Skoczeń (2012) on the basis of micromechanical considerations.

3.4 Effective material properties based on total energy equivalence

In the present work, the Helmholtz free energy density (per unit volume), ψ, is used as the thermodynamic potential which describes the current state of the material and, in real configuration (R), is a function of the state variables

$$\psi = \psi(\{V_\beta\}) = \psi(\boldsymbol{\varepsilon}^{\mathrm{E}}; \boldsymbol{\alpha}^{\mathrm{p}}, r^{\mathrm{p}}; \mathbf{D}^{\mathrm{d}}, \mathbf{D}^{\mathrm{b}}, r^{\mathrm{b}}; \xi) \tag{3.26}$$

Moreover, it is assumed that the state potential of the material in its real configuration (R) can be written as a sum of elastic (E), inelastic (I), and chemical (CH) terms:

$$\psi = \psi\left(V_\beta\right) = \psi^{\mathrm{E}} + \psi^{\mathrm{I}} + \psi^{\mathrm{CH}} \tag{3.27}$$

For the present study, the following functions for ψ^{E} and ψ^{I} are adopted:

$$\psi^{\mathrm{E}} = \frac{1}{2}\varepsilon^{\mathrm{E}}_{ij}\hat{\hat{E}}_{ijkl}\varepsilon^{\mathrm{E}}_{kl} \tag{3.28}$$

$$\psi^{\mathrm{I}} = \psi^{\mathrm{p}} + \psi^{\mathrm{bd}} = \frac{1}{2}\hat{\hat{C}}_{ijkl}\alpha^{\mathrm{p}}_{ij}\alpha^{\mathrm{p}}_{kl} + \frac{1}{2}\hat{\hat{Q}}^{\mathrm{p}}(r^{\mathrm{p}})^2 + \frac{1}{2}Q^{\mathrm{b}}(r^{\mathrm{b}})^2 \tag{3.29}$$

where $\hat{\hat{\mathbf{E}}}$, $\hat{\hat{\mathbf{C}}}$, $\hat{\hat{Q}}^{\mathrm{p}}$ and Q^{b} denote (damage affected) elastic stiffness tensor, (damage and phase transformation affected) plastic hardening moduli (respectively kinematic and isotropic) and damage isotropic hardening modulus in a current real configuration (R).
Term ψ^{CH} in Eq. (3.27) stands for the chemically stored energy:

$$\psi^{\mathrm{CH}} = \left[1 - f\left(\xi\right)\right]\psi^{\mathrm{CH}}_{\gamma} + f\left(\xi\right)\psi^{\mathrm{CH}}_{\alpha'} \tag{3.30}$$

Terms $\psi^{\mathrm{CH}}_{\gamma}$ and $\psi^{\mathrm{CH}}_{\alpha'}$ are the chemical energies of the respective phases, dependent on the specific heat, entropy and temperature (cf. e.g. Hallberg et al. (2007), Fischer et al. (2000)). Symbol $f(\xi)$ denotes a function of the current state of phase transformation, such that $f(0) = 0$ and $f(1) = 1$.
According to the used hypothesis of the total energy equivalence, it is reasonable to introduce the Helmholz free energy density, $\hat{\tilde{\psi}}$ related to the pseudo unchanged configuration $(\hat{\tilde{F}}) \equiv (\tilde{\hat{F}})$, which is

$$\hat{\tilde{\psi}}^{\mathrm{E}} = \frac{1}{2}\hat{\tilde{\varepsilon}}^{\mathrm{E}}_{ij}E^{0}_{ijkl}\hat{\tilde{\varepsilon}}^{\mathrm{E}}_{kl} \tag{3.31}$$

$$\hat{\tilde{\psi}}^{\mathrm{I}} = \hat{\tilde{\psi}}^{\mathrm{p}} + \hat{\psi}^{\mathrm{b}} = \frac{1}{2}C^{0}_{ijkl}\hat{\tilde{\alpha}}^{\mathrm{p}}_{ij}\hat{\tilde{\alpha}}^{\mathrm{p}}_{kl} + \frac{1}{2}Q^{\mathrm{p}0}(\hat{\tilde{r}}^{\mathrm{p}})^2 + \frac{1}{2}Q^{\mathrm{b}0}(r^{\mathrm{b}})^2 \tag{3.32}$$

$$\hat{\tilde{\psi}}^{\mathrm{CH}} = \tilde{\psi}_{\gamma}^{\mathrm{CH}} \tag{3.33}$$

where $\mathbf{E}^0$, $\mathbf{C}^0$, $Q^{\mathrm{p}0}$ and $Q^{\mathrm{b}0}$ denote material characteristics for the (virgin) undamaged and not transformed material. In view of the total energy equivalence the Helmholtz free energies in all configurations considered are equivalent, therefore:

$$\hat{\tilde{\psi}}^{\mathrm{E}} = \psi^{\mathrm{E}}, \quad \hat{\tilde{\psi}}^{\mathrm{I}} = \psi^{\mathrm{I}}, \quad \hat{\tilde{\psi}}^{\mathrm{CH}} = \psi^{\mathrm{CH}}. \tag{3.34}$$

In the case of $\gamma \rightarrow \alpha'$ phase transformation, it can be assumed that elastic behaviour of both phases is the same and therefore phase transformation does not affect elastic properties of the material (cf. e.g. Hallberg et al. (2007); Mahnken et al. (2012)). In such case, the phase transformation operator $\mathbf{N}$ (Eqs. 3.15) is a unit tensor, $\mathbf{N} = \mathbf{I}$, and, consequently, $\mathbf{P} = \mathbf{M}$ (see Eqs. 3.16). Equation (3.16_1) therefore takes the simplified form:

$$\hat{\tilde{\sigma}}_{ij} = (M_{ijkl})^{-1}\sigma_{kl} = \tilde{\sigma}_{ij} \tag{3.35}$$

Since $\gamma \rightarrow \alpha'$ phase transformation does not affect the elastic properties of the material, the current elastic stiffness tensor is affected only by damage, $\hat{\tilde{\mathbf{E}}}(\mathbf{D}) = \tilde{\mathbf{E}}(\mathbf{D})$. The tensor is related to the initial stiffness of the undamaged material, $\mathbf{E}^0$, by the use of the fourth-rank symmetric damage effect tensor $\mathbf{M}(\mathbf{D})$ (cf. Saanouni (2012)). Using relations (3.16), (3.28), (3.31), and (3.34) the relation between the initial and current stiffness tensors is obtained:

$$\tilde{E}_{ijkl}(\mathbf{D}) = M_{ijpq}E^0_{pqmn}M_{klmn} \tag{3.36}$$

The following expression for $\mathbf{M}(\mathbf{D})$, proposed by Cordebois and Sidoroff (1982a,b), will be used here:

$$M_{ikjl} = \frac{1}{2}\left[(\delta_{ik} - D_{ik})\delta_{jl} + \delta_{ik}(\delta_{jl} - D_{jl})\right] \tag{3.37}$$

Relations (3.34), (3.32) and (3.29) result in:

$$\hat{\tilde{C}}_{ijpq} = (1 + h_X\xi)^2 M_{ijkl}C^0_{klrs}M_{rspq} \tag{3.38}$$

$$\hat{\tilde{Q}}^{\mathrm{p}} = (1 + h_R\xi)^2(1 - D_{eq})^2 Q^{\mathrm{p}0} \tag{3.39}$$

while the material parameter related to damage isotropic hardening remains unchanged,

$$\hat{\tilde{Q}}^{\mathrm{b}} = Q^{\mathrm{b}0} \tag{3.40}$$

In the absence of the martensitic phase ($\xi \equiv 0$), and if there is no damage, the material is considered as isotropic, thus the plasticity tensor in the fictitious configuration $(\hat{\tilde{F}}) \equiv (\hat{\tilde{F}})$ is $C^0_{ijkl} = C^0 I_{ijkl}$. In such case, Eq. (3.38) is simplified into the following expression:

$$\hat{\tilde{C}}_{ijkl}(\mathbf{D}, \xi) = (1 + h_X \xi)^2 C^0 M_{ijmn}(\mathbf{D}) M_{mnkl}(\mathbf{D}) \tag{3.41}$$

It can be seen from Eqs. (3.36), (3.38) and (3.41) that in the presence of the (acquired) anisotropic behavior induced by damage, the generalized total energy equivalence leads to symmetric physical properties of multi-dissipative materials.

3.5 Equations of state

According to an approach widely used in the literature on damage mechanics, generalized here for all other dissipative phenomena, the mechanical behavior of a real dissipative medium is derived from the same state and dissipation potentials as a fictitious unchanged medium in which state variables are replaced by effective variables.
By eliminating all reversible processes from the Clausius-Duhem inequality, the following state equation, which expresses the thermodynamic force $\boldsymbol{\sigma}$ conjugated to the observable state variable $\boldsymbol{\varepsilon}^{\mathrm{E}}$, is obtained:

$$\sigma_{ij} = \frac{\partial \psi}{\partial \varepsilon^{\mathrm{E}}_{ij}} = \tilde{E}_{ijkl} \varepsilon^{\mathrm{E}}_{kl} \tag{3.42}$$

In addition, the forces conjugated to other state variables are defined in a like manner. For damage variable $\mathbf{D}$, the thermodynamic conjugated force has the form:

$$Y_{ij} = -\frac{\partial(\hat{\tilde{\psi}})}{\partial D_{ij}} = -\frac{\partial(\hat{\tilde{\psi}}^{\mathrm{E}})}{\partial D_{ij}} - \frac{\partial(\hat{\tilde{\psi}}^{\mathrm{I}})}{\partial D_{ij}} - \frac{\partial(\tilde{\psi}^{\mathrm{CH}}_{\gamma})}{\partial D_{ij}} = Y^{\mathrm{e}}_{ij} + Y^{\mathrm{p}}_{ij} + Y^{\mathrm{tr}}_{ij} \tag{3.43}$$

where Y^{e}_{ij}, Y^{p}_{ij} and Y^{tr}_{ij} stand for the contributions to the thermodynamic force Y_{ij} from elasticity, plastic hardening, and phase transformation respectively (cf. also Egner (2012); Egner and Ryś (2017)):

$$Y^{\mathrm{e}}_{ij} = -E^0_{pqkl} J_{rspqij} \varepsilon^{\mathrm{E}}_{kl} \varepsilon^{\mathrm{E}}_{rs}, \qquad J_{rspqij} = \frac{\partial M_{rspq}}{\partial D_{ij}} \tag{3.44}$$

$$Y^{\mathrm{p}}_{ij} = -C^{\mathrm{p}0}(1 + h_X \xi)^2 M_{klmn} J_{klrsij} \alpha^{\mathrm{p}}_{mn} \alpha^{\mathrm{p}}_{rs} + \frac{Q^{\mathrm{p}0}}{D_{eq}}(1 - D_{eq})(1 + h_R \xi)^2 (r^{\mathrm{p}})^2 D_{ij} \tag{3.45}$$

$$Y^{\mathrm{tr}}_{ij} = -\frac{\partial(\tilde{\psi}^{\mathrm{CH}}_{\gamma})}{\partial D_{ij}} \tag{3.46}$$

The conjugated force for phase transformation becomes:

$$Y^{\mathrm{CH}} = \frac{\partial(\hat{\tilde{\psi}})}{\partial \xi} = \frac{\partial(\hat{\tilde{\psi}}^{\mathrm{I}})}{\partial \xi} + \frac{\partial(\tilde{\psi}_{\gamma}^{\mathrm{CH}})}{\partial \xi} \tag{3.47}$$

The forces conjugated to plastic and damage hardening variables take the form:

$$X_{ij}^{\mathrm{p}} = \frac{\partial(\hat{\tilde{\psi}})}{\partial \alpha_{ij}^{\mathrm{p}}} = (1 + h_X \xi)^2 C^0 M_{ijmn} M_{mnkl} \alpha_{kl}^{\mathrm{p}} \tag{3.48}$$

$$R^{\mathrm{p}} = \frac{\partial(\hat{\tilde{\psi}})}{\partial r^{\mathrm{p}}} = (1 + h_R \xi)^2 (1 - D_{eq})^2 Q^{\mathrm{p}0} r^{\mathrm{p}} \tag{3.49}$$

$$R^{\mathrm{b}} = \frac{\partial(\hat{\tilde{\psi}})}{\partial r^{\mathrm{b}}} = Q^{\mathrm{b}0} r^{\mathrm{b}} \tag{3.50}$$

Equations (3.42)-(3.50) define the complete set $\{J_{cf}\} = \{\sigma_{ij}; -Y_{ij}, Y^{\mathrm{CH}}; X_{ij}^{\mathrm{p}}, R^{\mathrm{p}}, R^{\mathrm{b}}\}$ of thermodynamic forces conjugated to state variables (see Table 3.1).

3.6 Evolution of state variables

In the present study the following time-independent dissipative mechanisms: plastic flow, ductile damage, phase transformation, and brittle damage are considered. Each of these mechanisms is constrained by a separate scalar-valued potential function that is positive, null at the origin, and convex in its principal arguments. It should be pointed out that some of the considered phenomena, such as ductile damage in the austenitic phase and phase transformation, are strongly coupled with plastic flow, that is, if there is no plastic yielding, thus also neither ductile damage evolution nor phase transformation occur in a material. Brittle damage evolution is an independent process that can occur even in the elastic regime but only in the presence of the secondary phase. Generally, we can distinguish two types of coupling of plasticity with damage: the so called strong coupling and weak coupling. Weak coupling is obtained by using two separate uncoupled plastic and damage loading surfaces. Strong coupling is realized by using one single smooth generalized yield surface for the plasticity and damage evolution. Another approach to achieve strong coupling is using separate plasticity and damage surfaces with separate non-associated flow rules in such a way that both damage and plasticity flow rules are dependent on both plastic and damage potentials (Voyiadjis and Deliktas, 2000).

The plastic potential, F^{p} is here equal to von Mises-type yield surface plus additional terms

related to the isotropic and kinematic dynamic recovery (Chaboche, 2008)

$$F^{\mathrm{p}} = f^{\mathrm{p}} + \frac{1}{2}\frac{\hat{\tilde{b}}^{\mathrm{p}}}{\hat{\tilde{Q}}^{\mathrm{p}}}(R^{\mathrm{p}})^2 + \frac{3}{4}\hat{\tilde{\gamma}}X'^{\mathrm{p}}_{ij}\hat{\tilde{C}}^{-1}_{ijkl}X'^{\mathrm{p}}_{kl} \tag{3.51}$$

In the above equation, f^{p} denotes the von Mises yield surface:

$$f^{\mathrm{p}} = \sqrt{\frac{3}{2}(\sigma'_{ij} - X'^{\mathrm{p}}_{ij})(\sigma'_{ij} - X'^{\mathrm{p}}_{ij})} - \hat{\tilde{\sigma}}_{\mathrm{y}} - R^{\mathrm{p}} \tag{3.52}$$

Symbols σ'_{ij} and X'^{p}_{ij} stand for the stress and the back stress deviators (in the presence of anisotropic damage, the incompressibility of the plastic material is lost):

$$\sigma'_{ij} = \left(\delta_{im}\delta_{jn} - \frac{1}{3}\delta_{ij}\delta_{mn}\right)\sigma_{mn}, \quad X'^{\mathrm{p}}_{ij} = \left(\delta_{im}\delta_{jn} - \frac{1}{3}\delta_{ij}\delta_{mn}\right)X^{\mathrm{p}}_{mn} \tag{3.53}$$

while $\hat{\tilde{\gamma}}$ and $\hat{\tilde{b}}^{p}$ are additional material parameters which may be affected by the dissipative phenomena taking place in the material.

Ductile materials strained in cryogenic conditions develop micro-damage fields in a similar way like at room or enhanced temperatures. Evolution of damage fields (micro-cracks and micro-voids) is also driven by plastic strains and similar kinetic laws can be used. Thus for ductile damage dissipation the relevant potential F^{d} is assumed in the following form (cf. Saanouni (2012)):

$$F^{\mathrm{d}} = \frac{2S}{(s+1)(1-D^{\mathrm{d}}_{eq})^{\beta}}\left(\frac{Y^{\mathrm{d}}_{eq}}{S}\right)^{(s+1)} - B^{\mathrm{d}}\,, \qquad D^{\mathrm{d}}_{eq} = \sqrt{D^{\mathrm{d}}_{ij}D^{\mathrm{d}}_{ij}} \tag{3.54}$$

where S, s and β are characteristic damage-related parameters (that may be affected by phase transformation), and B^{d} is a threshold for the norm of the thermodynamic force associated with ductile damage, below which ductile damage does not develop. Symbol Y^{d}_{eq} stands for the norm of thermodynamic force conjugated to ductile damage, see Eq. (3.43):

$$Y^{\mathrm{d}}_{ij} = -\frac{\partial(\hat{\tilde{\psi}})}{\partial D^{\mathrm{d}}_{ij}} = -\frac{\partial(\hat{\tilde{\psi}})}{\partial D_{kl}}\frac{\partial D_{kl}}{\partial D^{\mathrm{d}}_{ij}} = (1-\xi)Y_{ij} \tag{3.55}$$

This norm is here defined as:

$$Y^{\mathrm{d}}_{eq} = \sqrt{\frac{1}{2}Y^{\mathrm{d}}_{ij}A_{ijkl}Y^{\mathrm{d}}_{kl}} \tag{3.56}$$

where A_{ijkl} is the anisotropy operator of ductile damage evolution (Hayakawa et al., 1998):

$$A_{ijkl} = \frac{1}{2}\left(\delta_{ij}\delta_{kl} + \delta_{il}\delta_{jk}\right) \tag{3.57}$$

The phase transformation dissipation potential, F^{tr}, is expressed as a function of Y^{CH} in a simple form:

$$F^{\mathrm{tr}} = (\xi_{\max} - \xi)\frac{m_\xi D_\xi}{(1 - D_{eq})}(D_\xi p)^{m_\xi - 1} Y^{\mathrm{CH}} - B^{\mathrm{tr}} \tag{3.58}$$

where factor $(\xi_{\max} - \xi)$ reflects the decreasing volume fraction available for transformation, m_ξ and D_ξ are parameters, and $p = \int_t \dot{\lambda}^{\mathrm{p}} dt$ ($\dot{\lambda}^{\mathrm{p}}$ is a plastic multiplier). Symbol B^{tr} denotes the barrier force for phase transformation (cf. Fischer et al. (2000), Mahnken and Schneidt (2010)).

The brittle damage evolution in martensitic inclusions is not governed by plasticity, and thus a separate brittle damage dissipation potential, F^{b}, is introduced in the following form (cf. Al-Rub and Voyiadjis (2003)):

$$\begin{aligned} F^{\mathrm{b}} = f^{\mathrm{b}} + \frac{1}{2}\frac{b^{\mathrm{b}}}{Q^{\mathrm{b0}}}(R^{\mathrm{b}})^2 &= \sqrt{\frac{1}{2}Y^{\mathrm{b}}_{ij} A_{ijkl} Y^{\mathrm{b}}_{kl}} - l_y - R^{\mathrm{b}} + \frac{1}{2}\frac{b^{\mathrm{b}}}{Q^{\mathrm{b0}}}(R^{\mathrm{b}})^2 \\ &= \xi\sqrt{\frac{1}{2}Y_{ij} A_{ijkl} Y_{kl}} - l_y - R^{\mathrm{b}} + \frac{1}{2}\frac{b^{\mathrm{b}}}{Q^{\mathrm{b0}}}(R^{\mathrm{b}})^2 \end{aligned} \tag{3.59}$$

where l_y denotes the initial size (radius) of the brittle damage surface, and b^{b} is an additional model parameter related to nonlinearity of the isotropic damage hardening. Symbol Y^{b}_{ij} is the thermodynamic force conjugated to brittle damage, see Eq. (3.43):

$$Y^{\mathrm{b}}_{ij} = -\frac{\partial(\hat{\tilde{\psi}})}{\partial D^{\mathrm{b}}_{ij}} = -\frac{\partial(\hat{\tilde{\psi}})}{\partial D_{kl}}\frac{\partial D_{kl}}{\partial D^{\mathrm{b}}_{ij}} = \xi Y_{ij} \tag{3.60}$$

As already mentioned before, the kinetic equations for a real dissipative medium can be derived from the dissipation potentials of a fictitious (non-dissipative) medium with the use of effective variables. Effective plastic potential $\hat{\tilde{F}}^{\mathrm{p}}$ (Eq. 3.51) in the fictitious $(\hat{\tilde{F}}) \equiv (\tilde{\hat{F}})$ configuration, expressed in effective variables, is:

$$\hat{\tilde{F}}^{\mathrm{p}} = \hat{\tilde{f}}^{\mathrm{p}} + \frac{1}{2}\frac{b^{\mathrm{p}}}{Q^{\mathrm{p0}}}(\hat{\tilde{R}}^{\mathrm{p}})^2 + \frac{3}{4}\frac{\gamma}{C^{\mathrm{p0}}}\hat{\tilde{X}}^{\mathrm{p}}_{ij}\hat{\tilde{X}}^{\mathrm{p}}_{ij} \tag{3.61}$$

where the effective conjugated variables are defined by Eqs. (3.35) and (3.19)-(3.24). Effective yield function $\hat{\tilde{f}}^{\mathrm{p}}$ is expressed in the following way:

$$\hat{\tilde{f}}^{p} = J_2(\tilde{\sigma}_{ij} - \hat{\tilde{X}}^{\mathrm{p}}_{ij}) - \sigma^0_{\mathrm{y}} - \hat{\tilde{R}}^{\mathrm{p}} = \\ = \sqrt{\frac{3}{2}\left[(M_{ijkl})^{-1}(s_{kl} - \frac{X'^{\mathrm{p}}_{kl}}{\sqrt{1+h_X\xi}})\right]\left[(M_{ijmn})^{-1}(s_{mn} - \frac{X'^{\mathrm{p}}_{mn}}{\sqrt{1+h_X\xi}})\right]} - \sigma^0_{\mathrm{y}} - \hat{\tilde{R}}^{\mathrm{p}} \quad (3.62)$$

In the above functional, all (dependent) state variables are expressed in the fictitious configuration. This approach is most general and consistent with the introduced concept, however there are also other possibilities, for example the functional can be based only on effective stress while other variables may be used in a real configuration. It can be easily seen that there are many other possibilities, which results in different couplings, thus there is quite much freedom of choosing a particular option (discussion about choosing different couplings in continuum damage mechanics can be found in Besson et al. (2009)).
The expression for the second invariant, J_2, may be presented in a form more convenient for numerical implementation. Taking into account Eqs. (3.35), (3.21$_1$) and (3.25) the relations (3.53) may be expressed in the following form:

$$\tilde{\sigma'}_{ij} = T^{-1}_{ijkl}\sigma_{kl}, \qquad \hat{\tilde{X}}'^{\mathrm{p}}_{ij} = T^{-1}_{ijkl}\frac{X^{\mathrm{p}}_{kl}}{1+h_X\xi} \quad (3.63)$$

where

$$T^{-1}_{ijkl} = \left(\delta_{im}\delta_{jn} - \frac{1}{3}\delta_{ij}\delta_{mn}\right)M^{-1}_{mnkl} = M^{-1}_{ijkl} - \frac{1}{3}M^{-1}_{mmkl}\delta_{ij} \quad (3.64)$$

Now, the second invariant of the effective stress deviator (3.62) can be rewritten as:

$$J_2(\tilde{\sigma}_{ij} - \hat{\tilde{X}}^{\mathrm{p}}_{ij}) = \sqrt{\frac{3}{2}\left[T^{-1}_{ijkl}\left(\sigma_{kl} - \frac{X^{\mathrm{p}}_{kl}}{1+h_X\xi}\right)\right]\left[T^{-1}_{ijmn}\left(\sigma_{mn} - \frac{X^{\mathrm{p}}_{mn}}{1+h_X\xi}\right)\right]} \quad (3.65)$$

By employing the normality rule, the following kinetic law for inelastic strain is obtained:

$$\dot{\varepsilon}^{\mathrm{I}}_{ij} = \dot{\lambda}^{\mathrm{p}}\frac{\partial\hat{\tilde{F}}^{\mathrm{p}}}{\partial\sigma_{ij}} + \dot{\lambda}^{\mathrm{p}}\frac{\partial F^{\mathrm{d}}}{\partial\sigma_{ij}} + \dot{\lambda}^{\mathrm{b}}\frac{\partial F^{\mathrm{b}}}{\partial\sigma_{ij}} + \dot{\varepsilon}^{\mathrm{tr}}_{ij} = \dot{\varepsilon}^{\mathrm{p}}_{ij} + \dot{\varepsilon}^{\mathrm{idd}}_{ij} + \dot{\varepsilon}^{\mathrm{ibd}}_{ij} + \dot{\varepsilon}^{\mathrm{tr}}_{ij} \quad (3.66)$$

where the strain rate components resulting from the mechanisms governed by plasticity are:

$$\dot{\varepsilon}^{\mathrm{p}}_{ij} = \dot{\lambda}^{\mathrm{p}}\frac{\partial\hat{\tilde{F}}^{\mathrm{p}}}{\partial\sigma_{ij}} = \dot{\lambda}^{\mathrm{p}}\frac{\frac{3}{2}T^{-1}_{pqij}T^{-1}_{pqkl}(\sigma_{kl} - \frac{X^{\mathrm{p}}_{kl}}{1+h_X\xi})}{J_2(\tilde{\sigma}_{ij} - \hat{\tilde{X}}^{\mathrm{p}}_{ij})} \quad (3.67)$$

$$\dot{\varepsilon}_{ij}^{\mathrm{idd}} = \dot{\lambda}^{\mathrm{p}} \frac{\partial F^{\mathrm{d}}}{\partial \sigma_{ij}} = \dot{\lambda}^{\mathrm{p}} \frac{2S}{(1 - D_{eq}^{\mathrm{d}})^{\beta}} \left(\frac{Y_{eq}^{\mathrm{d}}}{S} \right)^{s} \frac{A_{mnkl} Y_{kl}^{\mathrm{d}}}{Y_{eq}^{\mathrm{d}}} \frac{\partial Y_{mn}^{\mathrm{d}}}{\partial \sigma_{ij}} \tag{3.68}$$

The development of brittle damage gives the contribution:

$$\dot{\varepsilon}_{ij}^{\mathrm{ibd}} = \dot{\lambda}^{\mathrm{b}} \frac{\partial F^{\mathrm{b}}}{\partial \sigma_{ij}} = \dot{\lambda}^{\mathrm{b}} \frac{A_{klmn} Y_{mn}^{\mathrm{b}}}{\sqrt{\frac{1}{2} Y_{pq}^{\mathrm{b}} A_{pqsx} Y_{sx}^{\mathrm{b}}}} \frac{\partial Y_{kl}^{\mathrm{b}}}{\partial \sigma_{ij}} \tag{3.69}$$

The last term in (3.66) is related to the TRIP effect associated with phase transformation (cf. Stringfellow et al. (1992), Hallberg et al. (2007)):

$$\dot{\varepsilon}_{ij}^{\mathrm{tr}} = A \left(\frac{\partial \hat{\tilde{f}}^{\mathrm{p}}}{\partial \sigma_{ij}} + \frac{1}{3} \Delta \upsilon \delta_{ij} \right) \dot{\xi} \tag{3.70}$$

in which the dilatation term accounts for the volume change induced by transformation with $\Delta \upsilon > 0$ and $A = A_0 + A_1 \left(\frac{\sigma_{eq}}{\sigma_{\mathrm{y}}} \right)$ is dimensionless coefficient taking into account orientational charakter of the transformation strains (Stringfellow et al., 1992).
On the basis of the normality rule, the rate of plastic isotropic hardening internal variable is defined as follows:

$$\dot{r}^{\mathrm{p}} = -\dot{\lambda}^{\mathrm{p}} \frac{\partial \hat{\tilde{F}}^{\mathrm{p}}}{\partial R^{\mathrm{p}}} = \frac{\dot{\lambda}^{\mathrm{p}}}{(1 - D_{eq})(1 + h_R \xi)} \left(1 - \frac{b^{\mathrm{p}}}{Q^{\mathrm{p}0}} \frac{R^{\mathrm{p}}}{(1 - D_{eq})^3 (1 + h_R \xi)^3} \right) \tag{3.71}$$

Introducing state equation (3.49) in Eq. (3.71) results in the following relation:

$$\dot{r}^{\mathrm{p}} = -\dot{\lambda}^{\mathrm{p}} \frac{\partial \hat{\tilde{F}}^{\mathrm{p}}}{\partial R^{\mathrm{p}}} = \frac{\dot{\lambda}^{\mathrm{p}}}{(1 - D_{eq})(1 + h_R \xi)} \left(1 - \frac{b^{\mathrm{p}} r^{\mathrm{p}}}{(1 - D_{eq})(1 + h_R \xi)} \right) \tag{3.72}$$

The normality rule applied to plastic potential with respect to back stress $\mathbf{X}^{\mathrm{p}}$ gives:

$$\dot{\alpha}_{ij} = -\dot{\lambda}^{\mathrm{p}} \frac{\partial \hat{\tilde{F}}^{\mathrm{p}}}{\partial X_{ij}^{\mathrm{p}}} = \frac{3}{2} \frac{\dot{\lambda}^{\mathrm{p}}}{1 + h_X \xi} T_{pqij}^{-1} T_{pqkl}^{-1} \left[\frac{\left(\sigma_{kl} - \frac{X_{kl}^{\mathrm{p}}}{1 + h_X \xi} \right)}{J_2(\tilde{\sigma}_{ij} - \hat{\tilde{X}}_{ij}^{\mathrm{p}})} - \frac{\gamma}{C(1 + h_X \xi)^3} X_{kl}^{\mathrm{p}} \right] \tag{3.73}$$

The rates of damage state variables $\mathbf{D}^{\mathrm{d}}$, $\mathbf{D}^{\mathrm{b}}$ and r^{b} result from the normality rule applied to the relevant potentials, F^{d} and F^{b} (Eqs (3.54) and (3.59)):

$$\dot{D}_{ij}^{\mathrm{d}} = \dot{\lambda}^{\mathrm{p}} \frac{\partial F^{\mathrm{d}}}{\partial Y_{ij}^{\mathrm{d}}} = \frac{\dot{\lambda}^{\mathrm{p}}}{(1 - D_{eq}^{\mathrm{d}})^{\beta}} \left(\frac{Y_{eq}^{\mathrm{d}}}{S} \right)^{s} \frac{A_{ijkl} Y_{kl}^{\mathrm{d}}}{Y_{eq}^{\mathrm{d}}} H\left(p - p_D\right) \tag{3.74}$$

$$\dot{D}^{\mathrm{b}}_{ij} = \dot{\lambda}^{\mathrm{b}} \frac{\partial F^{\mathrm{b}}}{\partial Y^{\mathrm{b}}_{ij}} = \dot{\lambda}^{\mathrm{b}} \frac{A_{ijkl} Y^{\mathrm{b}}_{kl}}{\sqrt{\frac{1}{2} Y^{\mathrm{b}}_{pq} A_{pqsr} Y^{\mathrm{b}}_{sr}}} \tag{3.75}$$

$$\dot{r}^{\mathrm{b}} = -\dot{\lambda}^{\mathrm{b}} \frac{\partial F^{\mathrm{b}}}{\partial R^{\mathrm{b}}} = \dot{\lambda}^{\mathrm{b}} \left(1 - \frac{b^{\mathrm{b}}}{Q^{\mathrm{b}0}} R^{\mathrm{b}} \right) = \dot{\lambda}^{\mathrm{b}} \left(1 - b^{\mathrm{b}} r^{\mathrm{b}} \right) \tag{3.76}$$

For the phase transformation, the following kinetic equation is obtained:

$$\dot{\xi} = \dot{\lambda}^{\mathrm{p}} \frac{\partial F^{\mathrm{tr}}}{\partial Y^{\mathrm{CH}}} = \dot{\lambda}^{\mathrm{p}} (\xi_{\max} - \xi) \frac{m_\xi D_\xi}{(1 - D_{eq})} (D_\xi p)^{m_\xi - 1} \tag{3.77}$$

In the case of the absence of damage, the above formula is similar to the one proposed by Santacreu et al. (2006).

The constitutive model is completed with the following loading/unloading conditions:

$$\dot{\lambda}^{\mathrm{p}} \geqslant 0; \quad \hat{\tilde{f}}^{\mathrm{p}} \leqslant 0; \quad \dot{\lambda}^{\mathrm{p}} \hat{\tilde{f}}^{\mathrm{p}} = 0 \tag{3.78}$$

$$\dot{\lambda}^{\mathrm{b}} \geqslant 0; \quad f^{\mathrm{b}} \leqslant 0; \quad \dot{\lambda}^{\mathrm{b}} f^{\mathrm{b}} = 0 \tag{3.79}$$

The yield criterion (Eq. 3.62) is a function of the effective Cauchy stress, the backstress, the isotropic hardening, the damage tensor and the scalar magnitude of martensite content, and since (at plastic state, $\hat{\tilde{f}} = 0$) complementary conditions (Eq. 3.78) imply $\dot{\hat{\tilde{f}}} = 0$, thus the consistency condition can be expressed as follows:

$$\dot{\hat{\tilde{f}}}^{\mathrm{p}} = \frac{\partial \hat{\tilde{f}}^{\mathrm{p}}}{\partial \sigma_{ij}} \dot{\sigma}_{ij} + \frac{\partial \hat{\tilde{f}}^{\mathrm{p}}}{\partial X^{\mathrm{p}}_{ij}} \dot{X}^{\mathrm{p}}_{ij} + \frac{\partial \hat{\tilde{f}}^{\mathrm{p}}}{\partial R^{\mathrm{p}}} \dot{R}^{\mathrm{p}} + \frac{\partial \hat{\tilde{f}}^{\mathrm{p}}}{\partial D_{ij}} \dot{D}_{ij} + \frac{\partial \hat{\tilde{f}}^{\mathrm{p}}}{\partial \xi} \dot{\xi} = 0 \tag{3.80}$$

The conjugated forces X^{p}_{ij} and R^{p} are functions of the internal state variables α^{p}_{ij} and r^{p} (Eqs. 3.48, 3.49), hence the consistency condition can be rewritten in terms of the flux variables as follows:

$$\dot{\hat{\tilde{f}}}^{\mathrm{p}} = \frac{\partial \hat{\tilde{f}}^{\mathrm{p}}}{\partial \sigma_{ij}} \dot{\sigma}_{ij} + \frac{\partial \hat{\tilde{f}}^{\mathrm{p}}}{\partial X^{\mathrm{p}}_{kl}} \frac{\partial X^{p}_{kl}}{\alpha^{\mathrm{p}}_{ij}} \dot{\alpha}^{\mathrm{p}}_{ij} + \frac{\partial \hat{\tilde{f}}^{\mathrm{p}}}{\partial R^{\mathrm{p}}} \frac{\partial R^{\mathrm{p}}}{\partial r^{\mathrm{p}}} \dot{r}^{\mathrm{p}} + \frac{\partial \hat{\tilde{f}}^{\mathrm{p}}}{\partial D_{ij}} \dot{D}_{ij} + \frac{\partial \hat{\tilde{f}}^{\mathrm{p}}}{\partial \xi} \dot{\xi} = 0 \tag{3.81}$$

The use of the simplified rate form of the mixture rule (Eq. 3.8) and the definitions of the internal variable evolution equations (Eqs. 3.72, 3.73, 3.74, 3.75 and 3.77) results in the following relation

$$\begin{aligned} \dot{\hat{\tilde{f}}}^{\mathrm{p}} = \frac{\partial \hat{\tilde{f}}^{\mathrm{p}}}{\partial \sigma_{ij}} \dot{\sigma}_{ij} - \dot{\lambda}^{\mathrm{p}} \frac{\partial \hat{\tilde{f}}^{\mathrm{p}}}{\partial X^{\mathrm{p}}_{kl}} \frac{\partial X^{\mathrm{p}}_{kl}}{\alpha^{\mathrm{p}}_{ij}} \frac{\partial \hat{\tilde{F}}^{\mathrm{p}}}{\partial X^{\mathrm{p}}_{ij}} - \dot{\lambda}^{\mathrm{p}} \frac{\partial \hat{\tilde{f}}^{\mathrm{p}}}{\partial R^{\mathrm{p}}} \frac{\partial R^{\mathrm{p}}}{\partial r^{\mathrm{p}}} \frac{\partial \hat{\tilde{F}}^{\mathrm{p}}}{\partial R^{\mathrm{p}}} \\ + \dot{\lambda}^{\mathrm{p}} (1 - \xi) \frac{\partial \hat{\tilde{f}}^{\mathrm{p}}}{\partial D_{ij}} \frac{\partial F^{\mathrm{d}}}{\partial Y^{\mathrm{d}}_{ij}} + \dot{\lambda}^{\mathrm{b}} \xi \frac{\partial \hat{\tilde{f}}^{\mathrm{p}}}{\partial D_{ij}} \frac{\partial F^{\mathrm{b}}}{\partial Y^{\mathrm{b}}_{ij}} + \dot{\lambda}^{\mathrm{p}} \frac{\partial \hat{\tilde{f}}^{\mathrm{p}}}{\partial \xi} \frac{\partial F^{\mathrm{tr}}}{\partial Y^{\mathrm{CH}}} = 0 \end{aligned} \tag{3.82}$$

Thus the consistency condition can be written in the following simple form

$$\dot{\lambda}^{\mathrm{p}} H^{\mathrm{pp}} - \dot{\lambda}^{\mathrm{b}} H^{\mathrm{pd}} = Z^{\mathrm{p}} \tag{3.83}$$

where the following definitions were used

$$Z^{\mathrm{p}} = \frac{\partial \hat{\tilde{f}}^{\mathrm{p}}}{\partial \sigma_{ij}} \dot{\sigma}_{ij} \tag{3.84}$$

$$H^{\mathrm{pp}} = \frac{\partial \hat{\tilde{f}}^{\mathrm{p}}}{\partial X^{\mathrm{p}}_{kl}} \frac{\partial X^{\mathrm{p}}_{kl}}{\alpha^{\mathrm{p}}_{ij}} \frac{\partial \hat{\tilde{F}}^{\mathrm{p}}}{\partial X^{\mathrm{p}}_{ij}} + \frac{\partial \hat{\tilde{f}}^{\mathrm{p}}}{\partial R^{\mathrm{p}}} \frac{\partial R^{\mathrm{p}}}{\partial r^{\mathrm{p}}} \frac{\partial \hat{\tilde{F}}^{\mathrm{p}}}{\partial R^{\mathrm{p}}} - (1-\xi) \frac{\partial \hat{\tilde{f}}^{\mathrm{p}}}{\partial D_{ij}} \frac{\partial F^{\mathrm{d}}}{\partial Y^{\mathrm{d}}_{ij}} - \frac{\partial \hat{\tilde{f}}^{\mathrm{p}}}{\partial \xi} \frac{\partial F^{\mathrm{tr}}}{\partial Y^{\mathrm{CH}}} \tag{3.85}$$

$$H^{\mathrm{pd}} = \xi \frac{\partial \hat{\tilde{f}}^{\mathrm{p}}}{\partial D_{ij}} \frac{\partial F^{\mathrm{b}}}{\partial Y^{\mathrm{b}}_{ij}} \tag{3.86}$$

On the other hand, the consistency condition for the brittle damage criterion implies:

$$\dot{f}^{\mathrm{b}} = \frac{\partial f^{\mathrm{b}}}{\partial Y^{\mathrm{b}}_{ij}} \dot{Y}^{\mathrm{b}}_{ij} + \frac{\partial f^{\mathrm{b}}}{\partial R^{\mathrm{b}}} \dot{R}^{\mathrm{b}} = 0 \tag{3.87}$$

The use of the definition of the thermodynamic force, R^{b} (Eq. 3.50) gives

$$\dot{f}^{\mathrm{b}} = \frac{\partial f^{\mathrm{b}}}{\partial Y^{\mathrm{b}}_{ij}} \dot{Y}^{\mathrm{b}}_{ij} + \frac{\partial f^{\mathrm{b}}}{\partial R^{\mathrm{b}}} \frac{\partial R^{\mathrm{b}}}{\partial r^{\mathrm{b}}} \dot{r}^{\mathrm{b}} = 0 \tag{3.88}$$

However, based on Eq. (3.60), the above condition can be rewritten as follows:

$$\dot{f}^{\mathrm{b}} = \frac{\partial f^{\mathrm{b}}}{\partial \sigma_{ij}} \dot{\sigma}_{ij} + \frac{\partial f^{\mathrm{b}}}{\partial R^{\mathrm{b}}} \frac{\partial R^{\mathrm{b}}}{\partial r^{\mathrm{b}}} \dot{r}^{\mathrm{b}} + \frac{\partial f^{\mathrm{b}}}{\partial D_{ij}} \dot{D}_{ij} + \frac{\partial f^{\mathrm{b}}}{\partial \xi} \dot{\xi} \tag{3.89}$$

Again, substituting the definitions of the internal variable evolution equations (Eq. 3.76, 3.74, 3.75 and 3.77) results in

$$\begin{aligned} \dot{f}^{\mathrm{b}} = \frac{\partial f^{\mathrm{b}}}{\partial \sigma_{ij}} \dot{\sigma}_{ij} - \dot{\lambda}^{\mathrm{b}} \frac{\partial f^{\mathrm{b}}}{\partial R^{\mathrm{b}}} \frac{\partial R^{\mathrm{b}}}{\partial r^{\mathrm{b}}} \frac{\partial F^{\mathrm{b}}}{\partial R^{\mathrm{b}}} + \dot{\lambda}^{\mathrm{b}} \xi \frac{\partial f^{\mathrm{b}}}{\partial D_{ij}} \frac{\partial F^{\mathrm{b}}}{\partial Y^{\mathrm{b}}_{ij}} \\ + \dot{\lambda}^{\mathrm{p}} (1-\xi) \frac{\partial f^{\mathrm{b}}}{\partial D_{ij}} \frac{\partial F^{\mathrm{d}}}{\partial Y^{\mathrm{d}}_{ij}} + \dot{\lambda}^{\mathrm{p}} \frac{\partial f^{\mathrm{b}}}{\partial \xi} \frac{\partial F^{\mathrm{tr}}}{\partial Y^{\mathrm{CH}}} \end{aligned} \tag{3.90}$$

The above equation can be written in the following simple form

$$-\dot{\lambda}^{\mathrm{p}} H^{\mathrm{dp}} + \dot{\lambda}^{\mathrm{b}} H^{\mathrm{dd}} = Z^{\mathrm{d}} \tag{3.91}$$

where the following definitions were used

$$Z^{\mathrm{d}} = \frac{\partial f^{\mathrm{b}}}{\partial \sigma_{ij}} \dot{\sigma}_{ij} \tag{3.92}$$

$$H^{\mathrm{dd}} = \frac{\partial f^{\mathrm{b}}}{\partial R^{\mathrm{b}}} \frac{\partial R^{\mathrm{b}}}{\partial r^{\mathrm{b}}} \frac{\partial F^{\mathrm{b}}}{\partial R^{\mathrm{b}}} - \xi \frac{\partial f^{\mathrm{b}}}{\partial D_{ij}} \frac{\partial F^{\mathrm{b}}}{\partial Y^{\mathrm{b}}_{ij}} \tag{3.93}$$

$$H^{\mathrm{dp}} = (1-\xi) \frac{\partial f^{\mathrm{b}}}{\partial D_{ij}} \frac{\partial F^{\mathrm{d}}}{\partial Y^{\mathrm{d}}_{ij}} + \frac{\partial f^{\mathrm{b}}}{\partial \xi} \frac{\partial F^{\mathrm{tr}}}{\partial Y^{\mathrm{CH}}} \tag{3.94}$$

On the basis of the equations (3.83) and (3.91), we have

$$\begin{aligned} \dot{\lambda}^{\mathrm{p}} H^{\mathrm{pp}} - \dot{\lambda}^{\mathrm{b}} H^{\mathrm{pd}} &= Z^{\mathrm{p}} \\ -\dot{\lambda}^{\mathrm{p}} H^{\mathrm{dp}} + \dot{\lambda}^{\mathrm{b}} H^{\mathrm{dd}} &= Z^{\mathrm{d}} \end{aligned} \tag{3.95}$$

Thus the plastic and damage multipliers can be solved from the linear system of equations given such that

$$\begin{Bmatrix} \dot{\lambda}^{\mathrm{p}} \\ \dot{\lambda}^{\mathrm{b}} \end{Bmatrix} = \frac{1}{H} \begin{Bmatrix} H^{\mathrm{dd}} & H^{\mathrm{pd}} \\ H^{\mathrm{dp}} & H^{\mathrm{pp}} \end{Bmatrix} \begin{Bmatrix} Z^{\mathrm{p}} \\ Z^{\mathrm{d}} \end{Bmatrix} \tag{3.96}$$

where

$$H = H^{\mathrm{pp}} H^{\mathrm{dd}} - H^{\mathrm{pd}} H^{\mathrm{dp}} \tag{3.97}$$

Using this solution, the plastic and damage multipliers can be written in terms of the incremental stress as follows

$$\begin{aligned} \dot{\lambda}^{\mathrm{p}} &= \frac{1}{H} \left(H^{\mathrm{dd}} \frac{\partial \hat{\tilde{f}}^{\mathrm{p}}}{\partial \sigma_{ij}} + H^{\mathrm{pd}} \frac{\partial f^{\mathrm{b}}}{\partial \sigma_{ij}} \right) \dot{\sigma}_{ij} \\ \dot{\lambda}^{\mathrm{b}} &= \frac{1}{H} \left(H^{\mathrm{dp}} \frac{\partial \hat{\tilde{f}}^{\mathrm{p}}}{\partial \sigma_{ij}} + H^{\mathrm{pp}} \frac{\partial f^{\mathrm{bd}}}{\partial \sigma_{ij}} \right) \dot{\sigma}_{ij} \end{aligned} \tag{3.98}$$

In order to obtain equations of the plastic and damage multipliers in terms of the incremental strain, the incremental form of Eq. (3.42) must be inserted in Eq. (3.82) and Eq. (3.90), then one can obtain

$$\dot{\lambda}^{\mathrm{p}} h^{\mathrm{pp}} - \dot{\lambda}^{\mathrm{b}} h^{\mathrm{pd}} = z^{\mathrm{p}} \tag{3.99}$$

where

$$h^{\mathrm{pp}} = H^{\mathrm{pp}} + \frac{\partial \hat{\tilde{f}}^{\mathrm{p}}}{\partial \sigma_{ij}} \tilde{E}_{ijkl}(\mathbf{D}) \left(\frac{\partial \hat{\tilde{f}}^{\mathrm{p}}}{\partial \sigma_{kl}} + \frac{\partial F^{\mathrm{d}}}{\partial \sigma_{kl}} + A \left(\frac{\partial \hat{\tilde{f}}^{\mathrm{p}}}{\partial \sigma_{kl}} + \frac{1}{3} \Delta \upsilon \delta_{kl} \right) \frac{\partial F^{\mathrm{tr}}}{\partial Y^{\mathrm{CH}}} \right) - (1-\xi) \frac{\partial \hat{\tilde{f}}^{\mathrm{p}}}{\partial \sigma_{ij}} \frac{\partial \tilde{E}_{ijkl}(\mathbf{D})}{\partial D_{mn}} \left(\varepsilon_{kl} - \varepsilon^{\mathrm{I}}_{kl} \right) \frac{\partial F^{\mathrm{d}}}{\partial Y^{\mathrm{d}}_{mn}} \tag{3.100}$$

$$h^{\mathrm{pd}} = H^{\mathrm{pd}} - \frac{\partial \hat{\tilde{f}}^{\mathrm{p}}}{\partial \sigma_{ij}} \tilde{E}_{ijkl}(\mathbf{D}) \frac{\partial F^{\mathrm{b}}}{\partial \sigma_{kl}} + \xi \frac{\partial \hat{\tilde{f}}^{\mathrm{p}}}{\partial \sigma_{ij}} \frac{\partial \tilde{E}_{ijkl}(\mathbf{D})}{\partial D_{mn}} \left(\varepsilon_{kl} - \varepsilon^{\mathrm{I}}_{kl} \right) \frac{\partial F^{\mathrm{b}}}{\partial Y^{\mathrm{b}}_{mn}} \tag{3.101}$$

$$z^{\mathrm{p}} = \frac{\partial \hat{\tilde{f}}^{\mathrm{p}}}{\partial \sigma_{ij}} \tilde{E}_{ijkl}(\mathbf{D}) \dot{\varepsilon}_{kl} \tag{3.102}$$

and

$$-\dot{\lambda}^{\mathrm{p}} h^{\mathrm{dp}} + \dot{\lambda}^{\mathrm{bd}} h^{\mathrm{dd}} = z^{\mathrm{d}} \tag{3.103}$$

where

$$h^{\mathrm{dd}} = H^{\mathrm{dd}} + \frac{\partial f^{\mathrm{b}}}{\partial \sigma_{ij}} \tilde{E}_{ijkl}(\mathbf{D}) \frac{\partial F^{\mathrm{b}}}{\partial \sigma_{kl}} - \xi \frac{\partial f^{\mathrm{b}}}{\partial \sigma_{ij}} \frac{\partial \tilde{E}_{ijkl}(\mathbf{D})}{\partial D_{mn}} \left(\varepsilon_{kl} - \varepsilon^{\mathrm{I}}_{kl} \right) \frac{\partial F^{\mathrm{b}}}{\partial Y^{\mathrm{b}}_{mn}} \tag{3.104}$$

$$h^{\mathrm{dp}} = H^{\mathrm{dp}} - \frac{\partial f^{\mathrm{b}}}{\partial \sigma_{ij}} \tilde{E}_{ijkl}(\mathbf{D}) \left(\frac{\partial \hat{\tilde{f}}^{\mathrm{p}}}{\partial \sigma_{kl}} + \frac{\partial F^{\mathrm{d}}}{\partial \sigma_{kl}} + A \left(\frac{\partial \hat{\tilde{f}}^{\mathrm{p}}}{\partial \sigma_{kl}} + \frac{1}{3} \Delta \upsilon \delta_{kl} \right) \frac{\partial F^{\mathrm{tr}}}{\partial Y^{\mathrm{CH}}} \right) + (1-\xi) \frac{\partial f^{\mathrm{b}}}{\partial \sigma_{ij}} \frac{\partial \tilde{E}_{ijkl}(\mathbf{D})}{\partial D_{mn}} \left(\varepsilon_{kl} - \varepsilon^{\mathrm{I}}_{kl} \right) \frac{\partial F^{\mathrm{d}}}{\partial Y^{\mathrm{d}}_{mn}} \tag{3.105}$$

$$z^{\mathrm{d}} = \frac{\partial f^{\mathrm{b}}}{\partial \sigma_{ij}} \tilde{E}_{ijkl}(\mathbf{D}) \dot{\varepsilon}_{kl} \tag{3.106}$$

Thus, the plastic and damage multipliers can be obtained by solving the linear system of equations given by Eq. (3.99) and Eq. (3.103)

$$\begin{Bmatrix} \dot{\lambda}^{\mathrm{p}} \\ \dot{\lambda}^{\mathrm{b}} \end{Bmatrix} = \frac{1}{h} \begin{Bmatrix} h^{\mathrm{dd}} & h^{\mathrm{pd}} \\ h^{\mathrm{dp}} & h^{\mathrm{pp}} \end{Bmatrix} \begin{Bmatrix} z^{\mathrm{p}} \\ z^{\mathrm{d}} \end{Bmatrix} \tag{3.107}$$

where

$$h = h^{\mathrm{pp}} h^{\mathrm{dd}} - h^{\mathrm{pd}} h^{\mathrm{dp}} \tag{3.108}$$

thus

$$\begin{aligned}\dot{\lambda}^{\mathrm{p}} &= \frac{1}{h}\left(h^{\mathrm{dd}}\frac{\partial\hat{\tilde{f}}^{\mathrm{p}}}{\partial\sigma_{ij}} + h^{\mathrm{pd}}\frac{\partial f^{\mathrm{b}}}{\partial\sigma_{ij}}\right)\tilde{E}_{ijkl}\left(\mathbf{D}\right)\dot{\varepsilon}_{kl} \\ \dot{\lambda}^{\mathrm{b}} &= \frac{1}{h}\left(h^{\mathrm{dp}}\frac{\partial\hat{\tilde{f}}^{\mathrm{p}}}{\partial\sigma_{ij}} + h^{\mathrm{pp}}\frac{\partial f^{\mathrm{b}}}{\partial\sigma_{ij}}\right)\tilde{E}_{ijkl}\left(\mathbf{D}\right)\dot{\varepsilon}_{kl}\end{aligned} \tag{3.109}$$

3.7 Elastic-plastic-damage tangent modulus

On the basis of the rate form of the classical Hookean constitutive equation,

$$\dot{\boldsymbol{\sigma}} = \tilde{\mathbf{E}}\left(\mathbf{D}\right) : \left(\dot{\boldsymbol{\varepsilon}} - \dot{\boldsymbol{\varepsilon}}^{\mathrm{I}}\right) + \frac{\partial\tilde{\mathbf{E}}\left(\mathbf{D}\right)}{\partial\mathbf{D}} : \left(\boldsymbol{\varepsilon} - \boldsymbol{\varepsilon}^{\mathrm{I}}\right) : \dot{\mathbf{D}} \tag{3.110}$$

one can derive the tangent modulus of the elastic-plastic-damage and a partially transformed material. At first, the relation between the incremental stress and the incremental total damage measure must be find. This can be realized by substituting Eq. (3.98) into the following rate form of the mixture rule (Eq. 3.8), used in calculations

$$\dot{\mathbf{D}} = (1-\xi)\dot{\mathbf{D}}^{\mathrm{d}} + \xi\dot{\mathbf{D}}^{\mathrm{b}} = \left\langle\dot{\mathbf{D}}\right\rangle_{\mathrm{RVE}}^{\mathrm{d}} + \left\langle\dot{\mathbf{D}}\right\rangle_{\mathrm{RVE}}^{\mathrm{b}} = \dot{\lambda}^{\mathrm{p}}(1-\xi)\frac{\partial F^{\mathrm{d}}}{\partial\mathbf{Y}^{\mathrm{d}}} + \dot{\lambda}^{\mathrm{b}}\xi\frac{\partial F^{\mathrm{b}}}{\partial\mathbf{Y}^{\mathrm{b}}} \tag{3.111}$$

Thus, the relation can be written in the following general form

$$\dot{\mathbf{D}} = \mathbf{P} : \dot{\boldsymbol{\sigma}} \tag{3.112}$$

where $\mathbf{P}$ is a fourth order tensor defined as

$$\mathbf{P} = \frac{1}{H}\left[(1-\xi)\,\frac{\partial F^{\mathrm{d}}}{\partial\mathbf{Y}^{\mathrm{d}}} \otimes \left(H^{\mathrm{dd}}\frac{\partial\hat{\tilde{f}}^{\mathrm{p}}}{\partial\boldsymbol{\sigma}} + H^{\mathrm{pd}}\frac{\partial f^{\mathrm{b}}}{\partial\boldsymbol{\sigma}}\right) + \xi\frac{\partial F^{\mathrm{b}}}{\partial\mathbf{Y}^{\mathrm{b}}} \otimes \left(H^{\mathrm{dp}}\frac{\partial\hat{\tilde{f}}^{\mathrm{p}}}{\partial\boldsymbol{\sigma}} + H^{\mathrm{pp}}\frac{\partial f^{\mathrm{b}}}{\partial\boldsymbol{\sigma}}\right)\right] \tag{3.113}$$

Now, the substitution of the above relation into Eq. (3.110) results in the following general equation

$$\dot{\boldsymbol{\sigma}} = \mathbf{D}^{\mathrm{e}} : \dot{\boldsymbol{\varepsilon}}^{\mathrm{E}} = \mathbf{D}^{\mathrm{e}} : (\dot{\boldsymbol{\varepsilon}} - \dot{\boldsymbol{\varepsilon}}^{\mathrm{I}}) \tag{3.114}$$

where $\mathbf{D}^{\mathrm{e}}$ is the elastic tangent modulus, and it is expressed in the following way:

$$(\mathbf{D}^{\mathrm{e}})^{-1} = \begin{cases} \tilde{\mathbf{E}}^{-1} & if \quad \dot{\lambda}^{\mathrm{p}} = 0; \dot{\lambda}^{\mathrm{b}} = 0 \\ \tilde{\mathbf{E}}^{-1}(\mathbf{D}) - \frac{(1-\xi)}{H^{\mathrm{pp}}} \tilde{\mathbf{E}}^{-1}(\mathbf{D}) : \frac{\partial \tilde{\mathbf{E}}(\mathbf{D})}{\partial \mathbf{D}} : \boldsymbol{\varepsilon}^{\mathrm{E}} : \frac{\partial F^{\mathrm{d}}}{\partial \mathbf{Y}^{\mathrm{d}}} \otimes \frac{\partial \hat{\tilde{f}}^{\mathrm{p}}}{\partial \boldsymbol{\sigma}} & if \quad \dot{\lambda}^{\mathrm{p}} > 0; \dot{\lambda}^{\mathrm{b}} = 0 \\ \tilde{\mathbf{E}}^{-1}(\mathbf{D}) - \frac{\xi}{H^{\mathrm{dd}}} \tilde{\mathbf{E}}^{-1}(\mathbf{D}) : \frac{\partial \tilde{\mathbf{E}}(\mathbf{D})}{\partial \mathbf{D}} : \boldsymbol{\varepsilon}^{\mathrm{E}} : \frac{\partial F^{\mathrm{b}}}{\partial \mathbf{Y}^{\mathrm{b}}} \otimes \frac{\partial f^{\mathrm{b}}}{\partial \boldsymbol{\sigma}} & if \quad \dot{\lambda}^{\mathrm{p}} = 0; \dot{\lambda}^{\mathrm{b}} > 0 \\ \tilde{\mathbf{E}}^{-1}(\mathbf{D}) - \tilde{\mathbf{E}}^{-1}(\mathbf{D}) : \frac{\partial \tilde{\mathbf{E}}(\mathbf{D})}{\partial \mathbf{D}} : \boldsymbol{\varepsilon}^{\mathrm{E}} : \mathbf{P} & if \quad \dot{\lambda}^{\mathrm{p}} > 0; \dot{\lambda}^{\mathrm{b}} > 0 \end{cases} \tag{3.115}$$

On the other hand, te use of Eqs. (3.66-3.70) together with Eq. (3.98) in (3.114) results in the following general constitutive equation which relates the incremental stress and the total incremental strain

$$\dot{\boldsymbol{\sigma}} = \mathbf{D}^{\mathrm{epd}} : \dot{\boldsymbol{\varepsilon}} \tag{3.116}$$

where the tangent modulus, $\mathbf{D}^{\mathrm{epd}}$ of the elastic-plastic-damage and phase transformed material is as follows

$$\left(\mathbf{D}^{\mathrm{epd}}\right)^{-1} = \begin{cases} (\mathbf{D}^{\mathrm{e}})^{-1} & if \quad \dot{\lambda}^{\mathrm{p}} = 0; \dot{\lambda}^{\mathrm{b}} = 0 \\ (\mathbf{D}^{\mathrm{e}})^{-1} + \frac{1}{H^{\mathrm{pp}}} \left(\frac{\partial \hat{\tilde{F}}^{\mathrm{p}}}{\partial \boldsymbol{\sigma}} \otimes \frac{\partial \hat{\tilde{f}}^{\mathrm{p}}}{\partial \boldsymbol{\sigma}} + \frac{\partial F^{\mathrm{d}}}{\partial \boldsymbol{\sigma}} \otimes \frac{\partial \hat{\tilde{f}}^{\mathrm{p}}}{\partial \boldsymbol{\sigma}} + \mathbf{A}^{\mathrm{tr}} \otimes \frac{\partial \hat{\tilde{f}}^{\mathrm{p}}}{\partial \boldsymbol{\sigma}} \right) & if \quad \dot{\lambda}^{\mathrm{p}} > 0; \dot{\lambda}^{\mathrm{b}} = 0 \\ (\mathbf{D}^{\mathrm{e}})^{-1} + \frac{1}{H^{\mathrm{dd}}} \frac{\partial F^{\mathrm{b}}}{\partial \boldsymbol{\sigma}} \otimes \frac{\partial f^{\mathrm{b}}}{\partial \boldsymbol{\sigma}} & if \quad \dot{\lambda}^{\mathrm{p}} = 0; \dot{\lambda}^{\mathrm{b}} > 0 \\ (\mathbf{D}^{\mathrm{e}})^{-1} + \frac{1}{H} \left(\begin{array}{l} \frac{\partial \hat{\tilde{F}}^{\mathrm{p}}}{\partial \boldsymbol{\sigma}} \otimes \left(H^{\mathrm{dd}} \frac{\partial \hat{\tilde{f}}^{\mathrm{p}}}{\partial \boldsymbol{\sigma}} + H^{\mathrm{pd}} \frac{\partial f^{\mathrm{b}}}{\partial \boldsymbol{\sigma}} \right) \\ + \frac{\partial F^{\mathrm{d}}}{\partial \boldsymbol{\sigma}} \otimes \left(H^{\mathrm{dd}} \frac{\partial \hat{\tilde{f}}^{\mathrm{p}}}{\partial \boldsymbol{\sigma}} + H^{\mathrm{pd}} \frac{\partial f^{\mathrm{b}}}{\partial \boldsymbol{\sigma}} \right) \\ + \mathbf{A}^{\mathrm{tr}} \otimes \left(H^{\mathrm{dd}} \frac{\partial \hat{\tilde{f}}^{\mathrm{p}}}{\partial \boldsymbol{\sigma}} + H^{\mathrm{pd}} \frac{\partial f^{\mathrm{b}}}{\partial \boldsymbol{\sigma}} \right) \\ + \frac{\partial F^{\mathrm{b}}}{\partial \boldsymbol{\sigma}} \otimes \left(H^{\mathrm{dp}} \frac{\partial \hat{\tilde{f}}^{\mathrm{p}}}{\partial \boldsymbol{\sigma}} + H^{\mathrm{pp}} \frac{\partial f^{\mathrm{b}}}{\partial \boldsymbol{\sigma}} \right) \end{array} \right) & if \quad \dot{\lambda}^{\mathrm{p}} > 0; \dot{\lambda}^{\mathrm{b}} > 0 \end{cases} \tag{3.117}$$

and the following substitiusion has been used

$$\mathbf{A}^{\mathrm{tr}} = A \frac{\partial F^{\mathrm{tr}}}{\partial Y^{\mathrm{CH}}} \left(\frac{\partial \hat{\tilde{f}}^{\mathrm{p}}}{\partial \boldsymbol{\sigma}} + \frac{1}{3} \Delta \upsilon \mathbf{1} \right) \tag{3.118}$$

Chapter 4

Numerical approach – a fully implicit backward Euler scheme

The current constitutive formulation involves two convex and smooth yield surfaces (plastic and brittle damage) which intersect non-smoothly, which results in the presence of singular points in the boundary of the convex elastic domain. Basically, standard algorithms (e.g. return mapping algorithms) may be used to cope with such problems, however special attention must be paid to loading/unloading conditions for algorithmic implementation (cf. e.g. Simo and Hughes (1998); Brepols et al. (2017)). In general, even if loading conditions are fulfilled for both surfaces, it does not necessarily mean that both plastic and brittle damage processes are ultimately active. Recently, in a similar problem of two (plastic and damage) surfaces, The Closest Point Projection (CPP) algorithm was used in Voyiadjis and Dorgan (2007), and Ryś and Skoczeń (2017). In the present work, two return mapping algorithms will be presented. In the first algorithm, the Newton-Raphson scheme is used to solve a set of (rate-independent) nonlinear algebraic equations, while in the second algorithm a rate-dependent formulation is adopted as the regularization of the rate-independent model.

The constitutive model of the rate independent elastic-plastic-damage and partially transformed continuum, under the assumption of small strains, is defined by the following

set of evolution equations (cf. Eqs. 3.66, 3.72, 3.73, 3.74, 3.75, 3.76, 3.77)

$$\dot{\boldsymbol{\varepsilon}}^{\mathrm{I}} = \dot{\lambda}^{\mathrm{p}} \frac{\partial \hat{\tilde{F}}^{\mathrm{p}}}{\partial \boldsymbol{\sigma}} + \dot{\lambda}^{\mathrm{p}} \frac{\partial F^{\mathrm{d}}}{\partial \boldsymbol{\sigma}} + \dot{\lambda}^{\mathrm{b}} \frac{\partial F^{\mathrm{b}}}{\partial \boldsymbol{\sigma}} + \dot{\lambda}^{\mathrm{p}} \frac{\partial F^{\mathrm{tr}}}{\partial Y^{\mathrm{CH}}} \left(\frac{\partial \hat{\tilde{f}}^{\mathrm{p}}}{\partial \boldsymbol{\sigma}} + \frac{1}{3} \Delta v \mathbf{1} \right) A \tag{4.1}$$

$$\dot{\boldsymbol{\alpha}}^{\mathrm{p}} = -\dot{\lambda}^{\mathrm{p}} \frac{\partial \hat{\tilde{F}}^{\mathrm{p}}}{\partial \mathbf{X}^{\mathrm{p}}} \tag{4.2}$$

$$\dot{r}^{\mathrm{p}} = -\dot{\lambda}^{\mathrm{p}} \frac{\partial \hat{\tilde{F}}^{\mathrm{p}}}{\partial R^{\mathrm{p}}} \tag{4.3}$$

$$\dot{\mathbf{D}} = (1-\xi)\, \dot{\mathbf{D}}^{\mathrm{d}} + \xi \dot{\mathbf{D}}^{\mathrm{b}}, \quad \text{with} \quad \dot{\mathbf{D}}^{\mathrm{d}} = \dot{\lambda}^{\mathrm{p}} \frac{\partial F^{\mathrm{d}}}{\partial \mathbf{Y}^{\mathrm{d}}} \text{ and } \dot{\mathbf{D}}^{\mathrm{b}} = \dot{\lambda}^{\mathrm{b}} \frac{\partial F^{\mathrm{b}}}{\partial \mathbf{Y}^{\mathrm{b}}} \tag{4.4}$$

$$\dot{r}^{\mathrm{b}} = -\dot{\lambda}^{\mathrm{b}} \frac{\partial F^{\mathrm{b}}}{\partial R^{b}} \tag{4.5}$$

$$\dot{\xi} = \dot{\lambda}^{\mathrm{p}} \frac{\partial F^{\mathrm{tr}}}{\partial Y^{\mathrm{CH}}} \tag{4.6}$$

The above equations have to be solved together with the state laws,

$$\boldsymbol{\sigma} = \tilde{\mathbf{E}}\,(\mathbf{D}) : \boldsymbol{\varepsilon}^{\mathrm{E}} \tag{4.7}$$

$$\mathbf{X}^{\mathrm{p}} = \hat{\tilde{\mathbf{C}}}(\mathbf{D}, \xi) : \boldsymbol{\alpha}^{\mathrm{p}} \tag{4.8}$$

$$R^{\mathrm{p}} = \hat{\tilde{Q}}(\mathbf{D}, \xi) r^{\mathrm{p}} \tag{4.9}$$

$$R^{\mathrm{b}} = Q^{\mathrm{b}0} r^{\mathrm{b}} \tag{4.10}$$

$$-\mathbf{Y} = \underbrace{\frac{1}{2} \boldsymbol{\varepsilon}^{\mathrm{E}} : \frac{\partial \tilde{\mathbf{E}}(\mathbf{D})}{\partial \mathbf{D}} : \boldsymbol{\varepsilon}^{\mathrm{E}}}_{\mathbf{Y}^{\mathrm{e}}} + \underbrace{\frac{1}{2} \boldsymbol{\alpha}^{\mathrm{p}} : \frac{\partial \hat{\tilde{\mathbf{C}}}(\mathbf{D}, \xi)}{\partial \mathbf{D}} : \boldsymbol{\alpha}^{\mathrm{p}} + \frac{1}{2} \frac{\partial \hat{\tilde{Q}}^{\mathrm{p}}(\mathbf{D}, \xi)}{\partial \mathbf{D}} (r^{\mathrm{p}})^2}_{\mathbf{Y}^{\mathrm{p}}} \tag{4.11}$$

such that the yield criterion as well as the damage criterion have to be fulfilled:

$$\hat{\tilde{f}}^{\mathrm{p}} = \sqrt{\frac{3}{2} \left[\mathbf{T}^{-1} : (\boldsymbol{\sigma} - \hat{\mathbf{X}}) \right] : \left[\mathbf{T}^{-1} : (\boldsymbol{\sigma} - \hat{\mathbf{X}}) \right]} - \sigma_{\mathrm{y}}^{0} - \hat{\tilde{R}}^{\mathrm{p}} = 0 \tag{4.12}$$

$$f^{\mathrm{b}} = \sqrt{\frac{1}{2} \mathbf{Y}^{\mathrm{b}} : \mathbf{A} : \mathbf{Y}^{\mathrm{b}}} - l_y - R^{\mathrm{b}} = 0 \tag{4.13}$$

Using of the following time discretization scheme $\Delta(\bullet) = \Delta t(\dot{\bullet})$, where Δt is a time increment, and $\Delta(\bullet) = (\bullet)^{n+1} - (\bullet)^{n}$, employing the fully implicit backward Euler scheme allows to

rewrite differential equations (4.1-4.6) in the following incremental form:

$$\boldsymbol{\varepsilon}_j^{\mathrm{I}} = \boldsymbol{\varepsilon}_0^{\mathrm{I}} + \Delta\boldsymbol{\varepsilon}_j^{\mathrm{I}} \tag{4.14}$$

$$\boldsymbol{\alpha}_j^{\mathrm{p}} = \boldsymbol{\alpha}_0^{\mathrm{p}} + \Delta\boldsymbol{\alpha}_j^{\mathrm{p}} \tag{4.15}$$

$$r_j^{\mathrm{p}} = r_0^{\mathrm{p}} + \Delta r_j^{\mathrm{p}} \tag{4.16}$$

$$\mathbf{D}_j = \mathbf{D}_0 + \Delta\mathbf{D}_j, \quad \text{with} \quad \mathbf{D}_j^{\mathrm{d}} = \mathbf{D}_0^{\mathrm{d}} + \Delta\mathbf{D}_j^{\mathrm{d}} \text{ and } \mathbf{D}_j^{\mathrm{b}} = \mathbf{D}_0^{\mathrm{b}} + \Delta\mathbf{D}_j^{\mathrm{b}} \tag{4.17}$$

$$r_j^{\mathrm{b}} = r_0^{\mathrm{b}} + \Delta r_j^{\mathrm{b}} \tag{4.18}$$

$$\xi_j = \xi_0 + \Delta\xi_j \tag{4.19}$$

The subscripts "j" and "0" indicate the value of a variable at the current iteration and at the previously converged state, respectively, and "Δ" denotes the total increment from previously converged state to the current (unknown) state. The state at the end of the previous time increment "0" is known, which means that it is determined by the known set of values of internal variables $\{\boldsymbol{\varepsilon}_0^{\mathrm{I}}, \boldsymbol{\alpha}_0^{\mathrm{p}}, r_0^{\mathrm{p}}, \mathbf{D}_0^{\mathrm{d}}, \mathbf{D}_0^{\mathrm{b}}, r_0^{\mathrm{b}}, \xi_0\}$, and the following thermodynamic forces $\{\boldsymbol{\sigma}_0, \mathbf{X}_0^{\mathrm{p}}, R_0^{\mathrm{p}}, R_0^{\mathrm{b}}, \mathbf{Y}_0\}$. The total strain, $\boldsymbol{\varepsilon}_j$, at the current time step is also known and defined as follows:

$$\boldsymbol{\varepsilon}_j = \boldsymbol{\varepsilon}_0 + \Delta\boldsymbol{\varepsilon}_j \tag{4.20}$$

where $\Delta\boldsymbol{\varepsilon}_j$ denotes a prescribed value of the strain increment.
State equations (4.7-4.11) at the current time step are defined as follows:

$$\boldsymbol{\sigma}_j = \tilde{\mathbf{E}}_j : \boldsymbol{\varepsilon}_j^{\mathrm{E}} = \tilde{\mathbf{E}}_j : \left(\boldsymbol{\varepsilon}_j - \boldsymbol{\varepsilon}_j^{\mathrm{I}}\right) \tag{4.21}$$

$$\mathbf{X}_j^{\mathrm{p}} = \hat{\tilde{C}}_j^{\mathrm{p}}(\mathbf{D}, \xi) : \boldsymbol{\alpha}_j^{\mathrm{p}} \tag{4.22}$$

$$R_j^{\mathrm{p}} = \hat{\tilde{Q}}_j^{\mathrm{p}}(\mathbf{D}, \xi) r_j^{\mathrm{p}} \tag{4.23}$$

$$R_j^{\mathrm{b}} = Q^{\mathrm{b}0} r_j^{\mathrm{b}} \tag{4.24}$$

$$-\mathbf{Y}_j = \frac{1}{2}\boldsymbol{\sigma}_j : \frac{\partial \tilde{\mathbf{E}}_j^{-1}}{\partial \mathbf{D}_j} : \boldsymbol{\sigma}_j + \frac{1}{2}\boldsymbol{\alpha}_j^{\mathrm{p}} : \frac{\partial \hat{\tilde{\mathbf{C}}}_j(\mathbf{D}, \xi)}{\partial \mathbf{D}_j} : \boldsymbol{\alpha}_j^{\mathrm{p}} + \frac{1}{2}\frac{\partial \hat{\tilde{Q}}_j^{\mathrm{p}}(\mathbf{D}, \xi)}{\partial \mathbf{D}_j}(r_j^{\mathrm{p}})^2 \tag{4.25}$$

The explicit form of discretized Eqs. (4.1-4.6) is as follows [1]

$$\Delta\boldsymbol{\varepsilon}_j^{\mathrm{I}} = \Delta\lambda_j^{\mathrm{p}}\left(\hat{\tilde{f}}_{,\boldsymbol{\sigma}}^{\mathrm{p}} + F_{,\boldsymbol{\sigma}}^{\mathrm{d}} + F_{,Y^{\mathrm{CH}}}^{\mathrm{tr}}\left(\hat{\tilde{f}}_{,\boldsymbol{\sigma}}^{\mathrm{p}} + \frac{1}{3}\Delta\upsilon\mathbf{1}\right)A\right)_j + \Delta\lambda_j^{\mathrm{b}}\left(f_{,\boldsymbol{\sigma}}^{\mathrm{b}}\right)_j \tag{4.26}$$

$$\Delta\boldsymbol{\alpha}_j^{\mathrm{p}} = \frac{3}{2}\frac{\Delta\lambda_j^{\mathrm{p}}}{1+h_X\xi_j}\mathbf{T}_j^{-T}{:}\mathbf{T}_j^{-1}{:}\left[\frac{\left(\boldsymbol{\sigma}_j - \frac{\mathbf{X}_j^{\mathrm{p}}}{1+h_X\xi_j}\right)}{J_2(\tilde{\boldsymbol{\sigma}}_j - \hat{\tilde{\mathbf{X}}}_j^{\mathrm{p}})} - \frac{\gamma}{C^0(1+h_X\xi_j)^3}\mathbf{X}_j^{\mathrm{p}}\right] \tag{4.27}$$

$$\Delta r_j^{\mathrm{p}} = \frac{\Delta\lambda_j^{\mathrm{p}}}{(1-(D_{eq})_j)(1+h_R\xi_j)}\left(1 - \frac{b^{\mathrm{p}}r_j^{\mathrm{p}}}{(1-(D_{eq})_j)(1+h_R\xi_j)}\right) \tag{4.28}$$

$$\Delta r_j^{\mathrm{b}} = \Delta\lambda_j^{\mathrm{b}}\left(1 - b^{\mathrm{b}}r_j^{\mathrm{b}}\right) \tag{4.29}$$

$$\Delta\mathbf{D}_j = \Delta\lambda_j^{\mathrm{p}}\left(1-\xi_j\right)\left(F_{,\mathbf{Y}^{\mathrm{d}}}^{\mathrm{d}}\right)_j + \Delta\lambda_j^{\mathrm{b}}\xi_j\left(F_{,\mathbf{Y}^{\mathrm{b}}}^{\mathrm{b}}\right)_j \tag{4.30}$$

$$\Delta\xi_j = \Delta\lambda_j^{\mathrm{p}}(\xi_{\max} - \xi_j)\frac{m_\xi D_\xi}{(1-(D_{eq})_j)}(D_\xi p_j)^{m_\xi - 1} \tag{4.31}$$

where, $\Delta\lambda_j^{\mathrm{p}} = \lambda_j^{\mathrm{p}} - \lambda_0^{\mathrm{p}}$ and $\Delta\lambda_j^{\mathrm{b}} = \lambda_j^{\mathrm{b}} - \lambda_0^{\mathrm{b}}$.
In order to solve the problem, the elastic-predictor – plastic-corrector procedure is used and the Newton-Raphson scheme is employed in the plastic-corrector part of the algorithm to solve the nonlinear algebraic equations. In the elastic predictor step the trial stress ($\boldsymbol{\sigma}^{\mathrm{trial}}$) and the thermodynamic force conjugated to damage ($\mathbf{Y}^{\mathrm{trial}}$) is computed with the assumption that the applied total strain increment ($\Delta\boldsymbol{\varepsilon}$) is elastic and hence the damage state is frozen

$$\boldsymbol{\sigma}^{\mathrm{trial}} = \tilde{\mathbf{E}}_0 : \left(\boldsymbol{\varepsilon} - \boldsymbol{\varepsilon}_0^{\mathrm{I}}\right) = \boldsymbol{\sigma}_0 + \tilde{\mathbf{E}}_0 : \Delta\boldsymbol{\varepsilon} \qquad -\mathbf{Y}^{\mathrm{trial}} = \frac{1}{2}\boldsymbol{\sigma}^{\mathrm{trial}} : \left(\frac{\partial\tilde{\mathbf{E}}^{-1}}{\partial\mathbf{D}}\right)_0 : \boldsymbol{\sigma}^{\mathrm{trial}} + \mathbf{Y}_0^{\mathrm{p}} \tag{4.32}$$

It should be noted here that the time increment subscript "j" is omitted here. Thus, unless indicated otherwise, all quantities without subscript are actually evaluated at time "j".
During elastic-predictor step, the set of trial dependent state variables, $\{\boldsymbol{\sigma}^{\mathrm{trial}}, \mathbf{X}_0^{\mathrm{p}}, R_0^{\mathrm{p}}, \mathbf{Y}^{\mathrm{trial}}, R_0^{\mathrm{b}}, \mathbf{D}_0, \xi_0\}$, is used to check whether the yield criterion, $\hat{\tilde{f}}^{\mathrm{p,trial}}\left(\boldsymbol{\sigma}^{\mathrm{trial}}, \mathbf{X}_0^{\mathrm{p}}, R_0^{\mathrm{p}}, \mathbf{D}_0, \xi_0\right) \leqslant 0$, and the brittle damage criterion $f^{\mathrm{b,trial}}\left(\mathbf{Y}^{\mathrm{b,trial}}, R_0^{\mathrm{b}}\right) \leqslant 0$, are fulfilled. For the case when the yield and the brittle damage criteria are satisfied, i.e. $f^{\mathrm{p,trial}} \leqslant 0$ and $f^{\mathrm{b,trial}} \leqslant 0$, the current state $\{\boldsymbol{\sigma}, \mathbf{X}^{\mathrm{p}}, R^{\mathrm{p}}, \mathbf{Y}, R^{\mathrm{b}}\}$ is set to the trial state $\{\boldsymbol{\sigma}^{\mathrm{trial}}, \mathbf{X}_0^{\mathrm{p}}, R_0^{\mathrm{p}}, \mathbf{Y}^{\mathrm{trial}}, R_0^{\mathrm{b}}\}$. Similarly, the independent state variables are updated in the following way: $\{\boldsymbol{\varepsilon}^{\mathrm{I}}, \boldsymbol{\alpha}^{\mathrm{p}}, r^{\mathrm{p}}, r^{\mathrm{b}}, \mathbf{D}, \xi\}^T = \{\boldsymbol{\varepsilon}_0^{\mathrm{I}}, \boldsymbol{\alpha}_0^{\mathrm{p}}, r_0^{\mathrm{p}}, r_0^{\mathrm{b}}, \mathbf{D}_0, \xi_0\}^T$. Alternatively, three other situations may take place, i.e.:

1. $\hat{\tilde{f}}^{\mathrm{p,trial}} > 0$ and $f^{\mathrm{b,trial}} < 0$, then the current state resulting from the trial state lies outside the plastic yield surface. Since the plastic flow has occurred, the plastic corrector

[1] for simplicity, the following notation is used e.g. $\left(\hat{\tilde{f}}_{,\boldsymbol{\sigma}}^{\mathrm{p}}\right)_j \equiv \frac{\partial\hat{\tilde{f}}_j^p}{\partial\boldsymbol{\sigma}_j}$

step must be applied in order to return the trial state onto the yield surface (the brittle damage evolution process is not active),

2. $\hat{\tilde{f}}^{\mathrm{p,trial}} < 0$ and $f^{\mathrm{b,trial}} > 0$, thus, only the brittle damage criterion is violated and the brittle damage evolution has occurred, the damage-corrector step must be applied in order to return the trial state onto the brittle damage surface,

3. $\hat{\tilde{f}}^{\mathrm{p,trial}} > 0$ and $f^{\mathrm{b,trial}} > 0$, then the current state lies outside the plastic yield surface as well as the brittle damage surface. Such situation suggests that the plastic flow and the brittle damage evolution have occurred. Hovewer, as was mentioned, in the case of two non-smoothly intersected surfaces, even if loading conditions are fulfilled for both surfaces, this does not necessarily mean that both plastic and damage processes are ultimately active. A possible way to overcome such ambiguity will be presented at the end of the present section.

Equations (4.14-4.19) together with discretized equations (4.26-4.31) can be now written in the residual form as follows:

$$\mathbf{R}^{\varepsilon} = -\boldsymbol{\varepsilon}^{\mathrm{I}} + \boldsymbol{\varepsilon}_0^{\mathrm{I}} + (\lambda^{\mathrm{p}} - \lambda_0^{\mathrm{p}}) \left(\hat{\tilde{f}}^{\mathrm{p}}_{,\boldsymbol{\sigma}} + F^{\mathrm{d}}_{,\boldsymbol{\sigma}} + F^{\mathrm{tr}}_{,Y^{\mathrm{CH}}} \left(\hat{\tilde{f}}^{\mathrm{p}}_{,\boldsymbol{\sigma}} + \frac{1}{3}\Delta\upsilon \mathbf{1} \right) A \right) + (\lambda^{\mathrm{b}} - \lambda_0^{\mathrm{b}}) f^{\mathrm{b}}_{,\boldsymbol{\sigma}} \tag{4.33}$$

$$\mathbf{R}^{\boldsymbol{\alpha}^{\mathrm{p}}} = -\boldsymbol{\alpha}^{\mathrm{p}} + \boldsymbol{\alpha}_0^{\mathrm{p}} + \frac{3}{2}\frac{\lambda^{\mathrm{p}} - \lambda_0^{\mathrm{p}}}{1 + h_X \xi} \mathbf{T}^{-T} : \mathbf{T}^{-1} : \left[\frac{\left(\boldsymbol{\sigma} - \frac{\mathbf{X}^{\mathrm{p}}}{1 + h_X \xi} \right)}{J_2(\tilde{\boldsymbol{\sigma}} - \hat{\tilde{\mathbf{X}}}^{\mathrm{p}})} - \frac{\gamma}{C^0 (1 + h_X \xi)^3} \mathbf{X}^{\mathrm{p}} \right] \tag{4.34}$$

$$R^{r^{\mathrm{p}}} = -r^{\mathrm{p}} + r_0^{\mathrm{p}} + \frac{\lambda^{\mathrm{p}} - \lambda_0^{\mathrm{p}}}{(1 - D_{eq})(1 + h_R \xi)} \left(1 - \frac{b^{\mathrm{p}} r^{\mathrm{p}}}{(1 - D_{eq})(1 + h_R \xi)} \right) \tag{4.35}$$

$$R^{r^{\mathrm{b}}} = -r^{\mathrm{b}} + r_0^{\mathrm{b}} + (\lambda^{\mathrm{b}} - \lambda_0^{\mathrm{b}}) \left(1 - b^{\mathrm{b}} r^{\mathrm{b}} \right) \tag{4.36}$$

$$\mathbf{R}^{\mathbf{D}} = -\mathbf{D} + \mathbf{D}_0 + (\lambda^{\mathrm{p}} - \lambda_0^{\mathrm{p}}) (1 - \xi) \frac{\partial F^{\mathrm{d}}}{\partial \mathbf{Y}^{\mathrm{d}}} + (\lambda^{\mathrm{b}} - \lambda_0^{\mathrm{b}}) \xi \frac{\partial F^{\mathrm{b}}}{\partial \mathbf{Y}^{\mathrm{b}}} \tag{4.37}$$

$$R^{\xi} = -\xi + \xi_0 + (\lambda^{\mathrm{p}} - \lambda_0^{\mathrm{p}})(\xi_{\max} - \xi) \frac{m_\xi D_\xi}{(1 - D_{eq})} (D_\xi p)^{m_\xi - 1} \tag{4.38}$$

$$R^{\mathrm{p}} = \hat{\tilde{f}}^{\mathrm{p}} \left(\boldsymbol{\sigma}, \mathbf{X}^{\mathrm{p}}(\boldsymbol{\alpha}^{\mathrm{p}}), R^{\mathrm{p}}(r^{\mathrm{p}}), \mathbf{D}, \xi \right) = 0 \tag{4.39}$$

$$R^{\mathrm{b}} = f^{\mathrm{b}} \left(\mathbf{Y}^{\mathrm{b}}(\mathbf{D}, \xi), R^{\mathrm{b}}(r^{\mathrm{b}}) \right) = 0 \tag{4.40}$$

It is easy to see from the above equations that there are eight unknowns (of tensor or scalar type) that can be accumulated in the vector of unknowns $\mathbf{u} = \{\boldsymbol{\varepsilon}^{\mathrm{I}}, \boldsymbol{\alpha}^{\mathrm{p}}, r^{\mathrm{p}}, r^{\mathrm{b}}, \xi, \mathbf{D}, \lambda^{\mathrm{p}}, \lambda^{\mathrm{b}}\}$, residual functions can also be accumulated, $\mathbf{R}^T = \{\mathbf{R}^{\boldsymbol{\varepsilon}}, \mathbf{R}^{\boldsymbol{\alpha}^{\mathrm{p}}}, R^{r^{\mathrm{p}}}, R^{r^{\mathrm{b}}}, R^{\xi}, \mathbf{R}^{\mathbf{D}}, R^{\mathrm{p}}, R^{\mathrm{b}}\}$. It is evident that the condition

$$\mathbf{R}(\mathbf{u}) = \mathbf{0} \tag{4.41}$$

defines the solution. The above condition can be linearized and solved with the use of the

Newton-Raphson scheme at iteration (s), which can be written in the following general form:

$$\mathbf{R}(\mathbf{u}^s) + \left[\frac{\partial \mathbf{R}(\mathbf{u}^s)}{\partial \mathbf{u}}\right] \mathrm{d}\mathbf{u} = \mathbf{0} \tag{4.42}$$

Solving the above general equations allows to obtain the corrections $\mathrm{d}\mathbf{u} = \{\mathrm{d}\boldsymbol{\varepsilon}^{\mathrm{I}}, \mathrm{d}\boldsymbol{\alpha}^{\mathrm{p}}, \mathrm{d}r^{\mathrm{p}}, \mathrm{d}r^{\mathrm{b}}, \mathrm{d}\xi, \mathrm{d}\mathbf{D}, \mathrm{d}\lambda^{\mathrm{p}}, \mathrm{d}\lambda^{\mathrm{b}}\}$ for the current iteration (s) (and at current timen step j). Accordingly, the values of the unknowns for the next iteration are obtained from:

$$\mathbf{u}^{(s+1)} = \mathbf{u}^{(s)} + \mathrm{d}\mathbf{u}^{(s)} \tag{4.43}$$

The iteration procedure is stopped as soon as the norm of $\mathbf{R}(\mathbf{u})$ is sufficiently small, e.g. 10^{-8}.

As was mentioned, the case when the two criteria are fulfilled in the trial step ($\hat{\tilde{f}}^{\mathrm{p,trial}} > 0$ and $f^{\mathrm{b,trial}} > 0$), implies that the plastic flow and the brittle damage evolution have occurred. However, as was also mentioned, in the case of two non-smoothly intersected surfaces, even if loading conditions are fulfilled for both surfaces, it does not necessarily mean that both plastic and damage processes are ultimately active. To overcome such ambiguity, an algorithm proposed in Simo and Hughes (1998) is adopted.

The discrete counterparts of the loading/unloading conditions (Eqs. 3.78, 3.79) take the form:

$$\Delta\lambda^{\mathrm{p}} \geqslant 0; \quad \hat{\tilde{f}}^{\mathrm{p}} \leqslant 0; \quad \Delta\lambda^{\mathrm{p}} \hat{\tilde{f}}^{\mathrm{p}} = 0 \tag{4.44}$$

$$\Delta\lambda^{\mathrm{b}} \geqslant 0; \quad f^{\mathrm{b}} \leqslant 0; \quad \Delta\lambda^{\mathrm{b}} f^{\mathrm{b}} = 0 \tag{4.45}$$

Importantly, if only one process is active (either plastic or brittle damage), then the condition $\hat{\tilde{f}}^{\mathrm{p,trial}} > 0$ (or $f^{\mathrm{b,trial}} > 0$) implies that $\Delta\lambda^{\mathrm{p}} > 0$ (or $\Delta\lambda^{\mathrm{b}} > 0$), and the solution is reduced to single-surface problem. However, if two conditions are fulfilled, then the conditions $\hat{\tilde{f}}^{\mathrm{p,trial}} > 0$ and $f^{\mathrm{b,trial}} > 0$ do not necessarily imply that $\Delta\lambda^{\mathrm{p}} > 0$ and $\Delta\lambda^{\mathrm{b}} > 0$ (e.g. it is possible to have $\hat{\tilde{f}}^{\mathrm{p,trial}} > 0$ and, at the same time $\hat{\tilde{f}}^{\mathrm{p}} < 0$). Thus, the key point of the problem is the question how to define the set of active processes when $\hat{\tilde{f}}^{\mathrm{p,trial}} > 0$ and $f^{\mathrm{b,trial}} > 0$. This is done in two steps:

1. For $s = 0$, at every time step j (see Eq. 4.42), the nonlinear system of algebraic equations is solved by Newton-Raphson method for $\mathbf{u}^{s+1} = \{\boldsymbol{\varepsilon}^{\mathrm{I},s+1}, \boldsymbol{\alpha}^{\mathrm{p},s+1}, r^{\mathrm{p},s+1}, r^{\mathrm{b},s+1}, \xi^{s+1}, \mathbf{D}^{s+1}, \lambda^{\mathrm{p},s+1}, \lambda^{\mathrm{b},s+1}\}$.

2. The sign of $\mathrm{d}\lambda^{\mathrm{p}}$ and $\mathrm{d}\lambda^{\mathrm{b}}$ is checked. If $\mathrm{d}\lambda^{\mathrm{p}} < 0$, then the plastic process is deemed to be inactive, as well as if $\mathrm{d}\lambda^{\mathrm{b}} < 0$ then the brittle damage process is deemed to be inactive

and hence the corresponding constraint is dropped. If $\mathrm{d}\lambda^{\mathrm{p}} >$ and $\mathrm{d}\lambda^{\mathrm{b}} > 0$, then both processes are active.

Then set $s \leftarrow s+1$ and repeat step 1 and 2 until the convergence is obtained. Otherwise, if a limit of the number iteration is reached, the program is stopped.

The algorithm is summarized in the Table 4.1, and a simple example is also provided in Appendix 1.

Rate-dependent regularization of rate-independent model

It is well known that a rate-dependent formulation can be adopted as the regularization of the rate-independent plasticity (Simo and Hughes, 1998). Such numerical regularization is widely used in crystal plasticity computations to overcome the problem of determining the set of active plastic slips on slip surfaces (e.g. Peirce et al. (1983); Pan and Rice (1983)). Indeed, since in the rate-dependent plasticity all dissipative processes start from the very beginning of loading, the dilemma about active ones is avoided. A similar idea is used here. Writing Eqs. (3.52) and (3.59) in the following form

$$\begin{aligned} \hat{\tilde{\tau}}_{eq} &= \sigma_{\mathrm{y}}^0 + \hat{\tilde{R}}^{\mathrm{p}} \qquad \text{where} \quad \hat{\tilde{\tau}}_{eq} = J_2(\hat{\tilde{\sigma}}_{ij} - \hat{\tilde{X}}^{\mathrm{p}}_{ij}) \\ Y^{\mathrm{b}}_{eq} &= l_y + R^{\mathrm{b}} \qquad \text{where} \quad Y^{\mathrm{b}}_{eq} = \sqrt{\frac{1}{2} Y^{\mathrm{b}}_{ij} A_{ijkl} Y^{\mathrm{b}}_{kl}} \end{aligned} \tag{4.46}$$

the right hand sides of the above equations ($\sigma_{\mathrm{y}}^0 + \hat{\tilde{R}}^{\mathrm{p}}$ and $l_y + R^{\mathrm{b}}$) are understood as the current flow resistance and the current resistance against brittle damage evolution, respectively. In order to encompass a rate-dependent regularization in the present formulation, the following functions are assumed (cf. Gurtin et al. (2010))

$$\hat{\tilde{\tau}}_{eq} = \left(\frac{\dot{\lambda}^{\mathrm{p}}}{\dot{\lambda}^{\mathrm{p}}_0}\right)^m (\sigma_{\mathrm{y}}^0 + \hat{\tilde{R}}^{\mathrm{p}}) \qquad Y^{\mathrm{b}}_{eq} = \left(\frac{\dot{\lambda}^{\mathrm{b}}}{\dot{\lambda}^{\mathrm{b}}_0}\right)^m (l_y + R^{\mathrm{b}}) \qquad \text{with } m > 0 \tag{4.47}$$

where m is a rate sensivity parameter, and $\dot{\lambda}^{\mathrm{p}}_0$, $\dot{\lambda}^{\mathrm{b}}_0$ are reference rates (taken here equal to each other, for simplicity). The rate-independent model is recovered in the limit as $m \to 0$. The inversion of the above relations gives the explicit functions of the plastic and damage multipliers:

$$\dot{\lambda}^{\mathrm{p}} = \dot{\lambda}^{\mathrm{p}}_0 \left(\frac{\hat{\tilde{\tau}}_{eq}}{\sigma_{\mathrm{y}}^0 + \hat{\tilde{R}}^{\mathrm{p}}}\right)^{1/m} \qquad \dot{\lambda}^{\mathrm{b}} = \dot{\lambda}^{\mathrm{b}}_0 \left(\frac{Y^{\mathrm{b}}_{eq}}{l_y + R^{\mathrm{b}}}\right)^{1/m} \tag{4.48}$$

Table 4.1: Elastic predictor – plastic corrector algorithm*

Elastic predictor
$\boldsymbol{\varepsilon}_j = \boldsymbol{\varepsilon}_0 + \Delta\boldsymbol{\varepsilon}_j$
$\boldsymbol{\sigma}_j^{\text{trial}} = \tilde{\mathbf{E}}_0 : \left(\boldsymbol{\varepsilon}_j - \boldsymbol{\varepsilon}_0^{\text{I}}\right) = \boldsymbol{\sigma}_0 + \tilde{\mathbf{E}}_0 : \Delta\boldsymbol{\varepsilon}_j$
$-\mathbf{Y}_j^{\text{trial}} = \frac{1}{2}\boldsymbol{\sigma}_j^{\text{trial}} : \left(\frac{\partial\tilde{\mathbf{E}}^{-1}}{\partial\mathbf{D}}\right)_0 : \boldsymbol{\sigma}_j^{\text{trial}} + \frac{1}{2}\boldsymbol{\alpha}_0^{\text{p}} : \frac{\partial\hat{\tilde{\mathbf{C}}}(\mathbf{D}_0,\xi_0)}{\partial\mathbf{D}} : \boldsymbol{\alpha}_0^{\text{p}} + \frac{1}{2}\frac{\partial\hat{\tilde{Q}}^{\text{p}}(\mathbf{D}_0,\xi_0)}{\partial\mathbf{D}}(r_0^{\text{p}})^2$
$f_j^{\text{p,trial}} := f^{\text{p}}\left(\boldsymbol{\sigma}_j^{\text{trial}}, \mathbf{X}_0^{\text{p}}, R_0^{\text{p}}, \mathbf{D}_0, \xi_0\right)$
$f_j^{\text{b,trial}} := f_j^{\text{b}}\left(\mathbf{Y}_j^{\text{b,trial}}, R_0^{\text{b}}\right)$
Check for (possible) active processes
IF $f_j^{\text{p,trial}} < 0$ and $f_j^{\text{b,trial}} < 0$ THEN
$\{\boldsymbol{\sigma}_j, \mathbf{X}_j^{\text{p}}, R_j^{\text{p}}, \mathbf{Y}_j, R_j^{\text{b}}\} = \{\boldsymbol{\sigma}_j^{\text{trial}}, \mathbf{X}_0^{\text{p}}, R_0^{\text{p}}, \mathbf{Y}_j^{\text{trial}}, R_0^{\text{b}}\}$
$\{\boldsymbol{\varepsilon}_j^{\text{I}}, \boldsymbol{\alpha}_j^{\text{p}}, r^{\text{p}}, r_j^{\text{b}}, \mathbf{D}_j, \xi_j\} = \{\boldsymbol{\varepsilon}_0^{\text{I}}, \boldsymbol{\alpha}_0^{\text{p}}, r_0^{\text{p}}, r_0^{\text{b}}, \mathbf{D}_0, \xi_0\}$ and EXIT
ELSE
Define set J_{act} of active processes (α =p for plasticity α =b for brittle damage process)
$J_{\text{act}}^{(s=0)} := \{\alpha \in \{\text{p}, \text{b}\} \mid f_j^{\alpha,\text{trial}} > 0\}$
$\mathbf{u}_j^0 = \mathbf{u}_0$ and GO TO plastic-damage corrector
END IF
Plastic-damage corrector
DO
$\text{d}\mathbf{u}_j^s = \left[\frac{\partial\mathbf{R}(\mathbf{u}_j)}{\partial\mathbf{u}_j}\right]^{-1}\mathbf{R}(\mathbf{u}_j^s)$
$\mathbf{u}_j^{(s+1)} = \mathbf{u}_j^{(s)} + \text{d}\mathbf{u}_j^{(s)}$
Check whether $\left[\text{d}\mathbf{u}_j^{(s)}\right]_7 = \text{d}\lambda_j^{\text{p}(s)} > 0 \quad \text{and} \quad \left[\text{d}\mathbf{u}_j^{(s)}\right]_8 = \text{d}\lambda_j^{\text{b}(s)} > 0$
IF NOT obtain a new set of constraints $J_{\text{act}}^{(s+1)}$ by dropping f_j^{α} for which $\text{d}\lambda_j^{\alpha(s)} < 0$
Check convergence
IF $f_j^{\alpha(s+1)}$ <TOL$_1$ and $\|\mathbf{R}\|$ <TOL$_2$ THEN EXIT
ELSE $s \leftarrow s+1$
END IF
END DO

* Note that in the above Table 4.1, the following substitution is used $f_j^{\text{p,trial}} = \hat{\tilde{f}}_j^{\text{p,trial}}$

In order to minimize the time-dependency of the model in numerical simulations, and obtain results that are convergent to the rate-independent model, $m = 500$ was set, and $\dot{\lambda}_0^{\text{p}} = \dot{\lambda}_0^{\text{b}} = 0.01[1/s]$. The final set of discretized equations that are solved with the Newton-Raphson

scheme (Tab. 4.2) is summarized below.

$$\mathbf{R}^{\varepsilon} = -\boldsymbol{\varepsilon}^{\mathrm{I}} + \boldsymbol{\varepsilon}_0^{\mathrm{I}} + \Delta\lambda^{\mathrm{p}}\hat{\tilde{f}}^{\mathrm{p}}_{,\boldsymbol{\sigma}} + \Delta\lambda^{\mathrm{p}}F^{\mathrm{d}}_{,\boldsymbol{\sigma}} + \Delta\lambda^{\mathrm{p}}F^{\mathrm{tr}}_{,Y^{\mathrm{CH}}}\left(\hat{\tilde{f}}^{\mathrm{p}}_{,\boldsymbol{\sigma}} + \frac{1}{3}\Delta\upsilon\mathbf{1}\right)A + \Delta\lambda^{\mathrm{b}}f^{\mathrm{b}}_{,\boldsymbol{\sigma}} \tag{4.49}$$

$$\mathbf{R}^{\boldsymbol{\alpha}^{\mathrm{p}}} = -\boldsymbol{\alpha}^{\mathrm{p}} + \boldsymbol{\alpha}_0^{\mathrm{p}} + \frac{3}{2}\frac{\Delta\lambda^{\mathrm{p}}}{1+h_X\xi}\mathbf{T}^{-T}{:}\mathbf{T}^{-1}{:}\left[\frac{\left(\boldsymbol{\sigma} - \frac{\mathbf{X}^{\mathrm{p}}}{1+h_X\xi}\right)}{J_2(\tilde{\boldsymbol{\sigma}} - \hat{\tilde{\mathbf{X}}}^{\mathrm{p}})} - \frac{\gamma}{C^0(1+h_X\xi)^3}\mathbf{X}^{\mathrm{p}}\right] \tag{4.50}$$

$$R^{r^{\mathrm{p}}} = -r^{\mathrm{p}} + r_0^{\mathrm{p}} + \frac{\Delta\lambda^{\mathrm{p}}}{(1-D_{eq})(1+h_R\xi)}\left(1 - \frac{b^{\mathrm{p}}r^{\mathrm{p}}}{(1-D_{eq})(1+h_R\xi)}\right) \tag{4.51}$$

$$R^{r^{\mathrm{b}}} = -r^{\mathrm{b}} + r_0^{\mathrm{b}} + \Delta\lambda^{\mathrm{b}}\left(1 - b^{\mathrm{b}}r^{\mathrm{b}}\right) \tag{4.52}$$

$$\mathbf{R}^{\mathbf{D}} = -\mathbf{D} + \mathbf{D}_0 + \Delta\lambda^{\mathrm{p}}\left(1-\xi\right)\frac{\partial F^{\mathrm{d}}}{\partial \mathbf{Y}^{\mathrm{d}}} + \Delta\lambda^{\mathrm{b}}\xi\frac{\partial F^{\mathrm{b}}}{\partial \mathbf{Y}^{\mathrm{b}}} \tag{4.53}$$

$$R^{\xi} = -\xi + \xi_0 + \Delta\lambda^{\mathrm{p}}(\xi_{\max} - \xi)\frac{m_\xi D_\xi}{(1-D_{eq})}(D_\xi p)^{m_\xi - 1} \tag{4.54}$$

$$R^{\mathrm{p}} = \Delta\lambda^{\mathrm{p}} - \Delta t\dot{\lambda}_0^{\mathrm{p}}\left(\frac{\hat{\tilde{\tau}}_{eq}}{\sigma_{\mathrm{y}}^0 + \hat{\tilde{R}}^{\mathrm{p}}}\right)^{1/m} \tag{4.55}$$

$$R^{\mathrm{b}} = \Delta\lambda^{\mathrm{b}} - \Delta t\dot{\lambda}_0^{\mathrm{b}}\left(\frac{Y^{\mathrm{b}}_{eq}}{l_y + R^{\mathrm{b}}}\right)^{1/m} \tag{4.56}$$

Table 4.2: Newton-Raphson scheme for rate-dependent problem

Solve for every time step 'j'
DO
$\mathrm{d}\mathbf{u}_j^s = \left[\frac{\partial \mathbf{R}(\mathbf{u}_j)}{\partial \mathbf{u}_j}\right]^{-1}\mathbf{R}(\mathbf{u}_j^s)$
$\mathbf{u}_j^{(s+1)} = \mathbf{u}_j^{(s)} + \mathrm{d}\mathbf{u}_j^{(s)}$
Check convergence
IF $f_j^{\alpha(s+1)}$ <TOL$_1$ and $\|\|\mathbf{R}\|\|$ <TOL$_2$ THEN EXIT
ELSE $s \leftarrow s+1$
END IF
END DO

Chapter 5

Parametric studies

5.1 Elastic-brittle model

According to Eqs. (3.50), (3.59) and (3.76), the response of the elastic-brittle model can be changed by manipulating three parameters, i.e. l_{y}, which is a stress-type quantity above which the brittle damage evolution starts developing, and two parameters, $Q^{\mathrm{b}0}$ and b^{b}, that are related to non-linear isotropic-like hardening of the damage surface. The numerical results presented below were obtained for a fixed value of damage threshold $l_{\mathrm{y}} = 3\,[\mathrm{MPa}]$, initial Young modulus $E^0 = 200\,[\mathrm{GPa}]$, and Poisson ratio $\nu = 0.3$. In figures presented below the influence of parameters $Q^{\mathrm{b}0}$ and b^{b} on the stress-strain behaviour and thermodynamic force, R^{b}, is shown. As can be expected, increasing the value of $Q^{\mathrm{b}0}$ and decreasing the value of b^{b} implies significant increase in material strength, Fig. 5.1. This behavior is simply a consequence of steering the size of the damage surface, which can be seen as the restriction on damage evolution process and thus elastic-damage modulus degradation, Fig. 5.2. Increasing parameter b^{b} results in a fast saturation of the hardening variable, R^{b} (Fig. 5.1b). Moreover, it causes the sigmoidal character of the damage evolution curve (Fig. 5.2a). The use of a specific form of tensor A_{ijkl} describing the damage-induced change of the damage surface results in the anisotropy of damage evolution even in the case of uniaxial stress state without any additional parameters. The anisotropy of damage is shown in Fig. 5.3a, where a normalized strain is computed according to equation $\varepsilon^{\mathrm{I}}_{ii}/\mathrm{Max}\,\{\varepsilon^{\mathrm{I}}_{ii}\}$. It is also worth pointing out that including irreversible damage strain $\varepsilon^{\mathrm{ibd}}_{ij}$ (note that here $\varepsilon^{\mathrm{I}}_{ij} = \varepsilon^{\mathrm{ibd}}_{ij}$) in the model (see Eq. 3.69) has a significant influence on the stress–strain response since the value of this strain is pronounced, Fig. 5.4. The variation of different types of strains is shown in Fig. 5.3b, where the normalized damage denotes $D_{ii}/\mathrm{Max}\{D_{ii}\}$.

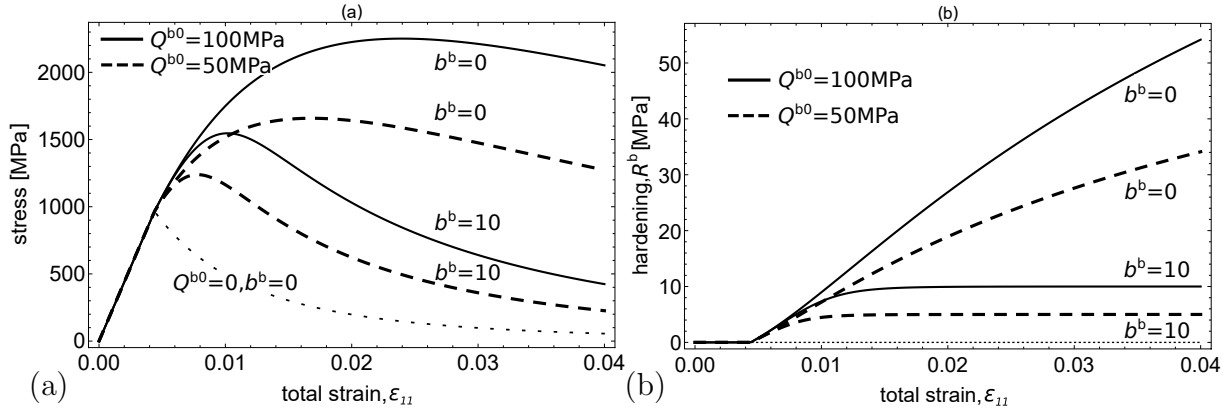

Figure 5.1: Influence of hardening parameters (Q^{b0},b^b) on (a) stress-strain relation and (b) isotropic hardening, R^b.

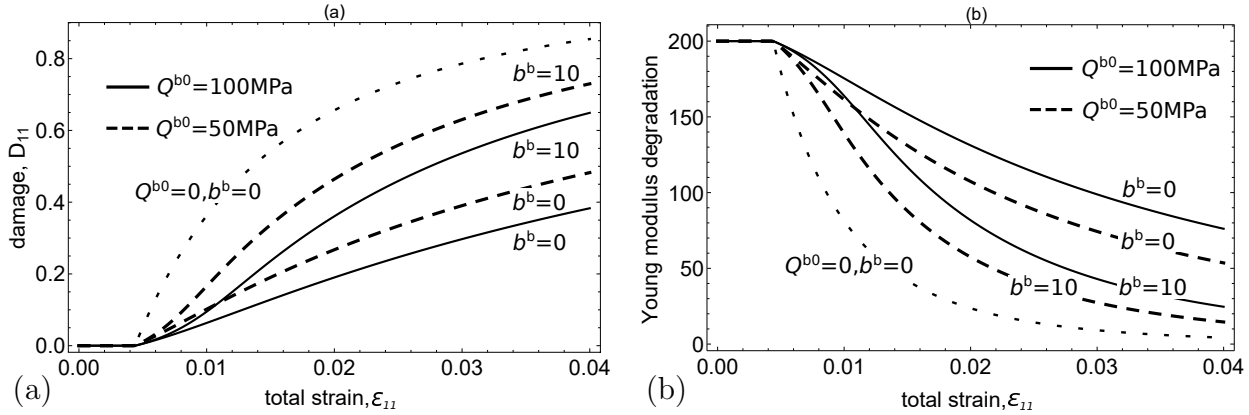

Figure 5.2: Influence of hardening parameters (Q^{b0},b^b) on (a) brittle damage evolution and (b) Young modulus degradation $\left(E(D_{11}) = E^0(1-D_{11})^2\right)$.

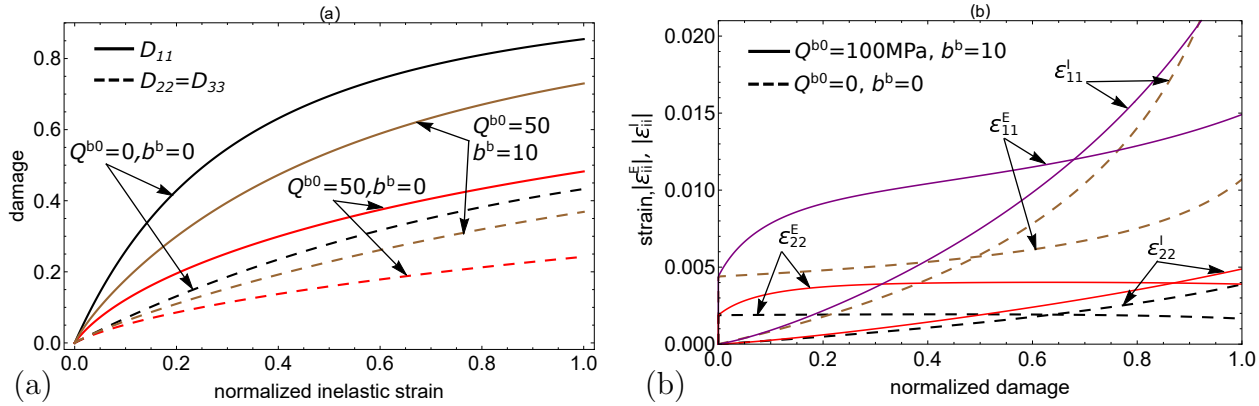

Figure 5.3: Anisotropy of damage (a) and variation of different types of strains with damage (b).

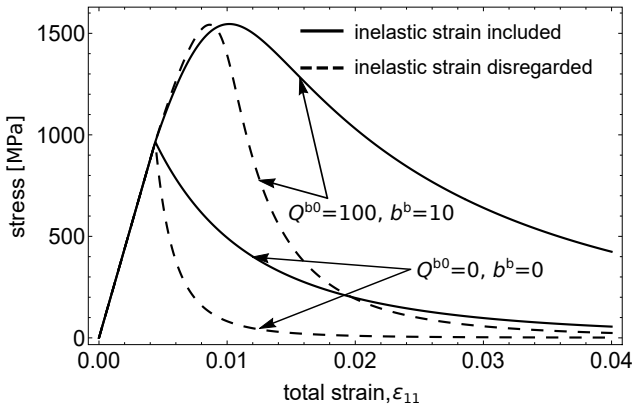

Figure 5.4: Influence of damage strain on stress-strain response.

5.2 Elastic–plastic ductile damage versus elastic–plastic with phase transformation model

To illustrate the influence of ductile damage and phase transformation on the model response, each phenomenon is examined separately. Importantly, brittle damage evolution is disregarded here. It is also assumed that ductile damage and phase transformation start to develop together with the onset of plastic yielding in a quite intensive way (see Fig. 5.7), hence the following parameters are used $p_D = 0$, $s = 1$, $\beta = 1$ for damage evolution (Eq. 3.74) and $D_\xi = 8$, $m_\xi = 2$ for phase transformation (Eq. 3.77). The value of yield stress is σ_y^0 =600[MPa] and additional strain related to phase transformation is neglected here ($\dot{\boldsymbol{\varepsilon}}^{\mathrm{tr}} = 0$).

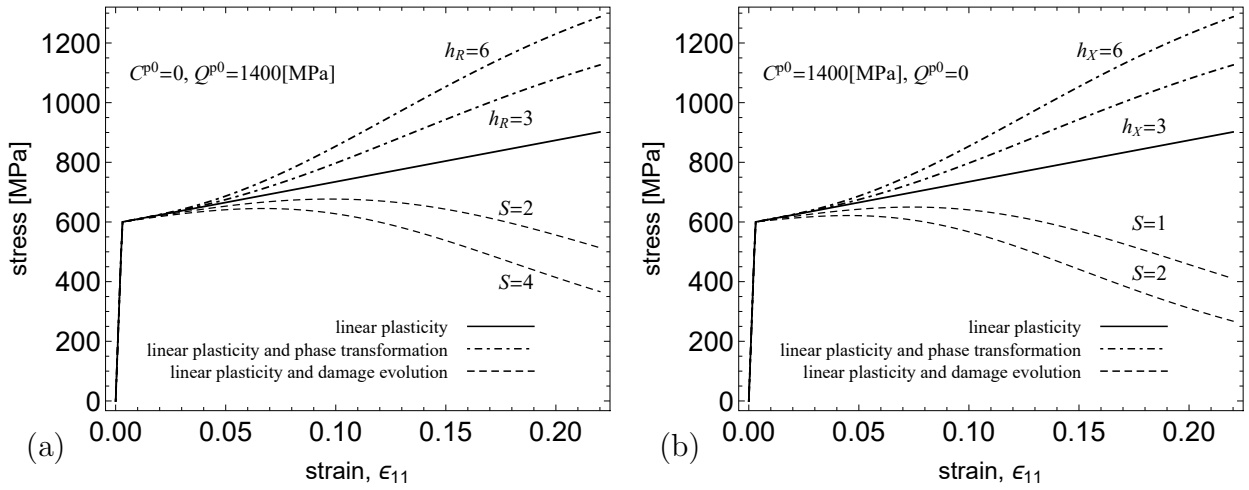

Figure 5.5: Influence of phase transformation or damage evolution on stress-strain response for model with (a) isotropic and (b) kinematic hardening.

The phase transformation influence functions (Eq. 3.25) are monotonic increasing functions of the secondary phase content to account for the experimentally observed strong hardening effect due to the phase transformation phenomenon. On the other hand, the damage influence tensor (Eq. 3.37) is a monotonic but decreasing function of the damage variable to enforce damage softening. These two effects are clearly visible in Fig. 5.5. Thermodynamic forces related to isotropic and kinematic hardenig affected by damage evolution and phase transformation are presented in Fig. 5.6.

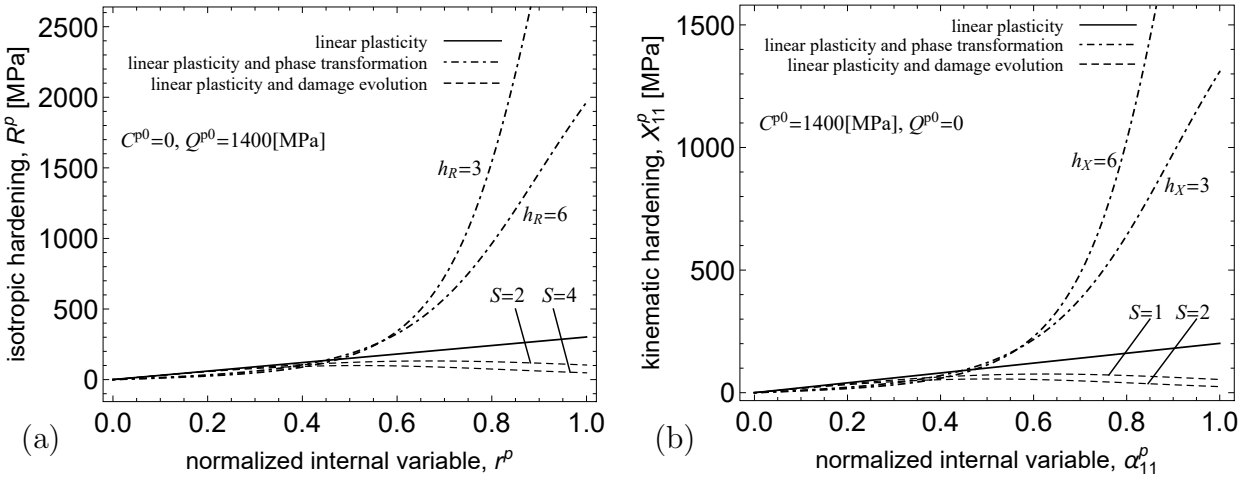

Figure 5.6: Influence of phase transformation or damage evolution on (a) isotropic hardening (with kinematic hardening disregarded) and (b) kinematic hardening (with isotropic hardening disregarded).

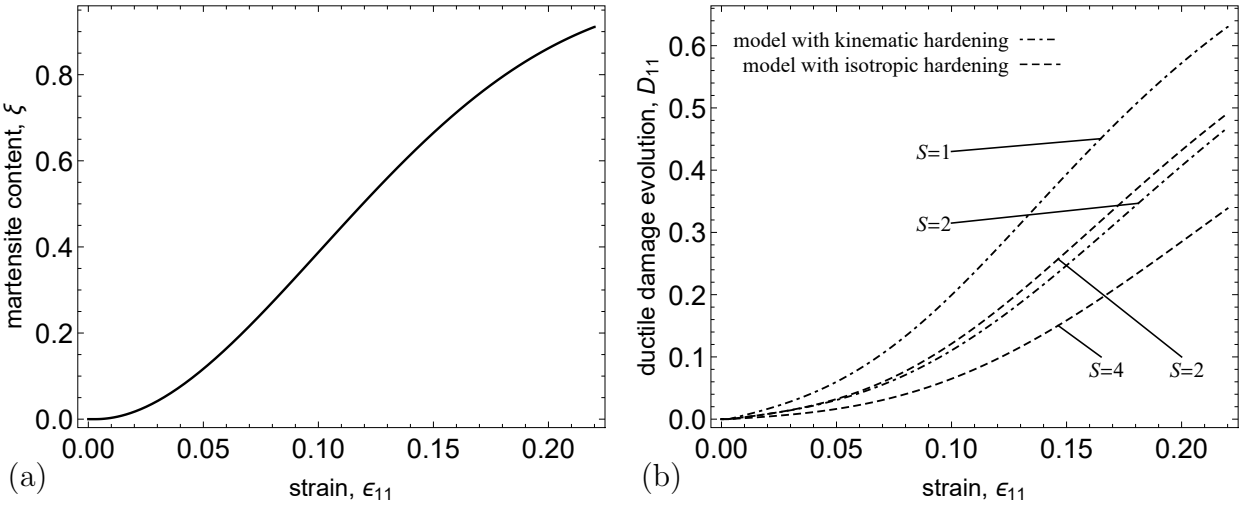

Figure 5.7: Kinetics of (a) phase transformation and (b) ductile damage evolution for the present parametric studies.

5.3 Plasticity, mixed ductile/brittle damage and phase transformation

The general model of plasticity, ductile damage in matrix, phase transformation, and brittle damage in the secondary phase are now considered. In Figures 5.8 – 5.10, the following cases are compared:

- nonlinear plasticity for $\sigma_{\mathrm{y}}^{0} = 600\mathrm{MPa}$, $Q^{\mathrm{p0}} = 1400\mathrm{MPa}$, $b = 2$, $C^{\mathrm{p0}} = 10000\mathrm{MPa}$ $\gamma = 100$ (dashed line);
- nonlinear plasticity coupled with ductile damage for $S = 10\mathrm{MPa}$, $p_{\mathrm{D}} = 0$, $s = 1$, $\beta = 1$ (dotted line);
- nonlinear plasticity coupled with phase transformation for $D_{\xi} = 5$, $m_{\xi} = 2$, $A = 0.01$, $h_X = 2$, $h_R = 15$ (dashed/dotted line);
- full coupled model, nonlinear plasticity, mixed ductile/brittle damage, and phase transformation, for parameters listed above and $Q^{\mathrm{b0}} = 20\mathrm{MPa}$, $l_y = 0.5\mathrm{MPa}$;

In accordance with the physical nature of the dissipative phenomena considered here (plastic strain hardening enhanced by phase transformation and damage softening), it seems that the proposed model captures all of these phenomena and couplings between them qualitatively in a proper way, which can be seen in the following figures, representing stress–strain relations (Fig. 5.8) and thermodynamic forces related to isotropic and kinematic hardening of the yield surface (Fig. 5.9).

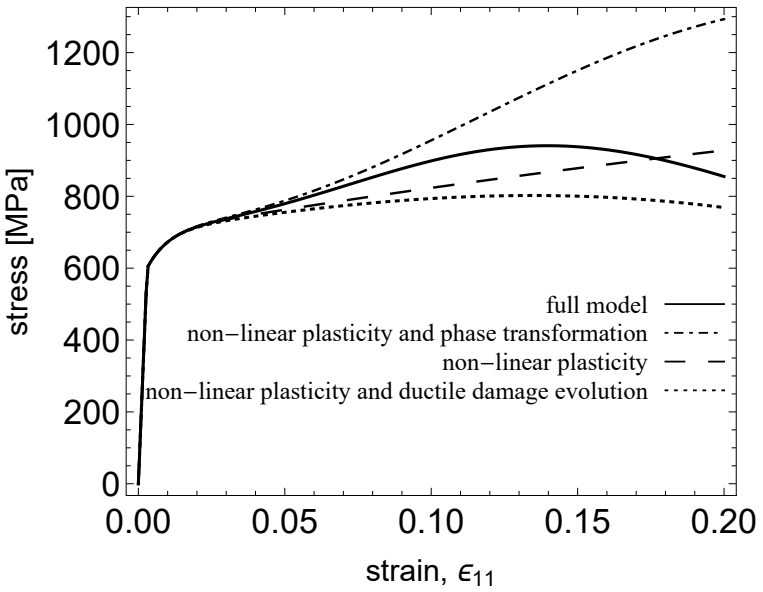

Figure 5.8: Stress-strain curves for different phenomena included.

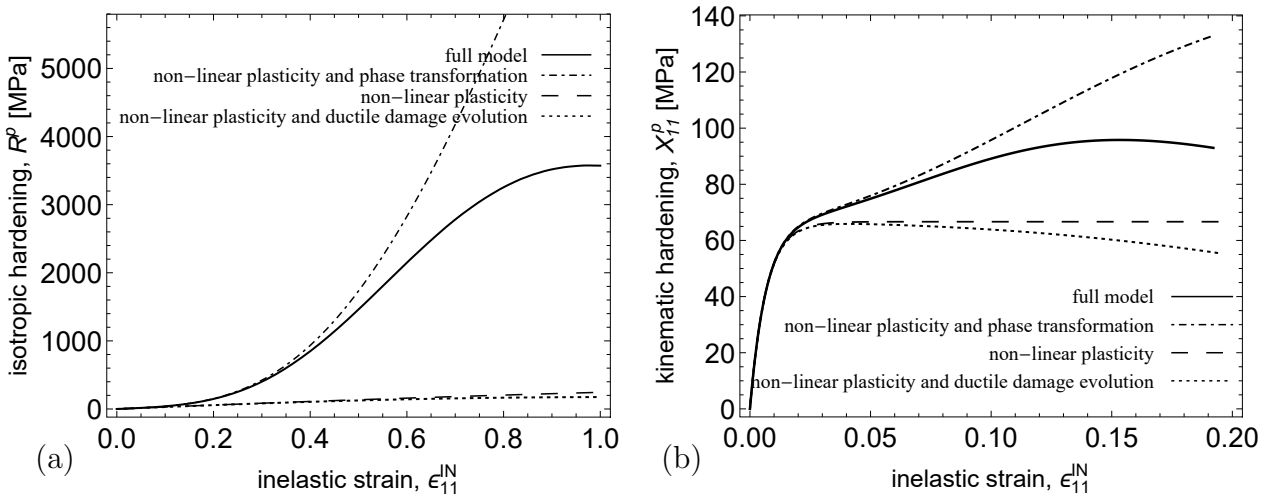

Figure 5.9: Influence of phase transformation and/or damage evolution on (a) isotropic and (b) kinematic hardening.

The damage evolution (in the direction of loading) correlated with the phase transformation for current model parametrs is presented in Fig. 5.10a whereas damage evolution in the principal directions, reflecting damage anisotropy, is presented in Fig. 5.10b. The components of ductile and brittle damage (see mixture rule Eq. (3.8)) were distinguished to show the fraction of both types of damage in the RVE. According to Eq. (3.8), the symbols appearing in the pictures are defined as follows:

$$
\begin{aligned}
D_{ij} = \int_t \dot{D}_{ij} dt, \quad D_{ij}^{\mathrm{d}} = \int_t \dot{D}_{ij}^{\mathrm{d}} dt, \quad D_{ij}^{\mathrm{b}} = \int_t \dot{D}_{ij}^{\mathrm{b}} dt, \\
\Big\langle D_{ij} \Big\rangle_{\mathrm{RVE}}^{\mathrm{d}} = \int_t \Big\langle \dot{D}_{ij} \Big\rangle_{\mathrm{RVE}}^{\mathrm{d}} dt = \int_t (1-\xi) \dot{D}_{ij}^{\mathrm{d}} dt, \\
\Big\langle D_{ij} \Big\rangle_{\mathrm{RVE}}^{\mathrm{b}} = \int_t \Big\langle \dot{D}_{ij} \Big\rangle_{\mathrm{RVE}}^{\mathrm{b}} dt = \int_t \xi \dot{D}_{ij}^{\mathrm{b}} dt
\end{aligned}
\tag{5.1}
$$

An important result is that the use of mixture rule (Eq. 3.8) results in the drop of the rate of the damage evolution (compare the difference between D_{ij}^{d} and $\Big\langle D_{ij} \Big\rangle_{\mathrm{RVE}}^{\mathrm{d}}$). Moreover, the introduction of the additional strain related to the phase transformation, $\dot{\varepsilon}_{ij}^{\mathrm{tr}}$ (Eq. 3.70) in the model reduces the value of the plastic strain (Fig. 5.11), and thus the rate of damage evolution since its value is significant. On the other hand, thermodynamic force conjugate to damage Y_{ij}^{p} strongly depends on the volume fraction of martensite and hence the growing volume fraction of martensite contributes to an increase in the rate of damage evolution. These features of the model agree with the experimental investigations presented in Section 2.4 where it was noted that, on the one hand martensite evolution can have a positive effect on damage evolution (e.g. because of absorbing energy that could otherwise be available for

crack extension, higher slip homogeneity resulting from phase transformation) but, on the other hand, can have a negative effect on damage state (e.g. martensitic phase is more brittle, additional strain resulting from phase transformation gives rise to the increase in dislocation density in the surrounding material, which may promote damage evolution). With the use of two separate evolution laws for ductile and brittle damage and employing the total energy equivalence hypothesis, the proposed model is able to capture these physical features.

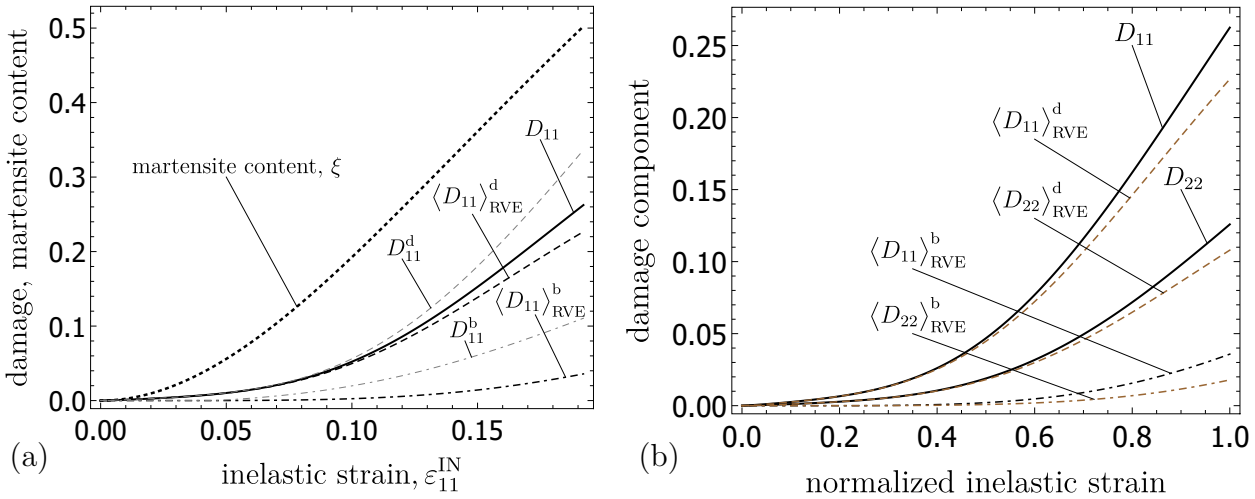

Figure 5.10: Evolution of (a) damage (in direction of loading) and phase transformation versus inelastic strain and (b) individual components of damage tensor versus normalized inelastic strain.

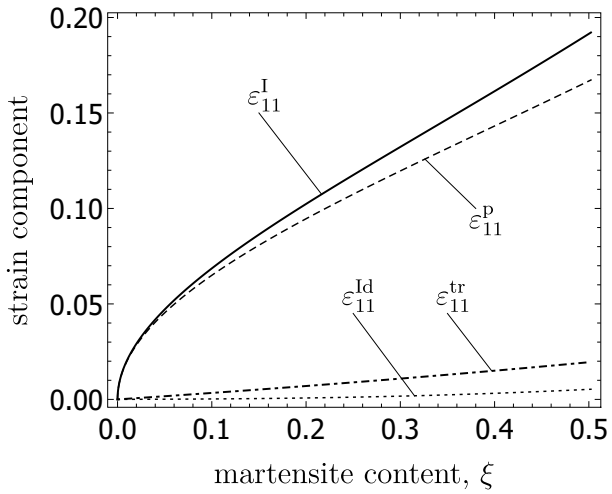

Figure 5.11: Variation of different types of strains with secondary phase content, ξ.

Chapter 6

Identification of model parameters for 316L and 304 stainless steels

6.1 Material parameters

The proposed model has been calibrated with the use of the experimental data from loading/unloading uniaxial tests performed for two stainless steel grades: 304 and 316L. The unloading procedure allows to trace the variation of the elastic-damage (unloading) modulus, and, in this way, to estimate the evolution of damage. The experimental stress-strain curves for 316L (after Garion et al. (2006); Egner and Skoczeń (2010)) and 304 (after Tabin et al. (2017)) stainless steels subjected to uniaxial tension (with unloading) are presented in Fig. 6.1, the measured subsequent unloading moduli ($\tilde{E}$) relative to the initial Young modulus (E^0) are also presented in the plots.

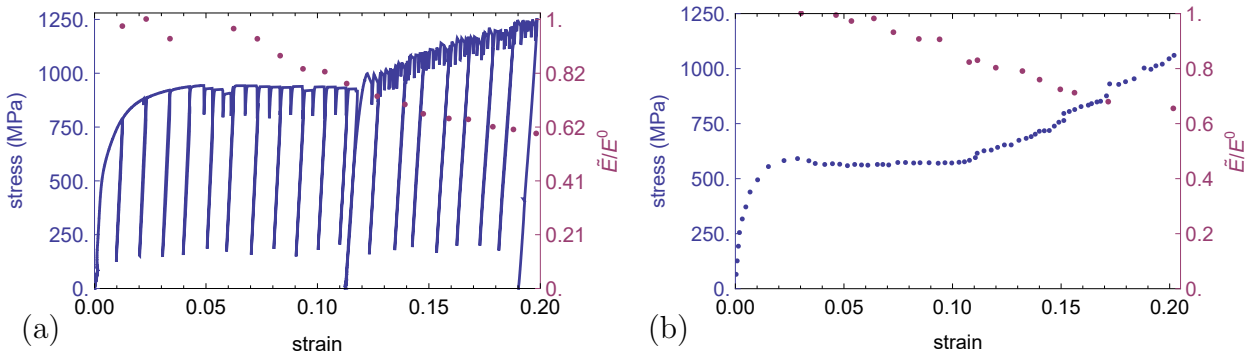

Figure 6.1: Stress-strain curves and unloading modulus for (a) 316L (after Garion et al. (2006); Egner and Skoczeń (2010)) and (b) 304 (after Tabin et al. (2017)) stainless steels.

According to the energy equivalence principle, in the uniaxial state of stress, damage evolution

can be calculated with the use of the following equation

$$D = 1 - \sqrt{\frac{\tilde{E}}{E^0}} \tag{6.1}$$

Such experimentally determined damage level is shown in Fig. 6.4 (black dots). It is worth mentioning that the experiments were performed at extremely low temperatures (liquid helium, 4.2 K). Such measurements are laborious, time-consuming and require a rather sophisticated equipment in order to maintain correct experimental conditions. A more detailed discussion about experimental setup may be found in Garion et al. (2006); Egner and Skoczeń (2010) and Tabin et al. (2016, 2017).

An automated Isight optimization workflow for the calibration of material parameters was used in order to fit the proposed model to the experimental results (Fig. 6.2). Three types of experimental results were loaded in the programme, i.e. stress-strain curve, damage evolution versus inelastic strain, and martensite volume fraction versus inelastic strain. The Pointer technique that consists of a complementary set of optimization algorithms was chosen to automatically find the optimal model parameters. Material parameters used in the following numerical examples are summarized in Table 6.1.

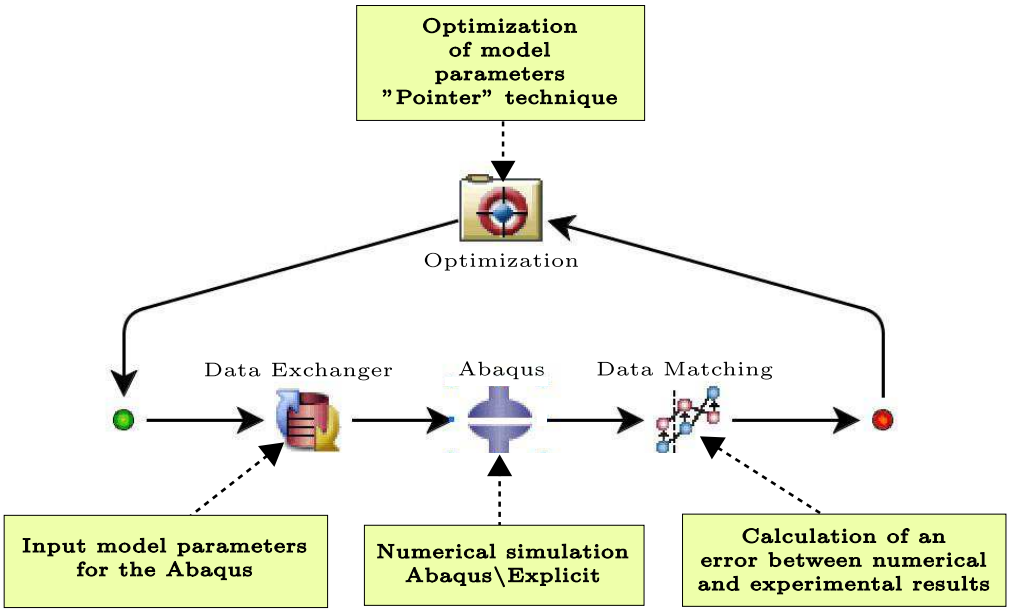

Figure 6.2: Optimization algorithm for calibration of model parameters.

Table 6.1: Material parameters

	SS 316L	SS 304	
Young modulus, E^0	247.266[a]	210[a]	GPa
Poisson's ratio, ν	0.3[a]	0.3[a]	-
Plasticity			
σ_y^0	515	320	MPa
Q^0	2625	2178	MPa
b	9	13.4	-
h_R	8	13	-
C^0	95591	73048	MPa
γ	290	409	-
h_X	0	0	-
Damage			
S	3.2	2.2	MPa
p_D	0.05	0.04	-
s	1	1	-
β	0	0	-
l_y	0.01	0.01	MPa
Q^{b0}	1600	1400	MPa
Phase transformation			
$\xi_{\max}$	0.9[a]	0.9[a]	-
m_ξ	25	40	-
D_ξ	8.5	8.2	-
A_0	0.02[b]	0.02[b]	-
A_1	0.05[b]	0.05[b]	-
dv	0.29[b]	0.29[b]	-
Additional parameters of rate-dependent regularization			
rate sensivity parameter, m	500	500	-
reference rate, $\dot{\lambda}_0^p = \dot{\lambda}_0^b$	0.01	0.01	$1/s$

[a] after Egner and Skoczeń (2010); Tabin et al. (2017); Garion et al. (2006)

[b] after Stringfellow et al. (1992); Hallberg et al. (2007)

[*] values without superscript were found with the Isight system

6.2 Uniaxial tension tests

Figures 6.3a,b show numerical and experimental stress-strain curves for 316L and 304 stainless steels, resulting from a uniaxial tension test. Three cases are distinguished in each figure: (1) full model (coupled plasticity, phase transformation, and ductile/brittle damage), (2) plasticity coupled with phase transformation, and (3) plasticity coupled with ductile damage evolution. Such a combination clearly shows the influence of individual effects (strong

hardening due to phase transformation and softening due to damage) as well as their mutual couplings. One can also see that the agreement between experimental and numerical results is satisfactory.

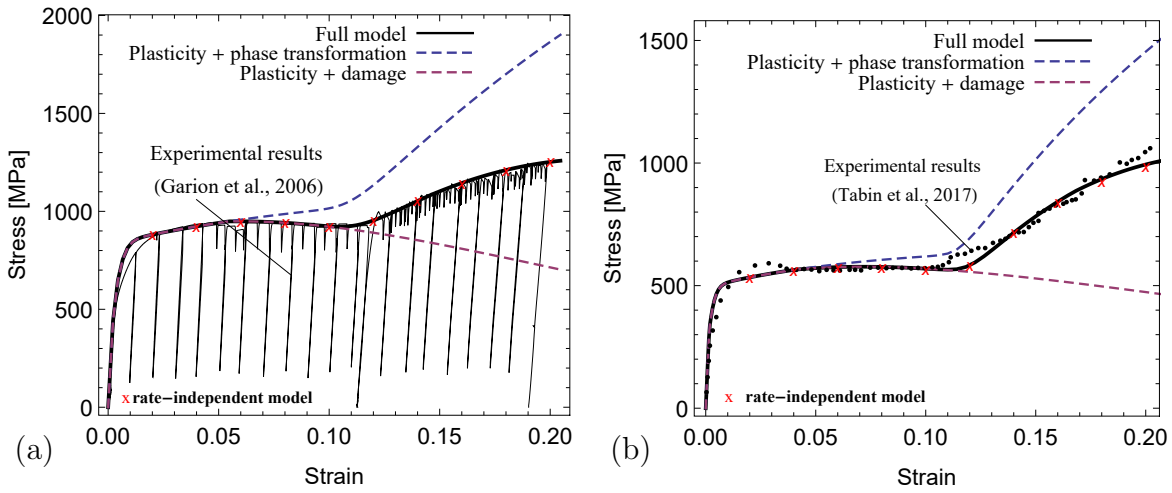

Figure 6.3: Stress-strain comparison of numerical and experimental results for (a) 316L and (b) 304 stainless steels. Presentation of various couplings.

Damage evolution (in the direction of loading) correlated with phase transformation for both materials is presented in Fig. 6.4 whereas damage evolution in the principal directions, reflecting damage anisotropy, is presented in Fig. 6.5. The components of ductile and brittle damage (see mixture rule (3.8)) were distinguished to show the fraction of both types of damage in the RVE. According to Eq. (3.8), the symbols appearing in the pictures are defined as follows (coupling with phase transformation rate is disregarded):

$$D_{ij} = \int_t \dot{D}_{ij} dt, \quad \Big\langle D_{ij} \Big\rangle^d_{\text{RVE}} = \int_t \Big\langle \dot{D}_{ij} \Big\rangle^d_{\text{RVE}} dt, \quad \Big\langle D_{ij} \Big\rangle^b_{\text{RVE}} = \int_t \Big\langle \dot{D}_{ij} \Big\rangle^b_{\text{RVE}} dt \tag{6.2}$$

In order to show the influence of phase transformation on the rate of damage, the result in which the martensitic transformation was disregarded is also shown (Fig. 6.4). One can see that, at the beginning, the damage evolves in a rather accelerated way and is purely ductile in nature. However, as soon as martensite starts to develop, a drop of the damage rate is observed, and brittle damage evolution accompanies the phenomenon of phase transformation. The observed effect of damage evolution deceleration in the parent phase is due to the transformation strain included in the constitutive model (Eq. 3.70) and the used mixture rule (Eq. 3.8). Strains resulting from damage evolution (Eqs. 3.68, 3.69) have a less significant impact.

In several papers mentioned in Section 1.2 the authors argument that the additional strain resulting from phase transformation gives rise to the increase in dislocation density in the

surrounding material, which may promote damage evolution. This effect is also included in the present model through the definition of the thermodynamic force $\mathbf{Y}$ conjugate to damage. Given that the part $\mathbf{Y}^{\mathrm{p}}$ strongly depends on the volume fraction of martensite, and hence the growing volume fraction of martensite contributes to an increase in the rate of damage evolution.

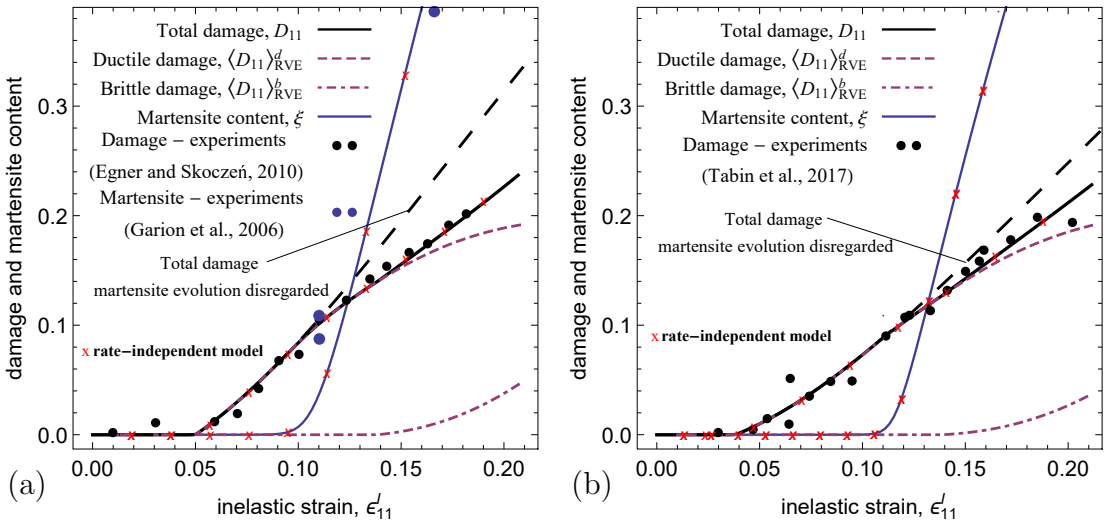

Figure 6.4: Damage evolution and martensite fraction in RVE for (a) 316L and (b) 304 stainless steels. Influence of phase transformation on ductile and brittle damage components in accordance with Eqs. (3.8) and (6.2).

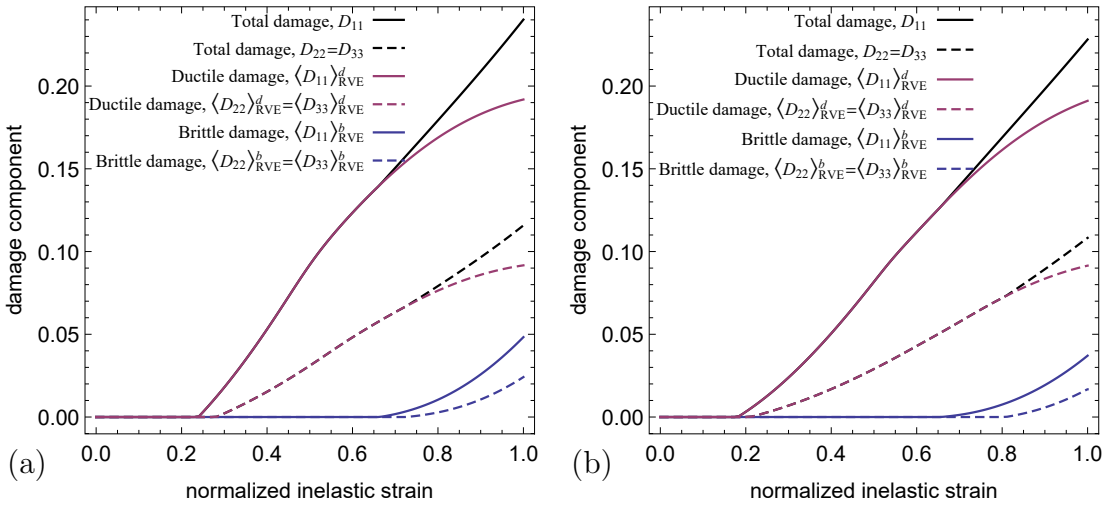

Figure 6.5: Individual components of damage tensor for (a) 316L and (b) 304 stainless steels.

6.3 Axisymmetric, corrugated thin-walled cryogenic bellows

Owing to the implementation of the constitutive model in the finite element software, the mechanical behaviour of various structures can be simulated. As an example, the analysis of an expansion bellows is presented here. Bellows expansion joints belong to thin-walled structures of high flexibility and are often key components of systems operating at high temperature gradients in which a significant shrinkage of structures may occur during the cooling process, hence the relative motion of two adjacent assemblies needs to be compensated. Since bellows expansion joints are subjected to severe conditions (cryogenic temperatures, radiation and mechanical loading, pressure), the choice of a relevant material is a key point in the design. Commonly, austenitic stainless steels are used for cryogenic applications because of their pronounced ductility at low temperatures, and good magnetic and vacuum properties. Here, a half convolution of a typical U-type bellows has been subjected to displacement-controlled cyclic mechanical loading. The parameters of 304SS (Tab. 6.1) were used, and the applied axial displacement amplitude was $u_{\mathrm{y}} = +42/-16$ mm (see Fig. 6.6), and 100 cycles were simulated. For simplicity, isotropic damage state variables were here used, so that $M_{ijkl} = (1-D)I_{ijkl}$ (see Eq. (3.37)). Basic geometrical parameters of the expansion bellows used in the simulation are listed in Tab. 6.2.

Table 6.2: Geometrical parameters of the expansion bellows (Skoczeń, 2004)

Material	Thickness of ply, t [mm]	Number of convultions	Outer diameter, D_0 [mm]	Inner diameter, D_b [mm]	Convoluted length, [mm]
SS 304	0.15	15	90.15	82	78

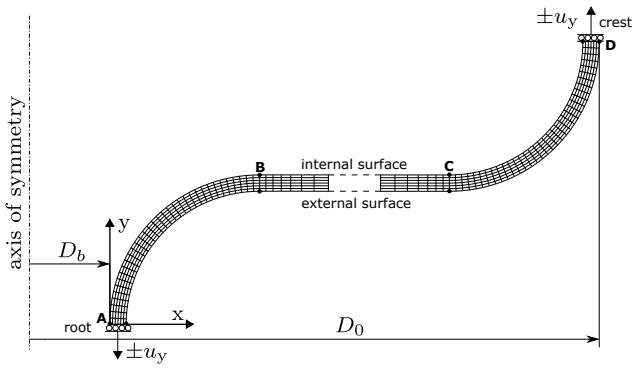

Figure 6.6: Boundary conditions and finite element mesh for single ply bellows (the mesh shown in the figure is two times coarser then that used in the computations).

The results obtained after 100 cycles are shown in Figs. 6.7-6.9. In Fig. 6.7 the distributions of chosen characteristic quantities related to state variables are presented. It can be seen that the most "efforted" area is placed at the internal surface near the bellows root. This is mainly due to the fact that the maximum meridional bending moment in the shell is localized at root and at crest (points A and D in Fig. 6.6). As a consequence of this highly localized bending and the relevant distribution of strain across the wall, the plastic strain fields develop on the external and internal surfaces of the shell. Figure 6.8 shows the evolution of damage through the thickness (at root and crest, Fig. 6.8a) and along the meridional line ABCD projected on x direction (Fig. 6.8b), while the profile of the martensite volume fraction in the same directions is presented in Fig. 6.9a,b. The most intensive damage accumulation occurs at root and at crest, where a strong localization of plastic strains takes place. It is accompanied by damage fields containing microcracks and microvoids, and by the plastic strain-induced phase transformation. This remains in a good agreement with the experimental observations, where the most intensive damage zones were observed at the internal side of the bellows root (cf. Garion and Skoczeń (2003)).

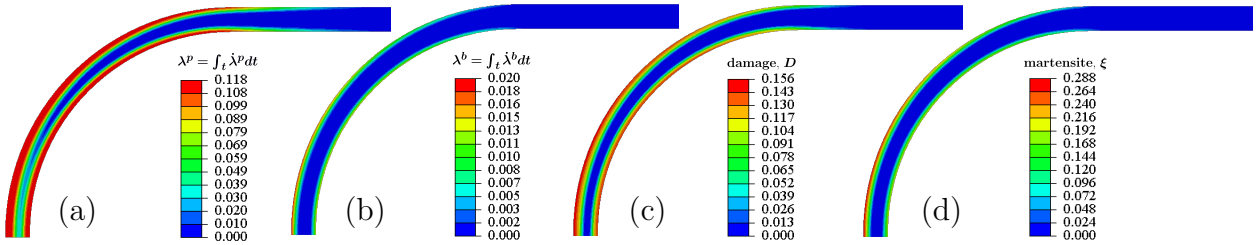

Figure 6.7: Distribution of: (a) $\lambda^{\mathrm{p}} = \int_t \dot{\lambda}^{\mathrm{p}} dt$; (b) $\lambda^{\mathrm{b}} = \int_t \dot{\lambda}^{\mathrm{b}} dt$; (c) damage, D and (d) martensite content, ξ after 100 cycles.

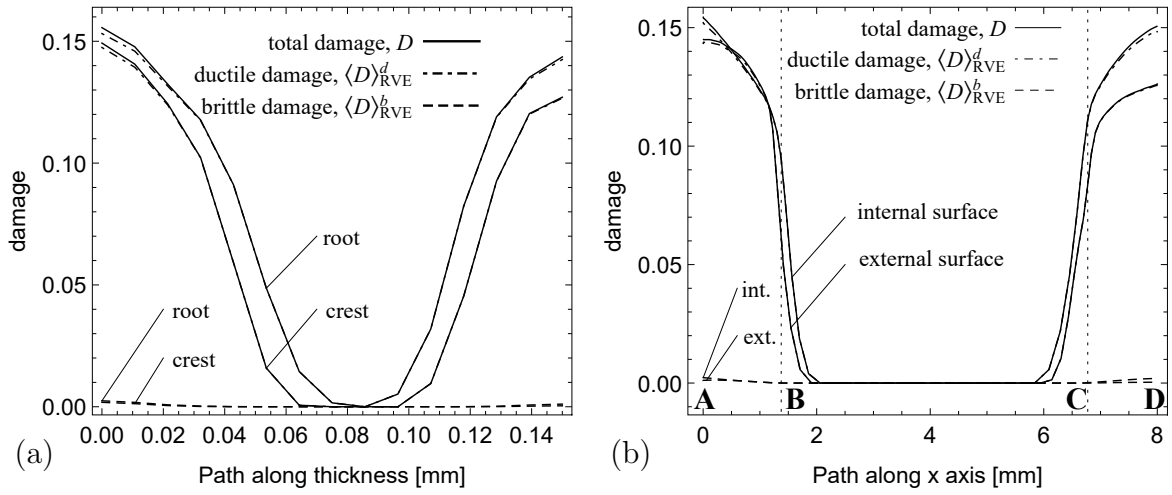

Figure 6.8: Distribution of various damage components through thickness (a) and along the meridional line ABCD projected on x direction (b).

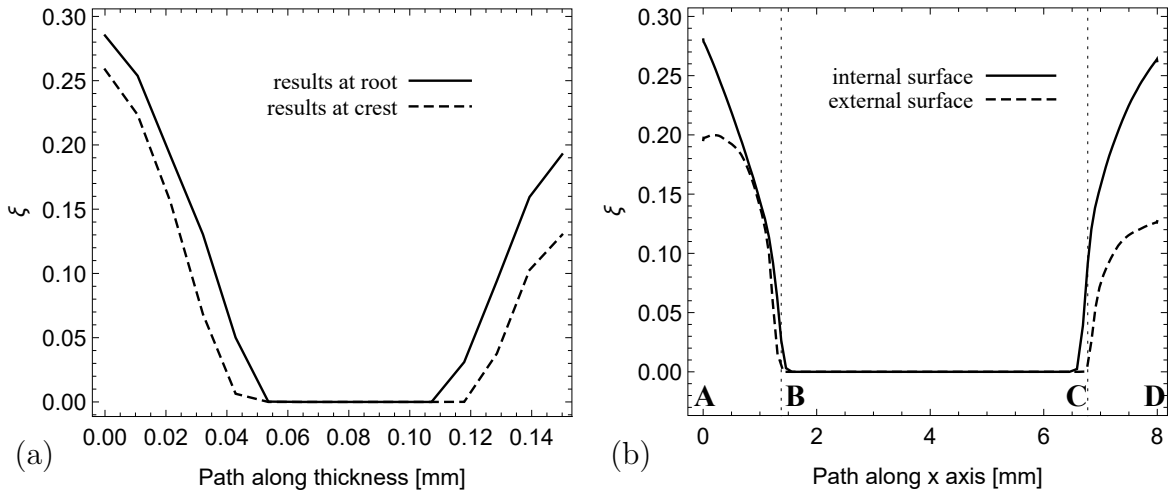

Figure 6.9: Distribution of martensite content through thickness (a) and along the meridional line ABCD projected on x direction (b).

Chapter 7

Summary

The constitutive model presented in the dissertation results from the identification of three fundamental phenomena that occur in a wide range of temperatures in the materials characterized by low stacking fault energy (e.g. austenitic steels):

- plastic flow resulting from the movement of dislocations,
- plastic strain-induced transformation from the parent phase (γ) to the secondary phase (α'), characteristic of meta-stable materials,
- evolution of micro-damage (micro-voids and micro-cracks) reflected by decreasing unloading modulus in the course of deformation.

A consistent thermodynamic framework has been built in order to describe all the phenomena, as well as coupling between them, in a unified way. The approach based on the total energy equivalence hypothesis, originally developed for damaged materials, extended to modelling not only damage but also other dissipative phenomena was used to derive the model. The hypothesis is based on introducing two main configurations: the real one in which a material is discontinuous (due to microcracks and microvoids) and heterogeneous (due to different phases present), and the equivalent fictitious configuration that is continuous (undamaged) and homogeneous (monophase). The novelty of this RVE based approach consists in introducing a mapping from the real to the fictitious configuration, defined as a combination of two physically different transformations. One is a classical mapping from a real, damaged (discontinuous but homogeneous) to a fictitious, undamaged (continuous) space. It involves a classical fourth rank damage effect tensor that allows to define damage-effective variables. The other transformation maps an RVE of a real, two-phase (heterogeneous but continuous) material into a point of a fictitious, mono-phase (homogeneous) configuration. The latter transformation requires a definition of another influence tensor, which allows to

obtain transformation-effective variables. The advantage of the proposed method lies in the possibility to describe all the dissipative phenomena by the use of the same thermodynamically consistent formalism, therefore the application of additional, usually complicated and laborious homogenization methods is not necessary.

To account for the damage-induced anisotropy of the ductile austenitic phase and the brittle martensitic content, the relevant second rank tensors were postulated. Ductile damage evolution has been described by an anisotropic model being a generalization of the classical isotropic model, known in the literature as the Chaboche–Lemaitre model. Ductile damage rate tensor depends on the 'ductile' strain energy density release rate tensor (Y_{ij}^{d}), not on the 'total' strain energy density release rate tensor (Y_{ij}) as in the original model. The ductile damage model is supplemented by an additional brittle-type damage model, to account for the stress-dependent damage state in the martensitic inclusions. The brittle damage surface based on the 'brittle' strain energy density release rate tensor (Y_{ij}^{b}) was used. The total material degradation is assumed to be a superposition of the ductile and the brittle parts, with the use of phase transformation variable as a composition factor (weight function). It allows for different coupling effects between damage and phase transformation to appear in a natural way: secondary phase volume fraction development results in a drop of the rate of ductile damage evolution. On the other hand, a high volume fraction of the brittle secondary phase may provide brittle macro-cracks and thus cause material failure.

Validation of the model is based on the available experimental data and very rare experiments carried out at extremely low temperatures, where multiple unloading technique was applied in order to monitor the evolution of micro-damage. Parameters included in the evolution equations for thermodynamic forces and kinetic laws of evolution of internal variables were found with the use of ISIGHT program.

Accounting for three dissipative phenomena: plasticity, damage evolution and phase transformation in the present constitutive model allows to obtain a satisfactory reproduction of the experimental stress-strain curve for 316L and 304 stainless steels subjected to uniaxial tension at the temperature of 4.2K.

References

Al-Rub, R. K. A. and Voyiadjis, G. Z. (2003). On the coupling of anisotropic damage and plasticity models for ductile materials. *Int. J. Sol. Struct.*, 40(11):2611–2643.

Amer, A. O., Gloanec, A.-L., Courtin, S., and Touze, C. (2013). Characterization of fatigue damage in 304L steel by an acoustic emission method. *Procedia Engineering*, 66:651–660.

Antolovich, S. D. and Singh, B. (1971). On the toughness increment associated with the austenite to martensite phase transformation in TRIP steels. *Metall. Mater. Trans. B*, 2(8):2135–2141.

Bag, A., Ray, K., and Dwarakadasa, E. (1999). Influence of martensite content and morphology on tensile and impact properties of high-martensite dual-phase steels. *Metall. Mater. Trans. A*, 30(5):1193–1202.

Bag, A., Ray, K., and Dwarakadasa, E. (2001). Influence of martensite content and morphology on the toughness and fatigue behavior of high–martensite dual-phase steels. *Metall. Mater. Trans. A*, 32(9):2207–2217.

Bailat, C., Gröschel, F., and Victoria, M. (2000). Deformation modes of proton and neutron irradiated stainless steels. *J. Nucl. Mat.*, 276(1-3):283–288.

Beese, A. M. and Mohr, D. (2011). Effect of stress triaxiality and lode angle on the kinetics of strain-induced austenite-to-martensite transformation. *Acta Mater.*, 59(7):2589–2600.

Beese, A. M. and Mohr, D. (2012). Anisotropic plasticity model coupled with lode angle dependent strain-induced transformation kinetics law. *J. Mech. Phys. Solids*, 60(11):1922–1940.

Berrahmoune, M., Berveiller, S., Inal, K., and Patoor, E. (2006). Delayed cracking in 301LN austenitic steel after deep drawing: Martensitic transformation and residual stress analysis. *Mater. Sci. Eng. A*, 438:262–266.

Besson, J., Cailletaud, G., Chaboche, J.-L., and Forest, S. (2009). *Non-linear mechanics of materials*, volume 167. Springer Science & Business Media.

Botshekan, M., Degallaix, S., Desplanques, Y., and Pol, J. (1998). Tensile and lcf properties of aisi 316ln ss at 300 and 77 k. *Fatig. Fract. Eng. Mater. Struct.*, 21(6):651–660.

Brepols, T., Wulfinghoff, S., and Reese, S. (2017). Gradient-extended two-surface damage-plasticity: micromorphic formulation and numerical aspects. *Int. J. Plast.*, 97:64–106.

Chaboche, J. (2008). A review of some plasticity and viscoplasticity constitutive theories. *International Journal of Plasticity*, 24(10):1642–1693.

Chaboche, J.-L. (1999). Thermodynamically Founded CDM Models for Creep and Other Conditions. In Altenbach, H. and Skrzypek, J. J., editors, *Creep and Damage in Materials and Structures*, pages 209–283, Vienna. Springer Vienna.

Chatterjee, S. and Bhadeshia, H. (2006). Trip–assisted steels: cracking of high–carbon martensite. *Mater. Sci. Technol.*, 22(6):645–649.

Cherkaoui, M., Berveiller, M., and Lemoine, X. (2000). Couplings between plasticity and martensitic phase transformation: overall behavior of polycrystalline TRIP steels. *Int. J. Plast.*, 16(10-11):1215–1241.

Cherkaoui, M., Berveiller, M., and Sabar, H. (1998). Micromechanical modeling of martensitic transformation induced plasticity (TRIP) in austenitic single crystals. *Int. J. Plast.*, 14(7):597–626.

Chow, C. and Lu, T. (1992). An analytical and experimental study of mixed-mode ductile fracture under nonproportional loading. *Int. J. Damage Mech.*, 1(2):191–236.

Cordebois, J. and Sidoroff, F. (1982a). Anisotropic damage in elasticity and plasticity. *J. Méc. Théor. Appl.*, pages 45–60.

Cordebois, J. and Sidoroff, F. (1982b). Damage induced elastic anisotropy. In Boechler, J., editor, *Mechanical Behavior of Anisotropic Solids/Comportment Méchanique des Solides Anisotropes*, pages 761–774. Springer.

Diani, J. and Parks, D. (1998). Effects of strain state on the kinetics of strain-induced martensite in steels. *J. Mech. Phys. Solids*, 46(9):1613–1635.

Diani, J., Sabar, H., and Berveiller, M. (1995). Micromechanical modelling of the transformation induced plasticity (TRIP) phenomenon in steels. *Int. J. Engng Sci.*, 33(13):1921–1934.

Egner, H. (2012). On the full coupling between thermo-plasticity and thermo-damage in thermodynamic modeling of dissipative materials. *Int. J. Sol. Struct.*, 49(2):279–288.

Egner, H. and Ryś, M. (2012). Modeling of coupling between damage and phase transformation in austenitic stainless steel at cryogenic temperatures. *Czasopismo Techniczne*, (Mechanika Zeszyt 8-M 22):27–44 (in polish).

Egner, H. and Ryś, M. (2017). Total energy equivalence in constitutive modeling of multi-dissipative materials. *Int. J. Damage Mech.*, 26(3):417–446.

Egner, H. and Skoczeń, B. (2010). Ductile damage development in two-phase metallic materials applied at cryogenic temperatures. *Int. J. Plast.*, 26(4):488–506.

Egner, H., Skoczeń, B., and Ryś, M. (2015a). Constitutive and numerical modeling of coupled dissipative phenomena in 316l stainless steel at cryogenic temperatures. *Int. J. Plast.*, 64:113–133.

Egner, H., Skoczeń, B., and Ryś, M. (2015b). Constitutive modeling of dissipative phenomena in austenitic metastable steels at cryogenic temperatures. In *Inelastic Behavior of Materials and Structures Under Monotonic and Cyclic Loading*, pages 35–48. Springer.

Fischer, F., Berveiller, M., Tanaka, K., and Oberaigner, E. (1994). Continuum mechanical aspects of phase transformations in solids. *Arch. Appl. Mech.*, 64(2):54–85.

Fischer, F., Oberaigner, E., Tanaka, K., and Nishimura, F. (1998). Transformation induced plasticity revised an updated formulation. *Int. J. Sol. Struct.*, 35(18):2209–2227.

Fischer, F. and Reisner, G. (1998). A criterion for the martensitic transformation of a microregion in an elastic-plastic material. *Acta Metall.*, 46(6):2095–2102.

Fischer, F. and Schlögl, S. (1995). The influence of material anisotropy on transformation induced plasticity in steel subject to martensitic transformation. *Mech. Mater.*, 21(1):1–23.

Fischer, F.-D., Reisner, G., Werner, E., Tanaka, K., Cailletaud, G., and Antretter, T. (2000). A new view on transformation induced plasticity (TRIP). *Int. J. Plast.*, 16(7-8):723–748.

Garion, C. and Skoczeń, B. (2002). Modeling of plastic strain-induced martensitic transformation for cryogenic applications. *J. Appl. Mech.*, 69(6):755–762.

Garion, C. and Skoczeń, B. (2003). Combined model of strain-induced phase transformation and orthotropic damage in ductile materials at cryogenic temperatures. *Int. J. Damage Mech.*, 12(4):331–356.

Garion, C., Skoczeń, B., and Sgobba, S. (2006). Constitutive modelling and identification of parameters of the plastic strain-induced martensitic transformation in 316L stainless steel at cryogenic temperatures. *Int. J. Plast.*, 22(7):1234–1264.

Greenwood, G. and Johnson, R. (1965). The deformation of metals under small stresses during phase transformations. *Proc. R. Soc. Lond. A*, 283(1394):403–422.

Gurtin, M. E., Fried, E., and Anand, L. (2010). *The mechanics and thermodynamics of continua*. Cambridge University Press.

Hallberg, H., Banks-Sills, L., and Ristinmaa, M. (2012). Crack tip transformation zones in austenitic stainless steel. *Eng. Fract. Mech.*, 79:266–280.

Hallberg, H., Håkansson, P., and Ristinmaa, M. (2007). A constitutive model for the formation of martensite in austenitic steels under large strain plasticity. *Int. J. Plast.*, 23(7):1213–1239.

Hallberg, H., Håkansson, P., and Ristinmaa, M. (2010). Thermo-mechanically coupled model of diffusionless phase transformation in austenitic steel. *Int. J. Sol. Struct.*, 47(11-12):1580–1591.

Han, H. N., Lee, C. G., Oh, C.-S., Lee, T.-H., and Kim, S.-J. (2004). A model for deformation behavior and mechanically induced martensitic transformation of metastable austenitic steel. *Acta Mater.*, 52(17):5203–5214.

Han, H. N., Lee, C. G., Suh, D.-W., and Kim, S.-J. (2008). A microstructure-based analysis for transformation induced plasticity and mechanically induced martensitic transformation. *Mater. Sci. Eng. A*, 485(1-2):224–233.

Han, H. N., Oh, C.-S., Kim, G., and Kwon, O. (2009). Design method for TRIP-aided multiphase steel based on a microstructure-based modelling for transformation-induced plasticity and mechanically induced martensitic transformation. *Mater. Sci. Eng. A*, 499(1-2):462–468.

Hayakawa, K., Murakami, S., and Liu, Y. (1998). An irreversible thermodynamics theory for elastic-plastic-damage materials. *Eur. J. Mech. A/Solids*, 17(1):13–32.

Huo, C. and Gao, H. (2005). Strain–induced martensitic transformation in fatigue crack tip zone for a high strength steel. *Materials Characterization*, 55(1):12–18.

Iwamoto, T., Tsuta, T., and Tomita, Y. (1998). Investigation on deformation mode dependence of strain-induced martensitic transformation in TRIP steels and modelling of transformation kinetics. *Int. J. Mech. Sci.*, 40(2-3):173–182.

Jacques, P., Furnemont, Q., Pardoen, T., and Delannay, F. (2001). On the role of martensitic transformation on damage and cracking resistance in TRIP–assisted multiphase steels. *Acta Mater.*, 49(1):139–152.

Lacroix, G., Furnemont, Q., Jacques, P., and Pardoen, T. (2006). Mechanisms of damage and fracture in TRIP assisted multiphase steels. In *Fracture of Nano and Engineering Materials and Structures*, pages 819–820. Springer.

Lacroix, G., Pardoen, T., and Jacques, P. J. (2008). The fracture toughness of TRIP–assisted multiphase steels. *Acta Mater.*, 56(15):3900–3913.

Leblond, J.-B. (1989). Mathematical modelling of transformation plasticity in steels ii: coupling with strain hardening phenomena. *Int. J. Plast.*, 5(6):573–591.

Leblond, J.-B., Devaux, J., and Devaux, J. (1989). Mathematical modelling of transformation plasticity in steels i: case of ideal-plastic phases. *Int. J. Plast.*, 5(6):551–572.

Lee, K. J., Chun, M. S., Kim, M. H., and Lee, J. M. (2009). A new constitutive model of austenitic stainless steel for cryogenic applications. *Comp. Mat. Sci.*, 46(4):1152–1162.

Lemaitre, J. (1971). Evaluation of dissipation and damage in metals. In *Proceeding ICM-1*, pages 15–20, Kyoto, Japan.

Lemaitre, J. (1992). *A course on damage mechanics*. Springer-Verlag, Berlin and New York.

Lemaitre, J. and Chaboche, J.-L. (1978). Aspect phénoménologique de la rupture par endommagement. *J. Méc. Appl.*, 2(3).

Magee, C. L. and Paxton, H. W. (1966). Transformation Kinetics, Microplasticity and Aging of Martensite in FE–31 Ni. Technical report, CARNEGIE INST OF TECH PITTSBURGH PA.

Mahnken, R. and Schneidt, A. (2010). A thermodynamics framework and numerical aspects for transformation-induced plasticity at large strains. *Arch. Appl. Mech.*, 80(3):229–253.

Mahnken, R., Wolff, M., Schneidt, A., and Böhm, M. (2012). Multi-phase transformations at large strains–Thermodynamic framework and simulation. *Int. J. Plast.*, 39:1–26.

Maugin, G. (1999). *The Thermomechanics of Nonlinear Irreversible Behaviors*. WORLD SCIENTIFIC.

Murakami, S. (2012). *Continuum Damage Mechanics: A Continuum Mechanics Approach to the Analysis of Damage and Fracture*, volume 185. Springer Science & Business Media.

Olson, G. (1996). Transformation plasticity and toughening. *Le Journal de Physique IV*, 6(C1):C1–407.

Olson, G. and Cohen, M. (1975). Kinetics of strain-induced martensitic nucleation. *Metall. Trans. A*, 6(4):791.

Ortwein, R., Ryś, M., and Skoczeń, B. (2016). Damage evolution in a stainless steel bar undergoing phase transformation under torsion at cryogenic temperatures. *Int. J. Damage Mech.*, 25(7):967–1016.

Pan, J. and Rice, J. R. (1983). Rate sensitivity of plastic flow and implications for yield-surface vertices. *Int. J. Sol. Struct.*, 19(11):973–987.

Parks, D. and Stringfellow, R. (1991). Strain-Induced Transformation Plasticity in Metastable Austenitic Steels. In *Anisotropy and Localization of Plastic Deformation*, pages 516–519. Springer.

Peirce, D., Asaro, R. J., and Needleman, A. (1983). Material rate dependence and localized deformation in crystalline solids. *Acta Metall.*, 31(12):1951–1976.

Petit, B., Gey, N., Cherkaoui, M., Bolle, B., and Humbert, M. (2007). Deformation behavior and microstructure/texture evolution of an annealed 304 AISI stainless steel sheet. Experimental and micromechanical modeling. *Int. J. Plast.*, 23(2):323–341.

Reisner, G., Werner, E., and Fischer, F. (1998). Micromechanical modeling of martensitic transformation in random microstructures. *Int. J. Sol. Struct.*, 35(19):2457–2473.

Ryś, M. (2014). Constitutive modelling and identification of parameters of 316L stainless steel at cryogenic temperatures. *Acta Mech. Autom.*, 8(3):136–140.

Ryś, M. (2015). Modeling of damage evolution and martensitic transformation in austenitic steel at cryogenic temperature. *Archive of Mechanical Engineering*, 62(4):523–537.

Ryś, M. (2016). Constitutive modelling of damage evolution and martensitic transformation in 316L stainless steel. *Acta Mech. Autom.*, 10(2):125–132.

Ryś, M. and Skoczeń, B. (2017). Coupled constitutive model of damage affected two-phase continuum. *Mech. Mater.*, 115:1–15.

Saanouni, K. (2012). *Damage Mechanics in Metal Forming: Advanced Modeling and Numerical Simulation*. John Wiley & Sons.

Saanouni, K., Forster, C., and Hatira, F. B. (1994). On the anelastic flow with damage. *Int. J. Damage Mech.*, 3(2):140–169.

Santacreu, P.-O., Glez, J.-C., Chinouilh, G., and Fröhlich, T. (2006). Behaviour model of austenitic stainless steels for automotive structural parts. *Steel Research International*, 77(9-10):686–691.

Simo, J. and Ju, J. (1987). Strain- and stress-based continuum damage models. I – Formulation, II – Computational aspects. *Int. J. Sol. Struct.*, 23(7):821–840, 841–869.

Simo, J. C. and Hughes, T. J. (1998). *Computational Inelasticity. Interdisciplinary Applied Mathematics*, volume 7. Springer, New York.

Sitko, M. and Skoczeń, B. (2012). Effect of γ–α' phase transformation on plastic adaptation to cyclic loads at cryogenic temperatures. *Int. J. Sol. Struct.*, 49(3-4):613–634.

Skoczeń, B. (2004). *Compensation systems for low temperature applications*. Springer, Berlin, Heidelberg, New York.

Socrate, S. (1995). *Mechanics of microvoid nucleation and growth in high–strength metastable austenitic steels*. PhD thesis, Massachusetts Institute of Technology.

Stavehaug, F. (1990). *Transformation toughening of γ'–strengthened metastable austenitic steels*. PhD thesis, Massachusetts Institute of Technology.

Stolarz, J., Baffie, N., and Magnin, T. (2001). Fatigue short crack behaviour in metastable austenitic stainless steels with different grain sizes. *Mater. Sci. Eng. A*, 319:521–526.

Stringfellow, R., Parks, D., and Olson, G. (1992). A constitutive model for transformation plasticity accompanying strain-induced martensitic transformations in metastable austenitic steels. *Acta Metall. Mater.*, 40(7):1703–1716.

Sugimoto, K.-I., Kobayashi, M., and Hashimoto, S.-I. (1992). Ductility and strain-induced transformation in a high-strength transformation-induced plasticity-aided dual-phase steel. *Metall. Trans. A*, 23(11):3085–3091.

Suiker, A. S. and Turteltaub, S. (2006). Numerical modelling of transformation-induced damage and plasticity in metals. *Modelling Simul. Mater. Sci. Eng.*, 15(1):S147.

Sun, X., Choi, K., Liu, W., and Khaleel, M. (2009). Predicting failure modes and ductility of dual phase steels using plastic strain localization. *Int. J. Plast.*, 25(10):1888–1909.

Tabin, J., Skoczeń, B., and Bielski, J. (2016). Strain localization during discontinuous plastic flow at extremely low temperatures. *Int. J. Sol. Struct.*, 97:593–612.

Tabin, J., Skoczeń, B., and Bielski, J. (2017). Damage affected discontinuous plastic flow (DPF). *Mech. Mater.*, 110:44–58.

Taleb, L. and Petit, S. (2006). New investigations on transformation induced plasticity and its interaction with classical plasticity. *Int. J. Plast.*, 22(1):110–130.

Taleb, L. and Sidoroff, F. (2003). A micromechanical modeling of the greenwood–johnson mechanism in transformation induced plasticity. *Int. J. Plast.*, 19(10):1821–1842.

Tomita, Y. and Iwamoto, T. (1995). Constitutive modeling of TRIP steel and its application to the improvement of mechanical properties. *Int. J. Mech. Sci.*, 37(12):1295–1305.

Tomita, Y. and Iwamoto, T. (2001). Computational prediction of deformation behavior of TRIP steels under cyclic loading. *Int. J. Mech. Sci.*, 43(9):2017–2034.

Turteltaub, S. and Suiker, A. (2005). Transformation-induced plasticity in ferrous alloys. *J. Mech. Phys. Solids*, 53(8):1747–1788.

Uthaisangsuk, V., Prahl, U., and Bleck, W. (2008). Micromechanical modelling of damage behaviour of multiphase steels. *Comp. Mat. Sci.*, 43(1):27–35.

Uthaisangsuk, V., Prahl, U., and Bleck, W. (2009). Failure modeling of multiphase steels using representative volume elements based on real microstructures. *Procedia Eng.*, 1(1):171–176.

Uthaisangsuk, V., Prahl, U., and Bleck, W. (2011). Modelling of damage and failure in multiphase high strength DP and TRIP steels. *Eng. Fract. Mech.*, 78(3):469–486.

Voyiadjis, G. Z. and Deliktas, B. (2000). A coupled anisotropic damage model for the inelastic response of composite materials. *Comp. Meth. Appl. Mech. Engng.*, 183(3-4):159–199.

Voyiadjis, G. Z. and Dorgan, R. J. (2007). Framework using functional forms of hardening internal state variables in modeling elasto-plastic-damage behavior. *Int. J. Plast.*, 23(10-11):1826–1859.

Appendix A

Rate-independent algorithm – an example

In the following section, a simulation of loading of a square of dimensions $h \times h$[mm] is shown. The purpose of this section is to present the main features of the rate-independent algorithm which is summarized in Table 4.1. On the bottom edge of the square, presented in Fig. A.1, the vertical displacement is zero ($u|_{y=0} = 0$) while the upper is $u|_{y=h} = 0.08h$. On the left and right side of the square, the horizontal displacement is $\pm 0.5u$. The computation is performed with the use of (linear) rectangular element and with a constant displacement rate 0.004[mm/s]. In this case, mixed linear-kinematic ($C^0 = 1000$[MPa], $\gamma = 0$) and linear–isotropic ($Q^{\mathrm{p}0}$=1000[MPa], $b^{\mathrm{p}} = 0$) hardening laws, affected by ductile ($S = 2$[MPa], $s = 1$, $\beta = 1$, $p_D = 0$) and brittle ($l_y = 0.01$[MPa], $Q^{\mathrm{b}0} = 100$[MPa]) damage and phase transformation ($h_{\mathrm{R}} = 5$, $h_{\mathrm{X}} = 5$), are used. The evolution of the secondary phase is quite rapid at the beginnig ($D_\xi = 20$, $m_\xi = 2$) as presented in Fig. A.2b. The rest of the used parameters is as in Table 6.1. The equivalent von Mises stress-strain as well as total damage and martensite content vs. total strain plots (in the direction of loading y) are presented in Fig. A.1, for better clarity of the macroscopic response for the present model parameters.

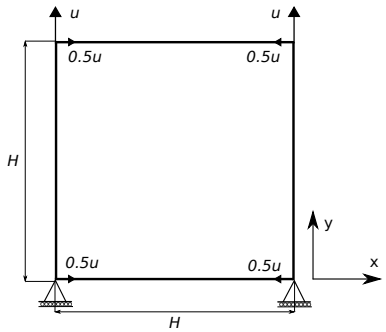

Figure A.1: Schematic sketch of loading of the square element.

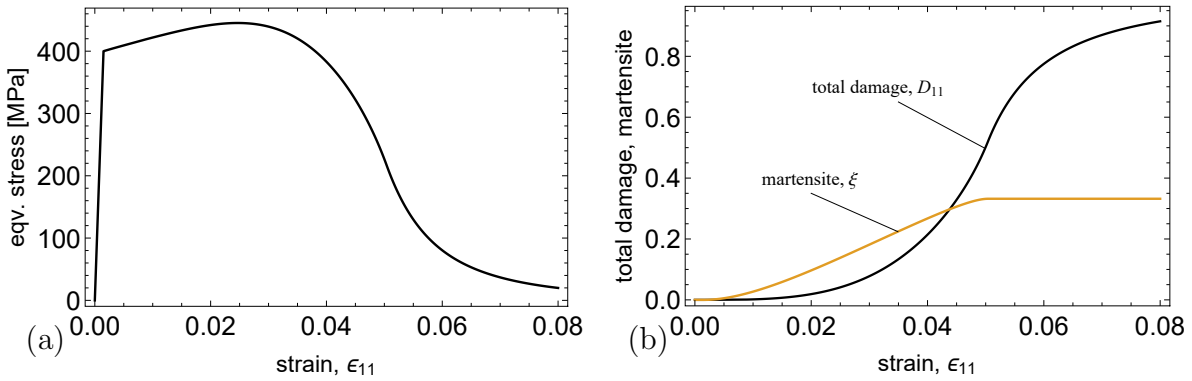

Figure A.2: Equivalent stress-strain plot (a) and damage (D_{11}), and martensite content (ξ) vs. total strain (b) for current parameters.

The values of the criterion of plastic yelding and brittle damage evolution for trial state ($\hat{\hat{f}}^{\mathrm{p,trial}}$, $f^{\mathrm{b,trial}}$) and at the end of every time step 'j' ($\hat{\hat{f}}^{\mathrm{p}}$, f^{b}) are presented in Fig. A.3. The values of the increments of plastic and brittle damage multipliers at the end of every time step 'j' denoted by $\Delta\lambda^{\mathrm{p}}$ and $\Delta\lambda^{\mathrm{b}}$, respectively and for some iteration 's' (usually for $s = 1$ or s for which a negative value of $\mathrm{d}\lambda^{\mathrm{p}}$ or $\mathrm{d}\lambda^{\mathrm{b}}$ was obtained in the case where two processes were active initially) are presented in Fig. A.5. The most interesting situation is between increments $86 \div 89$ for which the trial brittle damage criterion, $f^{\mathrm{b,trial}}$, is higher than zero (Fig. A.4b), which implies the onset of brittle damage evolution, however the increments for the first iteration, $\mathrm{d}\lambda^{\mathrm{b}(s=1)}$ are negative (Fig. A.6b), and thus, eventually, the brittle damage process is inactive for those time increments. Similarly, for increments between $506 \div 536$ the plastic yield criterion is higher than zero, however increments $\mathrm{d}\lambda^{\mathrm{p}(s=2)}$ for $j = 506, 507$ and $\mathrm{d}\lambda^{\mathrm{p}(s=1)}$ for $j = 508 \div 536$ are negative, which excludes plastic process from active ones. Importantly, the values of f^{b} and $\hat{\hat{f}}^{\mathrm{p}}$ at the end of time steps $j = 86 \div 89$ and $j = 506 \div 536$, respectively, are negative, which confirms the proper choice of active processes.

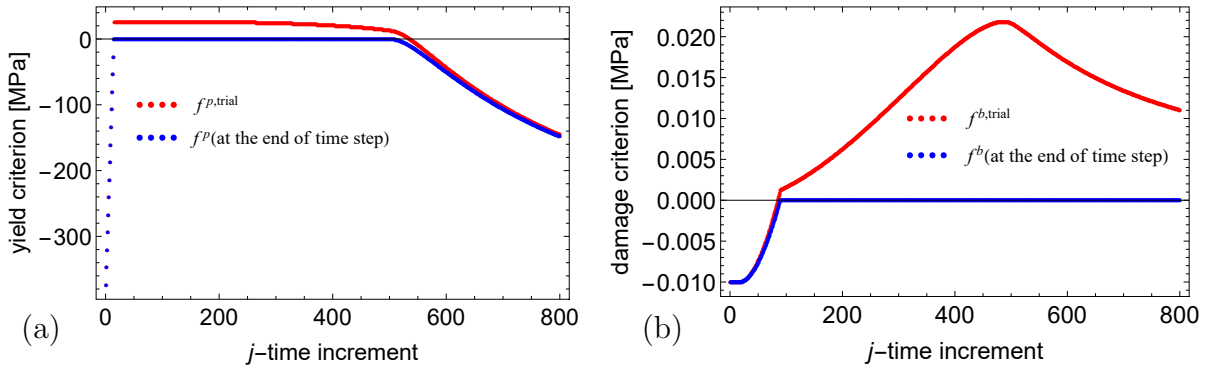

Figure A.3: Values of yield criterion, $\hat{\hat{f}}^{\mathrm{p}}$ (a) and damage criterion, f^{b} (b) at the beginning and the end for each time step.

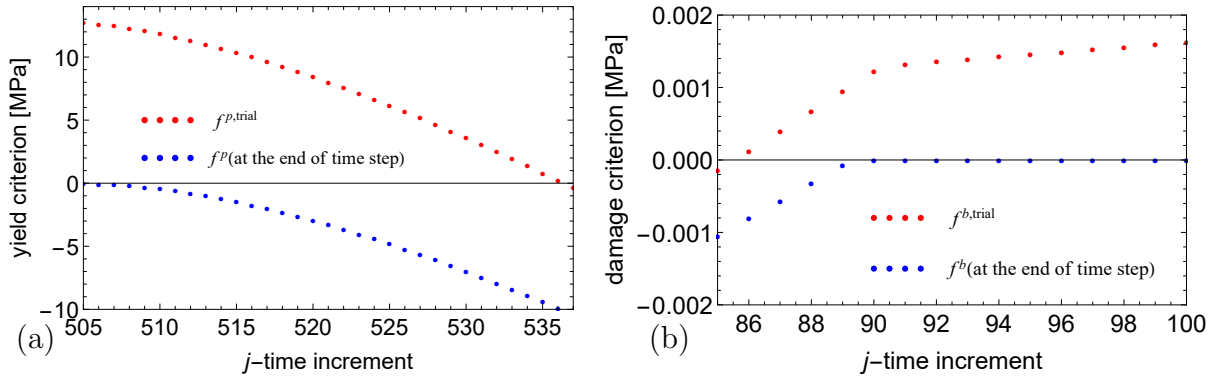

Figure A.4: Values of yield criterion, $\hat{\tilde{f}}^{\mathrm{p}}$ (a) and damage criterion, f^{b} (b) at the beginning and at the end for specific time steps.

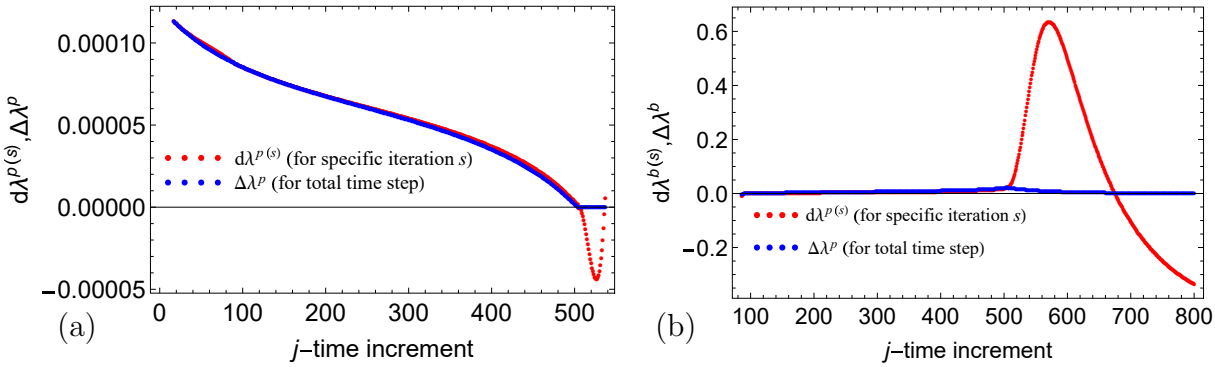

Figure A.5: Values of increments of plastic (a) and brittle damage (b) multipliers at the end of every time step 'j' ($\Delta\lambda^{\mathrm{p}}$, $\Delta\lambda^{\mathrm{b}}$) and for certain iteration 's' (for $s = 1$ or s for which negative value of $\mathrm{d}\lambda^{\mathrm{p}}$ or $\mathrm{d}\lambda^{\mathrm{b}}$ was obtained).

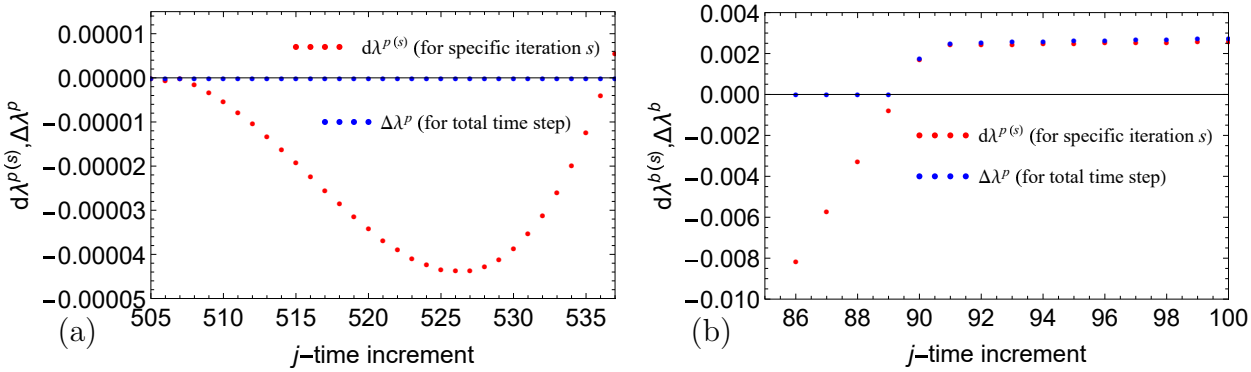

Figure A.6: Values of increments of plastic (a) and brittle damage (b) multipliers at the end of selected time steps 'j' ($\Delta\lambda^{\mathrm{p}}$, $\Delta\lambda^{\mathrm{b}}$) and for certain iteration 's' (for $s = 1$ or s for which negative value of $\mathrm{d}\lambda^{\mathrm{p}}$ or $\mathrm{d}\lambda^{\mathrm{b}}$ was obtained).